12-12-2018

The Utilization of Alternative Synthetic Methods for Further Optimization of Cyanine Dyes and their Potential Use in Imaging and Photodynamic Therapy

Fahad Marmarchi
fjrjes1@student.gsu.edu

The Utilization of Alternative Synthetic Methods for Further Optimization of Cyanine Dyes and

their Potential Use in Imaging and Photodynamic Therapy

by

Fahad Marmarchi

Under the Direction of Maged Henary, Ph.D

ABSTRACT

The work presented in this thesis aims utilizes the versatility of cyanine dyes. Although

large libraries have generated for these compounds, their remains an unmet need for alternative

synthetic procedures that both optimizes and allows the dyes to be tailored for the desired use.

The cyanine dye scaffold contains many points of modification but the central carbon remains a

point that requires further research. In addition, among the heterocyclic compound that can be

used in the synthesis of cyanine dyes, the quinoline heterocycle offer interesting optical

variations to the dyes and can be utilized in the applications that do not require highly fluorescent

compounds. The dyes presented showcase a superior synthetic procedure, and incorporate the

quinoline heterocycle in novel compounds.

INDEX WORDS: Organic Chemistry, Near-infrared Contrast Agents, Cyanine Dyes,

Photodynamic Therapy

The Utilization of Various Synthetic Methods for Further Optimization of Cyanine Dyes for their

Use in Imaging and Photodynamic Therapy

by

Fahad Marmarchi

A Thesis Submitted in Partial Fulfillment of the Requirements for the Degree of

Master of Science in the College of Arts and Sciences

Georgia State University

2018

The Utilization of Various Synthetic Methods for Further Optimization of Cyanine Dyes for their

Use in Imaging and Photodynamic Therapy

by

FAHAD MARMARCHI

Committee Chair: Maged Henary

Committee: Dr. Suazette Reid Mooring

Dr. Kathryn Gran

Electronic Version Approved:

Office of Graduate Studies

College of Arts and Sciences

Georgia State University

August 2018

DEDICATION

I would like to dedicate this thesis in loving memory of my mother, Merna Jardaq Marmarchi.

ACKNOWLEDGMENTS

First and foremost, I would like to thank my family and friends for their support throughout the years and especially during my graduate career. Next, I would like to thank all the professors and facility that has made my years at Georgia State University so memorable, especially Dr. Maged Henary for allowing me to join his research group. Through his mentorship, I was able to succeed in achieving my goal of obtaining my master's degree. Finally, I would like to thank all my labmates especially Dr. Andrew Ross Levitz, Matthew Laramie, Carl Kananda, Vincent Martinez, Ariana Laskey, Hector Argueta, Cory Holder, and Tyler Crawford whose loving spirit lives on with all of us.

TABLE OF CONTENTS

LIST OF TABLES

LIST OF FIGURES

1 INTRODUCTION: A REVIEW OF THE UNIQUE APPLICATIONS OF CYANINE DYES

1.1 PROPERTIES OF CYANINE DYES

Multiple families of cyanine dyes have been synthesized with various derivatives. NIR dyes have raised a great deal of interest due to their versatility in a wide array of applications, low energy absorption making for a safer alternative, and modifiability allowing for specific tailoring based on the desired application [1-3]. Their absorbance and emission fall outside the range of hemoglobin and water, making them ideal for medical applications [4]. Many NIR dyes have been screened and libraries have been generated, relating various properties (optical, physiochemical, etc.) of the dyes to a specific utility.

The Near Infrared (NIR) electromagnetic spectrum, is the region between infrared and visible light, with a wavelength of 600-900nm [5]. This is a lower energy of the spectrum and has opened a new and innovative path for scientific research, raising a great deal of interest in the medical field [6]. The low energy light makes for a safer alternative to current imaging techniques, while water and endogenous molecules have a low absorbance in this region (fig. 1) allowing for distinguishable difference and an enhanced signal to noise (S/N) ratio [6, 7]. The importance of this region can only be utilized upon the systematic design and synthesis of probes that have optical properties within this NIR wavelength.
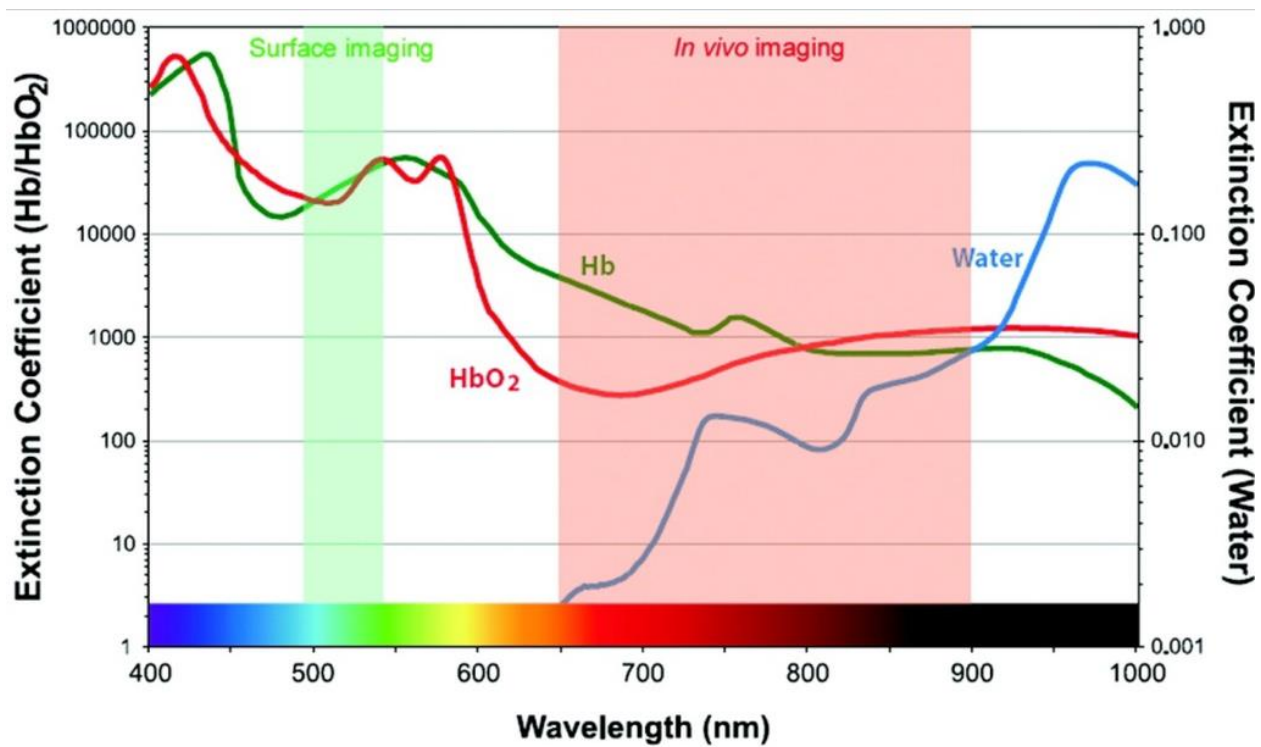
Figure 1.1.1: Spectra of endogenous molecule absorption [8]
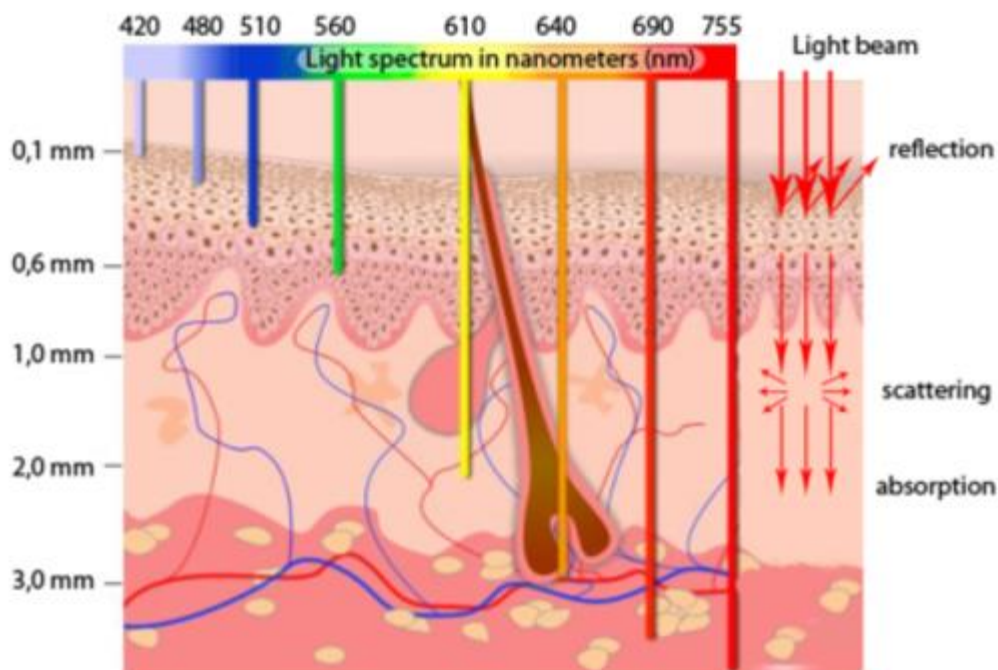
Figure 1.1.2: Dermal penetration at a different wavelength of light [9]

Among the various NIR probes synthesized, cyanine dyes have shown the greatest use in the medical imaging world. Their versatility and tunability allow them to be tailored for specific use. From the serendipitous discovery over a century ago to the FDA approval of indocyanine green (ICG) cyanine dyes continue to be used in a various application in the medical and industrial world [10]. As previously mentioned, ICG was approved by the FDA in 1955 but left room for optimization [11]. A myriad of cyanine dyes has been made since, focusing on fluorescent imaging and reviews have been written focusing on their use, but the aim of this manuscript is to focus on the recent advancements science has made using cyanine dyes and their incorporation to a wider array of applications.

Cyanine dyes are made of a two nitrogen-containing heterocycles linked together by a polymethine bridge which allow them to be tunable, modifiable, and versatile [12, 13]. Figure 3 represents the various points of modifications that can be made. First, the nitrogen-containing heterocycle (Fig. 3 blue) can be altered which can affect optical and physical properties. Along with the changes made to the heterocycle, varying alkyl groups can be incorporated to the nitrogen (Fig. 3 red) of the heterocycle which can alter characteristics such as solubility, the introduction of NHS ester for functionalizing and much more [14]. Next, the polymethine chain length can be varied (Fig. 3 green), predominately changing the absorbance wavelength by 100 nm per double bond which will ultimately change the fluorescence wavelength. The most common dyes used are penamethine (5 carbon chain) and heptamethine (7 carbon chain). Along with the changes discussed, the central carbon of the polymethine chain can be decorated with various substituents (Fig. 3 orange), as well as dyes can be made unsymmetrical by the incorporation of two different heterocycles [15-20].
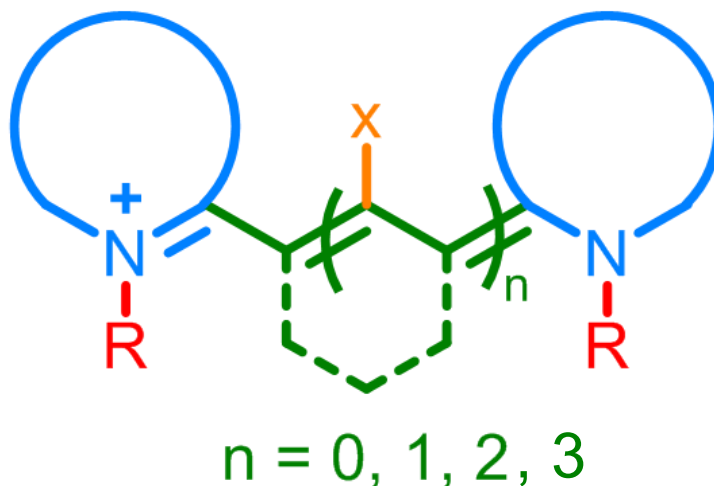
Figure 1.1.3: Cyanine dye scaffold

To understand cyanine dyes, the quantum and spectral properties have to be understood first. An altering of single and double bonds produces a conjugated system that allows for the electrons to have a $\pi \rightarrow \pi^*$ transition when excited, this transition has a small band gap allowing excitation to occur at higher wavelengths [21]. The two nitrogen-containing heterocycle red shifts the compound. Upon excitation of the dyes, based on their structure, various relaxation pathways may occur, each utilized for a specific use. These relaxation pathways include fluorescence emission, vibrational relaxation, and intersystem crossing [22-25].
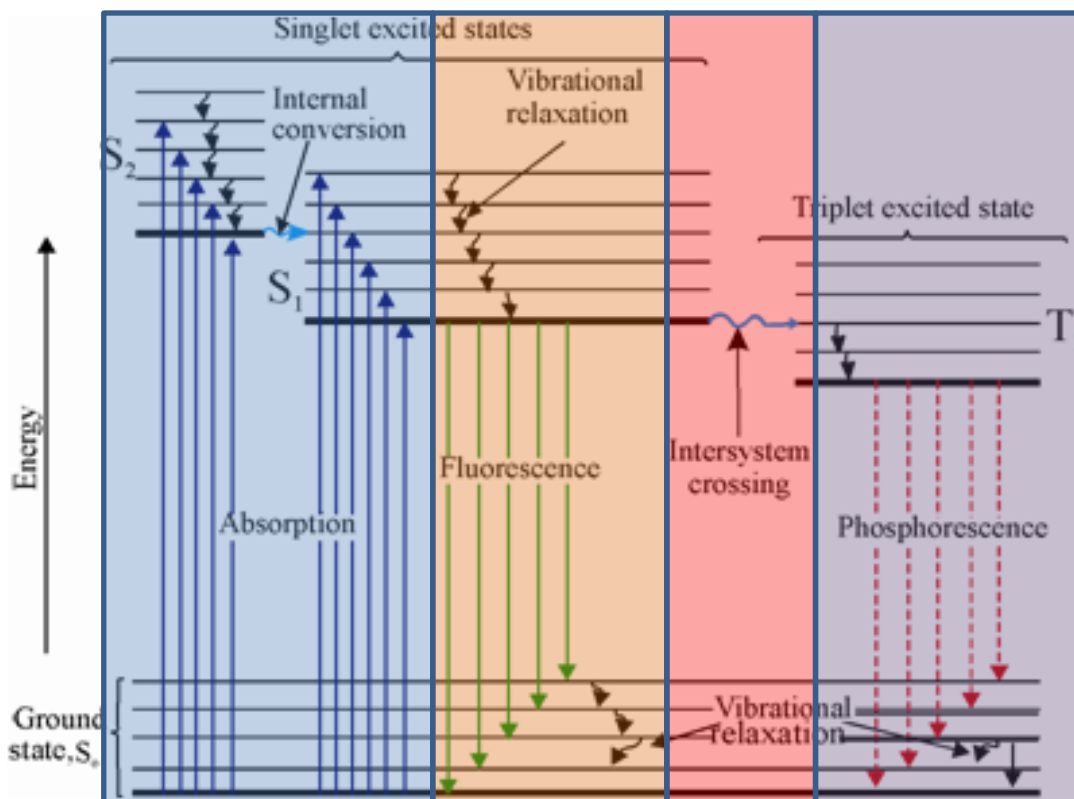
Figure 1.1.4: The Jablonski diagram [26]

The Jablonski diagram (fig. 4) illustrates the various relaxation pathways that fluorophores can take. Absorbance (fig. 4 blue) is a process by which a specific wavelength that excites electrons to the singlet excited state. Once excited, a combination of relaxation pathways are taken for the electron to return to the energy favorable ground state. Although an excited electron exhibits all of these relaxation pathways, we will focus on the dominate relaxation pathway that takes place and refer to these dyes as such. Fluorescent dyes use fluorescence (fig. 4 green) as the predominate relaxation pathway, these dyes emit light at a longer wavelength upon excitation. The longer wavelength is due to the energy lost with the various relaxation which yields a lower energy/longer wavelength photon. These dyes are commonly used in various applications in imaging. While, some weakly fluorescent dyes observe a greater rate of vibrational, non-radiative, relaxation, as

most excited electrons relax back to the ground state via vibrational relaxation. Dyes that demonstrate vibrational relaxation as dominate form show a great deal of utility in optoacoustic imaging (OAI) [27-37] [38-40], a new and innovative mode of imaging, and photothermal therapy (PTT). Other weakly fluorescent dyes, can interact with singlet oxygen, and upon collision, observe an electron flip which leads the excited electrons to undergo intersystem crossing (fig.3 red). Singlet oxygen too observes an electron flip that takes it to the triplet state, accumulation of triplet state oxygen, or reactive oxygen species (ROS) [41], is toxic to the cell. This phenomenon play a key role in photodynamic therapy (PDT) [42-47].

The goal of this review is to highlight key advances in developing cyanine dyes for imaging and the new and innovative applications utilizing the other relaxation pathways cyanine dyes can take. We aim to highlight unique, current and innovative uses of these dyes as contrast agents, optoacoustic imaging agents, photothermal therapy agents, and photodynamic therapy photosynthesizes.

Here in, we will separate the dyes based on their use and relaxation paths. Once again due to the vast number of reviews and research done on the more common applications of these dyes, the aim is to introduce innovative incorporations of cyanine dyes in a wider array of research avenues while still introducing some of the more common utilities.

1.2 The application of cyanine dyes as fluorescent probes

The most common use of these dyes remains in fluorescence imaging. Predominantly pentamethine and heptamethine dyes are used which emit light in the 700-800 nm range, and upon localization in specific organs can be used in image-guided surgery [28, 48-53]. This range is most utilized because it solves the direct setbacks that arise from the use of visible light contrast agent by avoiding auto-fluorescence and yielding high contrast. Most researchers done in this field

predominately uses ICG as a gold standard for fluorescent imaging due to its FDA approval and widespread medical usage [11]. Current research aims to alter and optimize the NIR compounds by changing the chain length and adding various functional groups to the many points of modification of the cyanine dye scaffold. Figure 5 illustrates the use of the dyes in a surgical setting for image-guided surgery yielding a great contrast due to the NIR emission of the dyes while endogenous tissue fluoresces in the visible range.
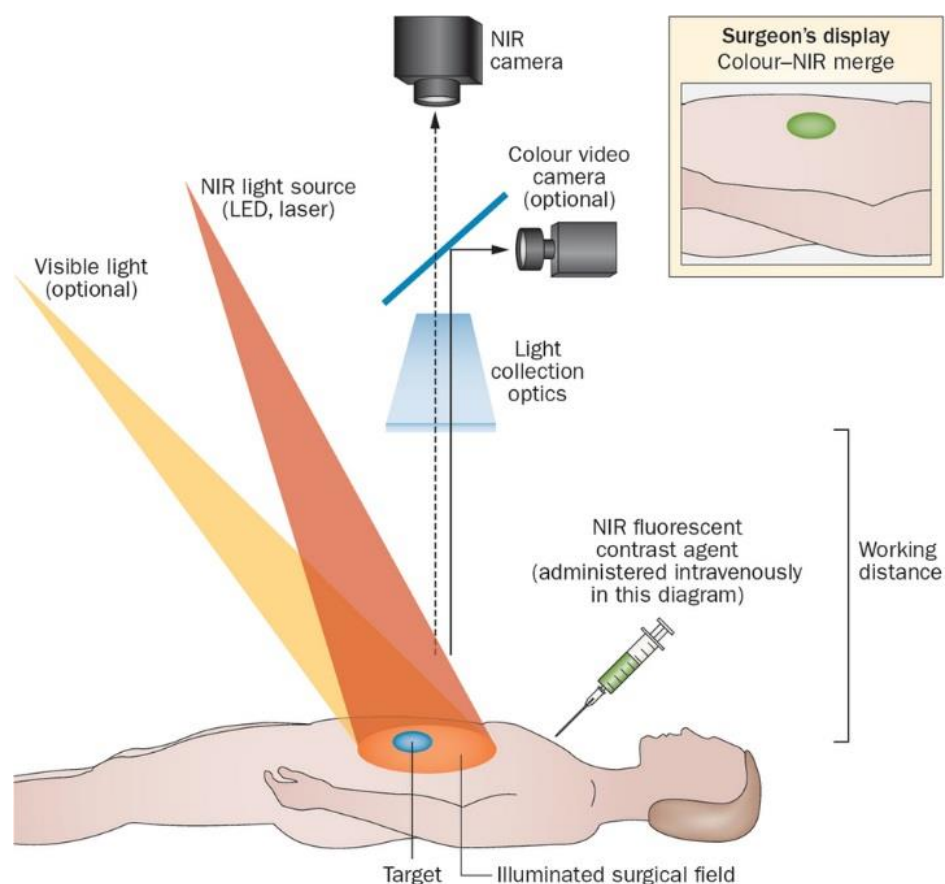
Figure 1.1.5: The surgical illustration of image-guided surgery [54]

With the modifiability of the cyanine dyes, certain substituents can be incorporated to dye scaffold that alters the absorbance, emission and stoke shift. Nagano *et. al* synthesized a two dye system wherein one is pentamethine (A) and the second is heptamethine (B) linked together by a cyclohexanediamine linker Figure 7 [55]. A key distinction between pentamethine and heptamethine cyanine dyes is the wavelength of the absorbance and fluorescence. Commonly pentamethine emission is within the range of heptamethine dye absorbance. Along with the differences in optical properties, the two dye used in this study have substantially different oxidative potential. Once a linked two dye system is synthesized, quenching occurs making the new dye optimal for Förster resonance energy transfer (FRET). FRET is energy transfer that occurs between two absorbing/emitting fluorophores [56-58]. Dyes must be close in proximity so that no fluorescence occurs, and contain one fluorophore that emits light which is then absorbed by the quencher. These two dyes also have widely different oxidative potential which allows for ROS detection. ROS is found in high concentrations in cancerous tissue, which gives these dyes medicinal relevancy [55] [59].

Upon excitation of pentamethine dye A, quenching occurs by heptamethine dye B. Once the two dyes system interacts with ROS, often found diseased (cancerous) area, dye B is cleaved due to it's high oxidative potential, and is no longer able to quench dye A, leading an observable fluorescent signal. The emitting light will only be found in the area with high ROS concentration, such as tumor sites. Although these dyes are not tumor targeting, they can be used for site-specific imaging due to the fact that fluorescence will only be observed at cancerous sites with high ROS concentrations. This process is illustrated in figure 6.
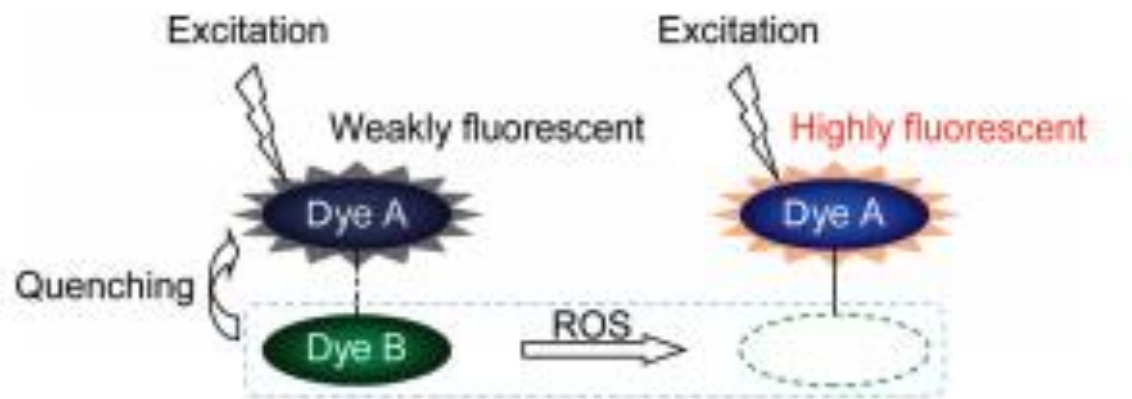
Figure 1.1.6: Representation of FRET and the two dye system [55]
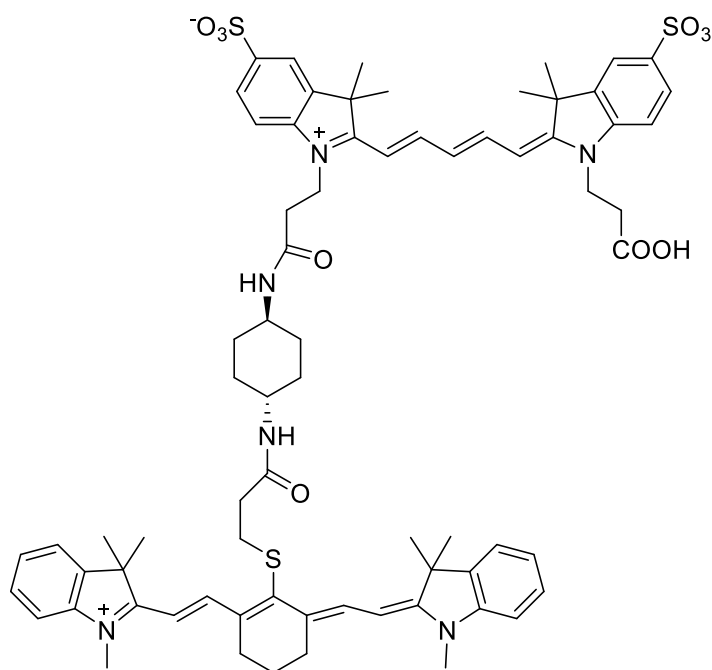
Figure 1.1.7: Dye used in this study [55]

Effective contrast agents must exhibit high contrast and be distinguishable from the endogenous tissue. It is ideal that the emission is specific to the target area and observes an increase in florescence or "turns-on" upon interaction with the desired target. Focusing on some of the key characteristics that differentiate diseased areas versus healthy tissue may enable the intelligent

design of the compound for the desired application. Among the vast number of differences, some inflamed tissue and tumors have a significantly more acidic environment in comparison to healthy tissue. This pH difference offers a condition that can be utilized for imaging [60]. Although numerous pH sensitive dyes have been synthesized, few have been in NIR region which offers a high contrast in comparison to visible range fluorophores. Additionally, the few NIR pH probes have not been used for *in vivo* applications, which is the future aim of this work.

Ohe *et. al* have synthesized ICG derivatives acting as pH probes for *in vivo* application. Incorporating nucleophilic amino-propyl, hydroxyl-propyl, and mercapto-propyl groups allowed for on-off fluorescence based on pH [61]. Compound 1C (figure 8) contained a closed ring structure of the nitrogen atom of the heterocycle, in physiological conditions the ring structure disables emission. Once the nitrogen of the cyclic structure is protonated, going from 1-C to 1-O, the ring is opened and the cyanine dye is then fluorescent. Once the series of dyes was screened, the optimal dye was chosen for testing and in hopes for future *in vivo* application in imaging.
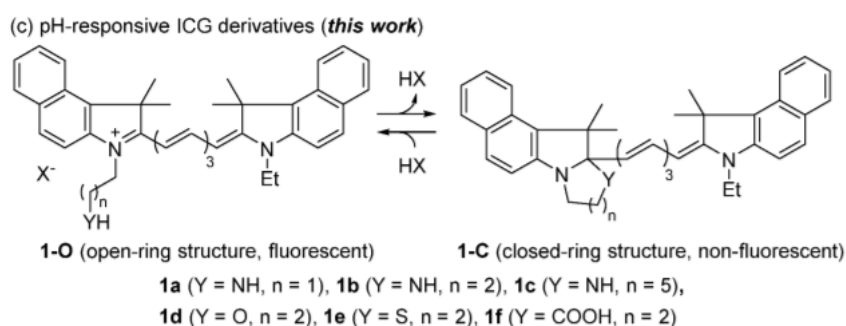
Figure 1.1.8: Dyes used in this study [61]

The recent advancement in imaging relies heavily on imaging diseased areas at a molecular level. Molecular imaging (MI) focuses on imaging at a molecular and cellular level, often utilizing ligands and binding sites of proteins. This mode of targeted imaging allows for more specific results and overcomes some of the limitations current imaging moieties have. Among the various

diseases, cancer is at the forefront of research due to the vast number of people that get the fatal disease. Some statistics show that nearly 1 out 6 deaths are cancer-related.

Although many chemotherapeutics have been studied, cancer is far from being cured and is heavily dependent on surgical resection and early detection for the best possible outcome. Studies have shown that early diagnosis can raise the rate of survival by 25% which can be raised even higher with full surgical resection [62].

Though the surgical processes have shown a great deal of advancement in recent years by the introduction of new technology into the operating room and advanced surgical procedures have been developed, it remains heavily dependent on the surgeon's experience and expertise. In order to better the process and obtain complete resection, contrast agents have been introduced in the surgical field. Among many contrast agents, cyanine dyes have been the most studied due to their superior properties and various modification sites [13].

Large libraries have been synthesized and screened for the medical application of cyanine dyes, most commonly these dyes localize in specific tissues and are used as contrast agents. While a great deal of success has been observed with this technique, another approach entails using more specific ligands for known receptors and attaching them to the dye.

Recent work has been done which synthesized a small library of dyes, tested their optical properties and photostability, and followed by attachment of folate to the dyes. Cancer cells have shown an overexpression of folate receptors at the surface of the cells. The folate receptor allows the dyes to be cancer-specific and can aid in the surgical process. The use of cyanine dyes adds greater contrast due to their NIR emission.

NIR contrast agents have found a great deal of success in the surgical process but are limited by the depth of penetration for NIR light. With an approximate 1 cm depth penetration

these dyes are unable to be used in noninvasive application [63]. Although more optimal NIR contrast agents have been made recently with high quantum yield and molar absorptivity, they remain only useful in surgical applications. However, taking advantage of other relaxation pathways can broaden the application of theses dyes and open a path for the synthesis of new chromophores.

Excited electrons observe various relaxation pathways but often have a dominant pathway. As illustrated in figure 5, laser excitation lead to an electron "jump" into the excited state, which for some dyes lead to vibrational relaxation, inducing thermal expansion which propagates an acoustic signal detectable by acoustic sensors (ultrasound detector) [24, 39, 40]. The incorporation of NIR contrast agents to ultrasound tomography is a new and innovative technique for disease imaging and image-guided surgery. With some promising results currently observed, there remains an unmet need for the understanding of what constitutes as good agents for OAI.

1.3   The application of cyanine dyes as optoacoustic contrast agents

With the many medical advances observed in past decades, among the most important is the various novel methods of screening and imaging. Computed tomography (CT), magnetic resonance imaging (MRI), positron emission tomography (PET), mammography, and ultrasonography are all fairly new imaging methods that have aided in early detection and diagnosis of disease, especially cancer. The chance of survival has been proven to be heavily reliant on the stage of the disease upon detection and diagnosis [62]. Although these imaging modalities have proven to be effective they are limited by their dependence on mass formation which might be far too late. Molecular imaging is often referred to as the future of modern medicine, allowing cancers and other diseases to be detected long before tumors have been formed. Optoacoustic imaging (OAI) has raised a great deal of interest lately, especially upon the

introduction of contrast agents. The contrast agent enhances the quality of the image while the sensing the acoustic signal increases the depth penetration of the contrast agent significantly.

The lack of depth penetration is a detrimental set back to NIR fluorescent imaging modality, limiting the usefulness of these compounds [63]. Optoacoustic imaging utilizes ultrasound detection (fig. 9), allowing for the acoustic signal to be picked up with much greater depth versus its fluorescent single. This mode of imaging enables the dyes to be used in a non-invasive format and applied for non-surgical imaging. Although acoustic signals can be detected without the dyes, it lacks the ability to differentiate healthy versus diseased tissue which is made possible by the introduction of NIR contrast agents. The incorporation of NIR dyes and optoacoustic imaging technology aids in the earlier detection and demonstrates the versatility of NIR dyes. Current literature has found some correlation between signal strength and the number of rotatable bonds [64]. Other characteristics that enhance the optophore include high molar absorptivity and low quantum yield.

Herein, we attempt to introduce a new and innovative application of NIR contrast agents in optoacoustic imaging and provide examples of this application
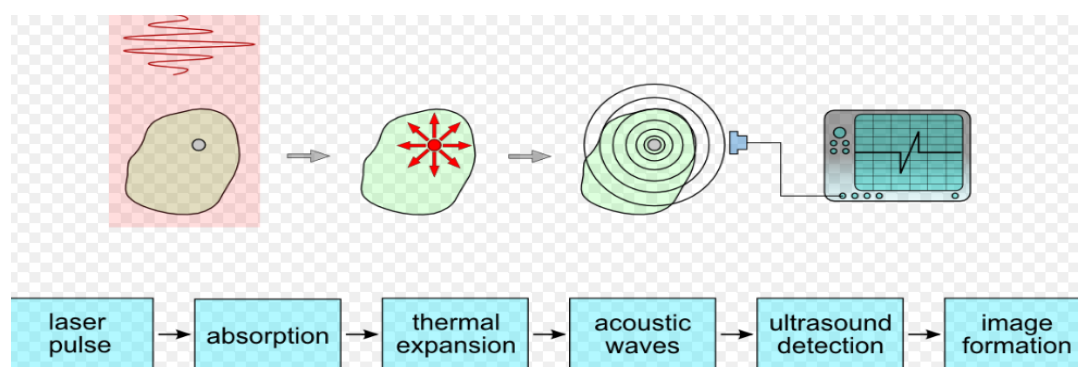
Figure 1.1.9: Depiction of the optoacoustic imaging [65]

Optoacoustic imaging (OAI) combine photosynthesizers and ultrasound tomography providing superior contrast at greater depth. Ultras sound imaging is operational without NIR

contrast agents but can be optimized with the introduction of them. With an immense selection of contrast agents to choose from, NIR contrast agents show great potential due to their low toxicity and the low absorption of endogenous tissue and water in the NIR spectral region. Among NIR dyes, cyanine dyes remain the most useful in biological application.

Although far from optimal due to low molar absorptivity, ICG serves as the gold standard for cyanine dyes, often used a representative compound due to its commercial availability and FDA approval [11]. Several studies were done using OAI with ICG as the contrast agent in mice and found that the NIR contrast agent had a 25% spectral enhancement to spectra observed without the incorporation of the dyes, allowing the targeted area to be better observed and with greater resolution and contrast [66]. Figure 10 illustrates the enhanced image upon the introduction of ICG. Results also indicate that the enhancement was concentration dependent and with varying concentration, the signal intensity differed. The study results depict the spectral differences observed with varying concentrations. In conclusion, the introduction of ICG allows for greater resolution of the OAI image, while OAI allows for greater depth penetration in comparison to the NIR dye's fluorescent signal. This dual benefit shows promising results for the incorporation of cyanine dyes into OAI and leaves an unmet need for a synthesis of optimized derivatives for this particular and useful application.
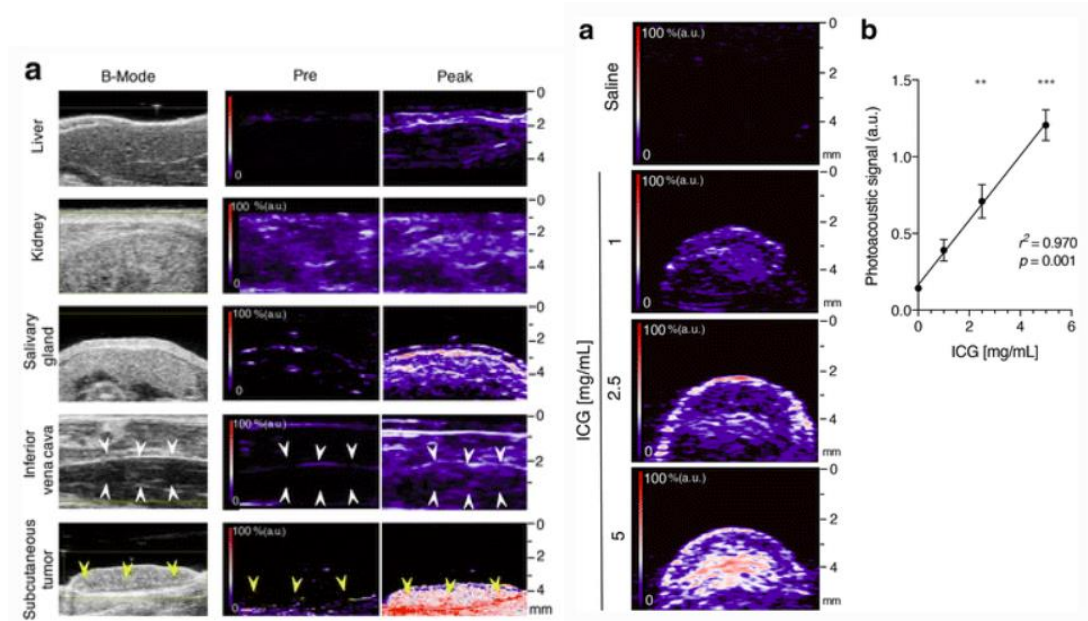
Figure 1.1.10: Imaging data of OAI upon introduction of ICG [66]

What truly determines the optimal contrast agent for OAI remains to be determined as various groups aim to correlate key features of different contrast agents versus the resolution of the OAI signal. By generating a larger library and further screening a wide array of compounds, researchers aim to better understand this new field.

Upon determination and diagnosis of cancers, determining the extent of metastasis is crucial in limiting the disease. Introduction of ICG, adsorbed to gold nanoprobes (AuNR), into the lymphatic system, has been shown to allow the tracking of the cancer tissue [67]. ICG along with other cyanine dyes are limited by their depth pentation, hence why they have shown success in the surgical setting but not as much in pre-surgical imaging. The use of OAI technology enhances the depth penetration and is a feasible option for surgical application due to the fact hospitals already possess the technology necessary; while AuNR increases the acoustic signal by a factor of 2.3.
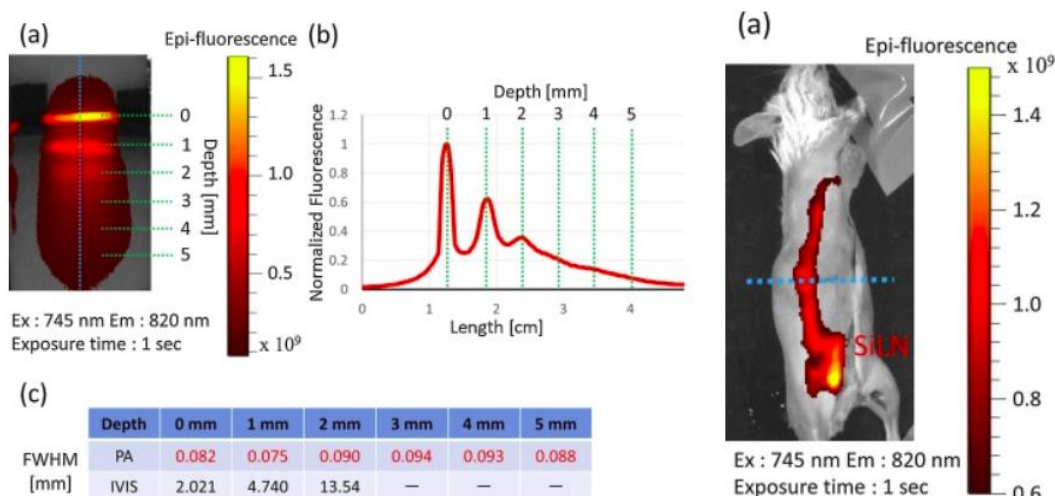
Figure 1.1.11: In-vivo studies of OAI [67]

The ICG was deemed a suitable contrast agent for OAI due to ICG's efficient signal generation and strong absorption in the proper wavelength region (700–1000 nm). The lymph vessels of mice affected by cancer were visualized using ICG and OAI technology. The lymph vessels were clearly visualized with ICG. These results indicate that an OAI with ICG shows promising results in lymph node imaging and cancer tracking for breast cancer metastases.

The vibrational relaxation and thermal expansion observed in OAI can also be utilized in non-imaging methods. Photothermal therapy (PTT) is an innovative therapeutic process that has seen some success in treating cancers and other diseases [30, 34, 37]. NIR contrast agents that do not use fluorescent or intersystem crossing as the dominate relaxation pathway have been used in PTT. NIR laser serves a great deal of purpose due to the high wavelength of light making it both safer, due to low energy light, and increase the depth penetration due to the low absorbance of endogenous tissue in this region. Among their many advantages, cyanine dyes serve a great purpose in this application due to their ability to absorb light in this wavelength. Although high

energy radiation is effective on its own, the introduction of NIR contrast agents allows for a more optimal process that deters the need for high energy laser. Optimistic results have been observed upon the introduction of squaraine cyanine dyes for PTT application and remain to be further investigated and optimized [68] [69-71].

| Cancer diagnosed | Targeted nanogold particles | Homing on the tumer | Laser exposure | Recovery |
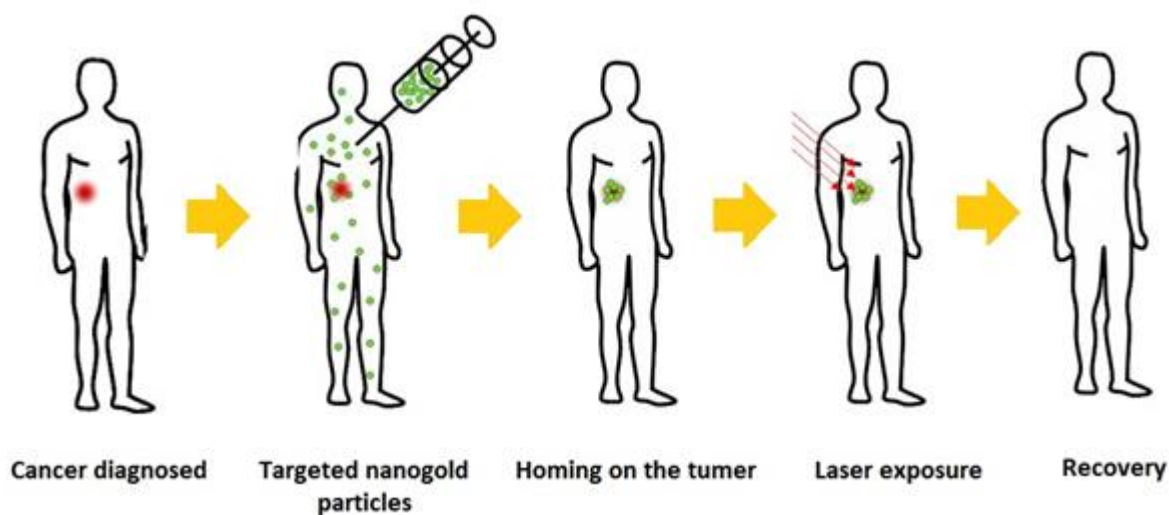
Figure 1.1.12: Photothermal therapy [72]

1.4   The application of cyanine dyes as therapeutic agents

Cyanine dyes have also shown success in other therapeutic applications. Photodynamic therapy (PDT), similar to PTT (fig. 13) in that it uses NIR lasers in killing the diseased cell; however, PDT relies excited electrons interacting with singlet oxygen leading to intersystem crossing of the dye and triplet oxygen formation which is leads the cells to a apoptotic state [30, 42-47].
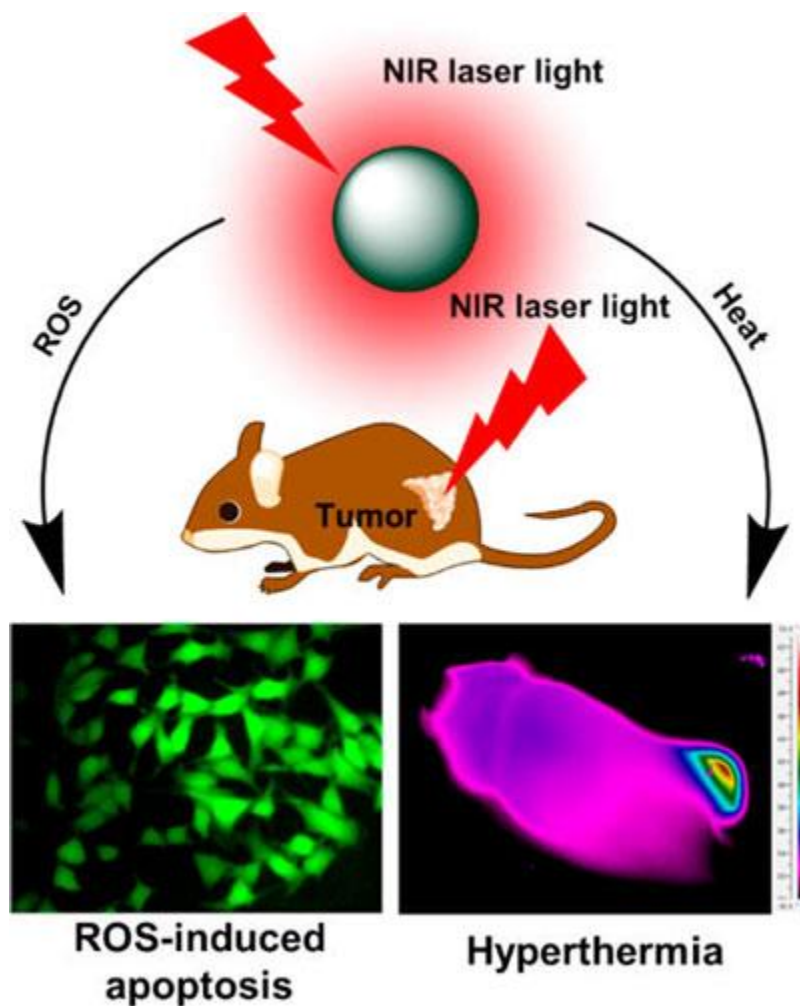
Figure 1.1.13: PDT vs PTT [73]

Photodynamic therapy (PDT) is a cancer treatment method that uses the combination of light and photosensitizers to treat the target area. This process works by utilizing organic molecules that are non-cytotoxic, creating a safer treatment method. With localized radiation using lower energy lights, the treatment method allows for minimal toxicity to the non-diseased area. These compounds, in the presence of molecular oxygen, will have no reaction. Once a light source is introduced, the compound goes into the singlet excited state, undergoes intersystem crossing to the triplet state. The conversation of the photosensitizers to the triplet state transforms triplet oxygen into singlet oxygen which produces reactive oxygen species (ROS). Some ROS includes

singlet oxygen, peroxide, and hydroxide, all of which are toxic to cells. This allows for specificity through targeted irradiation [15, 46, 69]. Preliminary tests may include the introduction of the photosensitizers in the presence of plasmid DNA, then screened for linear and nicked cleavage of the strands, both processes leads to cell death.

Ideal compounds include non- or weakly fluorescent dyes that undergo intersystem crossing. Current agents used in PDT, such as porphyrins and psoralen, have a major setback. Psoralen absorbs in the UV region allowing them to be used only for topical applications. Porphyrins also predominantly absorb in the visible region and also have poor clearance forcing the patient to be out of sunlight for long periods of times [15, 46, 69]. Porphyrins are also plighted by major synthetic troubles, often having difficult purification methods that include a mixture of monomers, dimers, and polymers [74-78]. An alternative was direly needed which lead to the investigation of NIR dyes. Among the various NIR dye family, cyanine dyes showed success in this application.

Although ICG has been fairly successful in an imaging application, various other heptamethine derivatives have been synthesized for the various application mentioned above. Among those derivatives, IR-783 was used in this particular PDT study. Ordinarily quinoline pentamethine dyes have shown a great deal of success in PDT assays; however, the introduction of a single iodine substituent to the 1,2,3,3-tetramethyl-3*H*-indol-1-ium salt using the IR-783 scaffold proved very successful for PDT. The iodine lowered the fluorescent quantum yield significantly and showed the most ROS production. Although the symmetric iodine substituted IR-783 scaffold (containing an iodine substituents on both salts) showed even lower quantum yield it was not as successful in generating ROS, which was concluded using the *in vitro* studies. Upon determining that the optimal dye for PDT was the singly substituted version, *in vivo* studies were

done with BxPC3-Luc mice. Results show that nearly no tumor growth was present for 11 days for mice that received the treatment where a 500% growth was observed for those mice that did not receive any treatment [79].
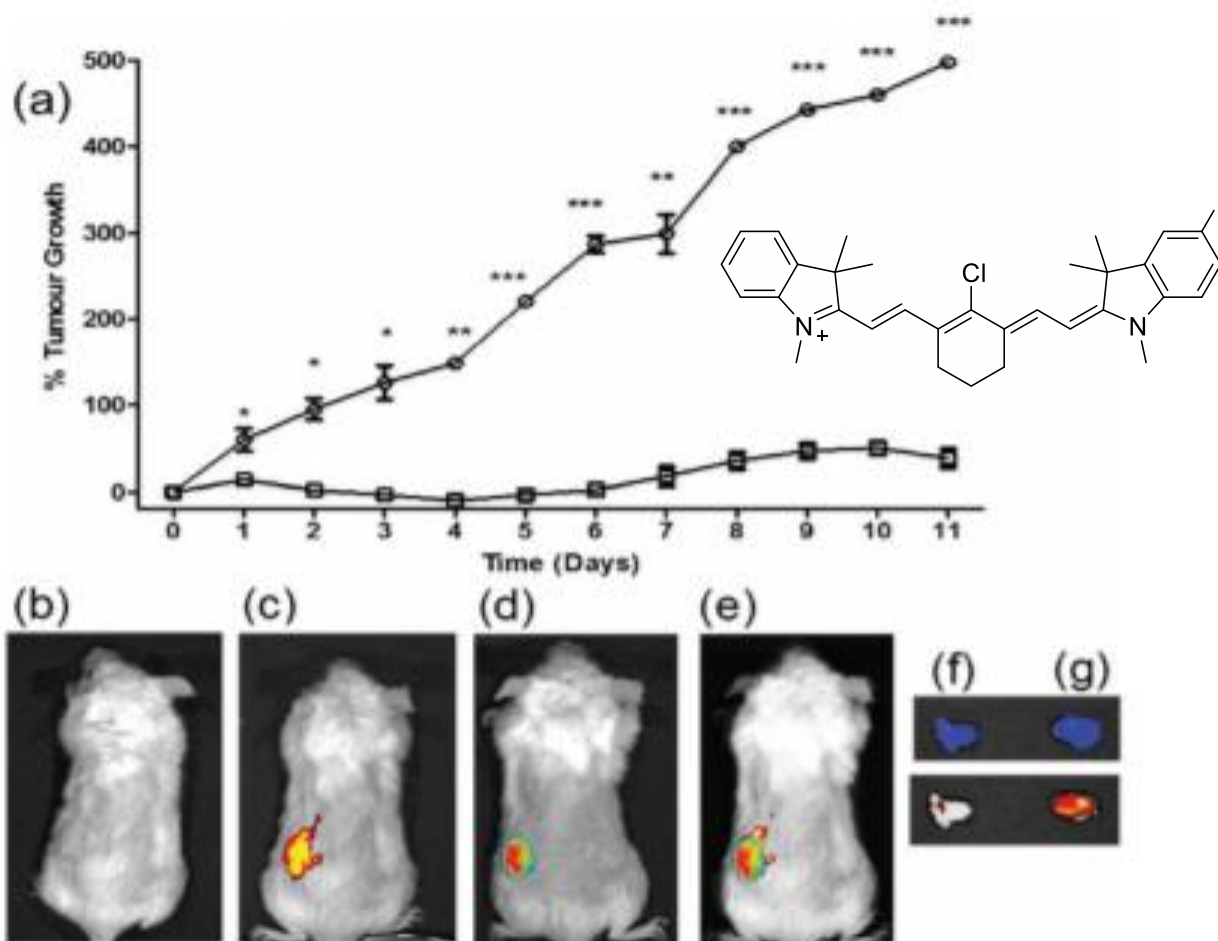
Figure 1.1.14: Results and dye structure used [79]

Photodynamic therapy (PDT) has been widely studied in the past decade but is still limited by the non-optimal photosynthesizing agents. Often these agents are not water soluble, have low molar absorptivity, low ROS generation capabilities, are unconjugatable, and have dark toxicity. Large libraries have been screened and found that IR-780 showed promising results. IR-780 is a

known mitochondrial targeting agent which is ideal due to the large abundance of oxygen in this organelle, negating the issue of hypoxia [80]. IR-780, although somewhat successful, lacks water solubility and has unselective dark toxicity [81]. Using the IR-780 scaffold for its mitochondrial targeting, while decorating it with different substituents in order to optimize the negative qualities allows for synthesis for an ideal PDT agent.

In order to overcome the water solubility issue, alkylating agents containing pyridine were incorporated into the IR-780 scaffold. This enhanced both the water solubility and simultaneously the mitochondrial targeting ability. Along with the enhanced physical properties, the charged molecule allows for the incorporation hyaluronic acid (HA), a known cancer-specific drug carrying ligand. HA is highly selective to CD44 binding sites, which is overexpressed in cancer cells, this combines cancer specificity to newly enhanced physical properties of IR-780 dye [82] [83] [84].

Upon synthesis of the HA-IR-Pyr dye, *in vitro* and *in vivo* studies were done to conclude if the new substituents added to the IR-780 scaffold proved to be successful for PDT application or significantly altered the dye's properties limiting its effectivity in the application. First cell assays were prepared in a competitive study using cancerous cells versus non-cancerous cells, in order to determine the selectivity [82] [83].

Next cancerous cell assays were prepared with HA-IR-Pyr and received irradiation. The cells were surveyed using flow cytometry in order to determine the magnitude of apoptosis. Figure 15 (illustrating the flow cytometry data) indicated that cells with HA-IR-pyr (no laser) had no occurrence of apoptosis but after 3 minutes of irradiation a great deal cell death occurred [84] [82]. Concluding that the dye complex has negligible dark toxicity and significant toxicity upon irradiation.
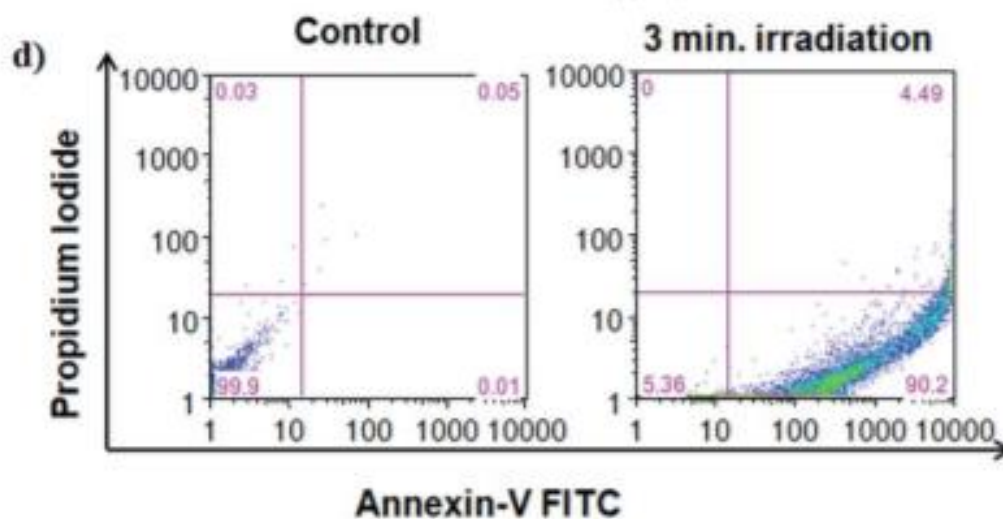
Figure 1.1.15: Flow cytometry results of the study [84]

Following the *in vitro* study, mouse studies were done, using mice SCC7 cancerous cell line. The dye was injected into the mice followed by laser irradiation of the diseased region, and the tumors were then resected to observe levels growth suppression. Figure 16 depicts the effectivity of irradiation plus HA-IR-Pyr dye in comparison to multiple controls (PBS, light, HA-IR-Pyr without light) [84]. As illustrated the tumor, in comparison with PBS treated control, saw a great deal of shrinkage in with irradiated HA-IR-Pyr, while very limited shrinkage using the dye alone (negligible dark toxicity) and with just light alone [84]. Concluding that the modifiability of these dyes allows for various incorporation of substituents for optimization allowing for the synthesis of the ideal agent for the desired use [84] [83].
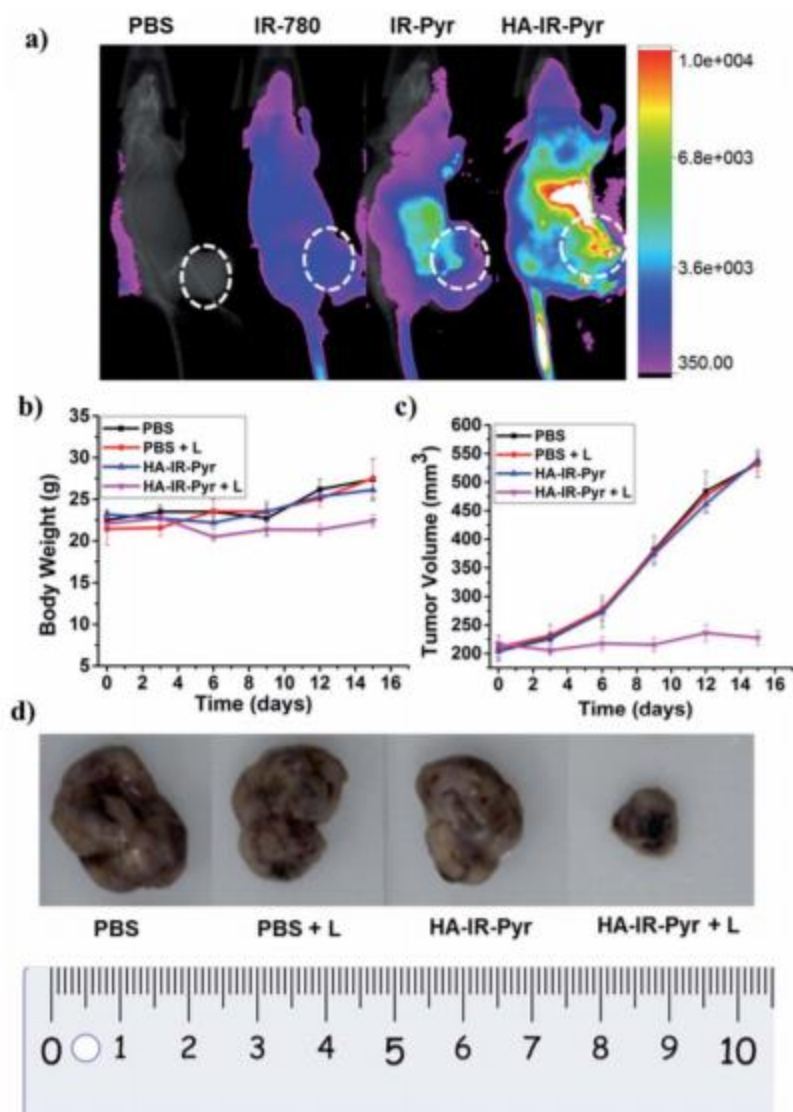
Figure 1.1.16: In-vivo results of the study [84]

1.5   Conclusion

With the extensive work done with cyanine dyes since their discovery, these dyes continue to find utility in innovative fields. Although the predominant research remains focused on the introduction of these NIR contrast agents in image-guided surgery, their alternative uses are highlighted in this review. These dyes, due to their versatility and numerous points of modifications have found success as fluorophores, optaphores, and as therapeutic agents. As their research continues to grow these dyes will continue to be optimized for their respective application.

1.6 **References**

1. Hyun, H.; Owens, E. A.; Wada, H.; Levitz, A.; Park, G.; Park, M. H.; Frangioni, J. V.; Henary, M.; Choi, H. S., Cartilage-Specific Near-Infrared Fluorophores for Biomedical Imaging. *Angew Chem Int Ed Engl* **2015,** 54, (30), 8648-52.
2. Choi, H. S.; Gibbs, S. L.; Lee, J. H.; Kim, S. H.; Ashitate, Y.; Liu, F.; Hyun, H.; Park, G.; Xie, Y.; Bae, S.; Henary, M.; Frangioni, J. V., Targeted zwitterionic near-infrared fluorophores for improved optical imaging. *Nat Biotechnol* **2013,** 31, (2), 148-53.
3. Ye, Y.; Akers, W.; Xu, B.; Bloch, S.; Odonkor, C.; Achilefu, S., Near-infrared fluorescent divalent RGD ligand for integrin alphavbeta(3)-targeted optical imaging. *Bioorg Med Chem Lett* **2012,** 22, (17), 5405-9.
4. Cheng-Lun Tsai*, J.-C. C., Wen-Jwu Wang1, Near-infrared Absorption Property of Biological Soft Tissue Constituents *Journal of Medical and Biological Engineering* **2001,** 21, (1), 7-14.
5. Pu, S.; Nakagome, K.; Yamada, T.; Ikezawa, S.; Itakura, M.; Satake, T.; Ishida, H.; Nagata, I.; Mogami, T.; Kaneko, K., A pilot study on the effects of cognitive remediation on hemodynamic responses in the prefrontal cortices of patients with schizophrenia: a multi-channel near-infrared spectroscopy study. *Schizophr Res* **2014,** 153, (1-3), 87-95.
6. Hilderbrand, S. A.; Weissleder, R., Near-infrared fluorescence: application to in vivo molecular imaging. *Curr Opin Chem Biol* **2010,** 14, (1), 71-9.
7. Sitaram, R.; Zhang, H.; Guan, C.; Thulasidas, M.; Hoshi, Y.; Ishikawa, A.; Shimizu, K.; Birbaumer, N., Temporal classification of multichannel near-infrared spectroscopy signals of motor imagery for developing a brain-computer interface. *Neuroimage* **2007,** 34, (4), 1416-27.
8. Joshi, B. P.; Wang, T. D., Exogenous Molecular Probes for Targeted Imaging in Cancer: Focus on Multi-modal Imaging. *Cancers (Basel)* **2010,** 2, (2), 1251-87.
9. Dermatology, I. t. f., Rapini Ronald P Jorizzo Joseph L Bolognia Jean L.
10. Mishra, A.; Behera, R. K.; Behera, P. K.; Mishra, B. K.; Behera, G. B., Cyanines during the 1990s: A Review. *Chem Rev* **2000,** 100, (6), 1973-2012.
11. FDA Drug Approval information. https://www.accessdata.fda.gov/scripts/cder/daf/index.cfm?event=overview.process&ApplNo=011525 (October 2017),
12. Oswald, B.; Patsenker, L.; Duschl, J.; Szmacinski, H.; Wolfbeis, O. S.; Terpetschnig, E., Synthesis, spectral properties, and detection limits of reactive squaraine dyes, a new class of diode laser compatible fluorescent protein labels. *Bioconjug Chem* **1999,** 10, (6), 925-31.
13. Levitz, A.; Marmarchi, F.; Henary, M., Synthesis and Optical Properties of Near-Infrared meso-Phenyl-Substituted Symmetric Heptamethine Cyanine Dyes. *Molecules* **2018,** 23, (2).
14. Lin, Y.; Weissleder, R.; Tung, C. H., Novel near-infrared cyanine fluorochromes: synthesis, properties, and bioconjugation. *Bioconjug Chem* **2002,** 13, (3), 605-10.
15. Yang, H. M.; Park, C. W.; Park, S.; Kim, J. D., Cross-linked magnetic nanoparticles with a biocompatible amide bond for cancer-targeted dual optical/magnetic resonance imaging. *Colloids Surf B Biointerfaces* **2018,** 161, 183-191.
16. Uno, K.; Sasaki, T.; Sugimoto, N.; Ito, H.; Nishihara, T.; Hagihara, S.; Higashiyama, T.; Sasaki, N.; Sato, Y.; Itami, K., Key Structural Elements of Unsymmetrical Cyanine Dyes for Highly Sensitive Fluorescence Turn-On DNA Probes. *Chem Asian J* **2017,** 12, (2), 233-238.
17. Tan, X.; Luo, S.; Long, L.; Wang, Y.; Wang, D.; Fang, S.; Ouyang, Q.; Su, Y.; Cheng, T.; Shi, C., Structure-Guided Design and Synthesis of a Mitochondria-Targeting Near-Infrared Fluorophore with Multimodal Therapeutic Activities. *Adv Mater* **2017,** 29, (43).
18. Sun, H.; Jin, X.; Long, N.; Zhang, R., Improved biodegradation of synthetic azo dye by horseradish peroxidase cross-linked on nano-composite support. *Int J Biol Macromol* **2017,** 95, 1049-1055.

19.   Konig, S. G.; Kramer, R., Accessing Structurally Diverse Near-Infrared Cyanine Dyes for Folate Receptor-Targeted Cancer Cell Staining. *Chemistry* **2017,** 23, (39), 9306-9312.

20.   Gbahou, F.; Cecon, E.; Viault, G.; Gerbier, R.; Jean-Alphonse, F.; Karamitri, A.; Guillaumet, G.; Delagrange, P.; Friedlander, R. M.; Vilardaga, J. P.; Suzenet, F.; Jockers, R., Design and validation of the first cell-impermeant melatonin receptor agonist. *Br J Pharmacol* **2017,** 174, (14), 2409-2421.

21.   Hunault, M.; Lelong, G.; Gauthier, M.; Gelebart, F.; Ismael, S.; Galoisy, L.; Bauchau, F.; Loisel, C.; Calas, G., Assessment of Transition Element Speciation in Glasses Using a Portable Transmission Ultraviolet-Visible-Near-Infrared (UV-Vis-NIR) Spectrometer. *Appl Spectrosc* **2016,** 70, (5), 778-84.

22.   Del Valle, J. C.; Diaz-Oliva, C., Steady-State Spectroscopy of the 2-(N-methylacetimidoyl)-1-naphthol Molecule. *Photochem Photobiol* **2015,** 91, (3), 660-71.

23.   Dixon, I. M.; Boissard, G.; Whyte, H.; Alary, F.; Heully, J. L., Computational Estimate of the Photophysical Capabilities of Four Series of Organometallic Iron(II) Complexes. *Inorg Chem* **2016,** 55, (11), 5089-91.

24.   Leen, V.; Laine, M.; Ngongo, J. M.; Lipkowski, P.; Verbelen, B.; Kochel, A.; Dehaen, W.; Van der Auweraer, M.; Nadtochenko, V.; Filarowski, A., Impact of the Keto-Enol Tautomeric Equilibrium on the BODIPY Chromophore. *J Phys Chem A* **2018,** 122, (28), 5955-5961.

25.   Thyrhaug, E.; Sorensen, T. J.; Gryczynski, I.; Gryczynski, Z.; Laursen, B. W., Polarization and symmetry of electronic transitions in long fluorescence lifetime triangulenium dyes. *J Phys Chem A* **2013,** 117, (10), 2160-8.

26.   diagram", I. T. f. Q. J.

27.   An, H. W.; Qiao, S. L.; Hou, C. Y.; Lin, Y. X.; Li, L. L.; Xie, H. Y.; Wang, Y.; Wang, L.; Wang, H., Self-assembled NIR nanovesicles for long-term photoacoustic imaging in vivo. *Chem Commun (Camb)* **2015,** 51, (70), 13488-91.

28.   Bai, L. Y.; Yang, X. Q.; An, J.; Zhang, L.; Zhao, K.; Qin, M. Y.; Fang, B. Y.; Li, C.; Xuan, Y.; Zhang, X. S.; Zhao, Y. D.; Ma, Z. Y., Multifunctional magnetic-hollow gold nanospheres for bimodal cancer cell imaging and photothermal therapy. *Nanotechnology* **2015,** 26, (31), 315701.

29.   Guberman-Pfeffer, M. J.; Greco, J. A.; Samankumara, L. P.; Zeller, M.; Birge, R. R.; Gascon, J. A.; Bruckner, C., Bacteriochlorins with a Twist: Discovery of a Unique Mechanism to Red-Shift the Optical Spectra of Bacteriochlorins. *J Am Chem Soc* **2017,** 139, (1), 548-560.

30.   Hou, L.; Shan, X.; Hao, L.; Feng, Q.; Zhang, Z., Copper sulfide nanoparticle-based localized drug delivery system as an effective cancer synergistic treatment and theranostic platform. *Acta Biomater* **2017,** 54, 307-320.

31.   Mallidi, S.; Larson, T.; Tam, J.; Joshi, P. P.; Karpiouk, A.; Sokolov, K.; Emelianov, S., Multiwavelength photoacoustic imaging and plasmon resonance coupling of gold nanoparticles for selective detection of cancer. *Nano Lett* **2009,** 9, (8), 2825-31.

32.   Patel, M. A.; Yang, H.; Chiu, P. L.; Mastrogiovanni, D. D.; Flach, C. R.; Savaram, K.; Gomez, L.; Hemnarine, A.; Mendelsohn, R.; Garfunkel, E.; Jiang, H.; He, H., Direct production of graphene nanosheets for near infrared photoacoustic imaging. *ACS Nano* **2013,** 7, (9), 8147-57.

33.   Wang, B.; Su, J. L.; Amirian, J.; Litovsky, S. H.; Smalling, R.; Emelianov, S., Detection of lipid in atherosclerotic vessels using ultrasound-guided spectroscopic intravascular photoacoustic imaging. *Opt Express* **2010,** 18, (5), 4889-97.

34.   Yang, Z.; Tian, R.; Wu, J.; Fan, Q.; Yung, B. C.; Niu, G.; Jacobson, O.; Wang, Z.; Liu, G.; Yu, G.; Huang, W.; Song, J.; Chen, X., Impact of Semiconducting Perylene Diimide Nanoparticle Size on Lymph Node Mapping and Cancer Imaging. *ACS Nano* **2017,** 11, (4), 4247-4255.

35.   Yasun, E.; Kang, H.; Erdal, H.; Cansiz, S.; Ocsoy, I.; Huang, Y. F.; Tan, W., Cancer cell sensing and therapy using affinity tag-conjugated gold nanorods. *Interface Focus* **2013,** 3, (3), 20130006.

36. Yu, J.; Yin, W.; Zheng, X.; Tian, G.; Zhang, X.; Bao, T.; Dong, X.; Wang, Z.; Gu, Z.; Ma, X.; Zhao, Y., Smart MoS2/Fe3O4 Nanotheranostic for Magnetically Targeted Photothermal Therapy Guided by Magnetic Resonance/Photoacoustic Imaging. *Theranostics* **2015,** 5, (9), 931-45.

37. Zhang, S.; Huang, Q.; Zhang, L.; Zhang, H.; Han, Y.; Sun, Q.; Cheng, Z.; Qin, H.; Dou, S.; Li, Z., Vacancy engineering of Cu2-xSe nanoparticles with tunable LSPR and magnetism for dual-modal imaging guided photothermal therapy of cancer. *Nanoscale* **2018,** 10, (7), 3130-3143.

38. He, H.; Prakash, J.; Buehler, A.; Ntziachristos, V., Optoacoustic Tomography Using Accelerated Sparse Recovery and Coherence Factor Weighting. *Tomography* **2016,** 2, (2), 138-145.

39. Dean-Ben, X. L.; Razansky, D., Optoacoustic signal excitation with a tone-burst of short pulses. *Photoacoustics* **2018,** 11, 1-5.

40. Abeyakoon, O.; Morscher, S.; Dalhaus, N.; Ford, S. J.; Mendichovszky, I. A.; Manavaki, R.; Wallis, M.; Moyle, P.; Woitek, R.; Patterson, A.; Torheim, T.; Joseph, J.; Gonzalez, I. Q.; Bohndiek, S.; Gilbert, F. J., Optoacoustic Imaging Detects Hormone-Related Physiological Changes of Breast Parenchyma. *Ultraschall Med* **2018**.

41. Trachootham, D.; Alexandre, J.; Huang, P., Targeting cancer cells by ROS-mediated mechanisms: a radical therapeutic approach? *Nat Rev Drug Discov* **2009,** 8, (7), 579-91.

42. Jajarm, H. H.; Asadi, R.; Bardideh, E.; Shafaee, H.; Khazaei, Y.; Emadzadeh, M., The effects of photodynamic and low-level laser therapy for treatment of oral lichen planus-A systematic review and meta-analysis. *Photodiagnosis Photodyn Ther* **2018**.

43. Yu, X.; Zheng, H.; Chan, M. T. V.; Wu, W. K. K., Immune consequences induced by photodynamic therapy in non-melanoma skin cancers: a review. *Environ Sci Pollut Res Int* **2018,** 25, (21), 20569-20574.

44. Davoudi, A.; Ebadian, B.; Nosouhian, S., Role of laser or photodynamic therapy in treatment of denture stomatitis: A systematic review. *J Prosthet Dent* **2018**.

45. Seyed Jafari, S. M.; Cazzaniga, S.; Hunger, R. E., Photodynamic therapy as an alternative treatment for mycosis fungoides: a systemic review and meta-analysis. *G Ital Dermatol Venereol* **2018**.

46. Grandi, V.; Sessa, M.; Pisano, L.; Rossi, R.; Galvan, A.; Gattai, R.; Mori, M.; Tiradritti, L.; Bacci, S.; Zuccati, G.; Cappugi, P.; Pimpinelli, N., Photodynamic therapy with topical photosensitizers in mucosal and semimucosal areas: review from a dermatologic perspective. *Photodiagnosis Photodyn Ther* **2018**.

47. Liu, J.; Xue, P.; Deng, J., Therapeutic effect of photodynamic therapy for nonresectable cholangiocarcinoma: Protocol for a meta-analysis and systematic review. *Medicine (Baltimore)* **2018,** 97, (8), e9863.

48. Buckle, T.; van Willigen, D. M.; Spa, S. J.; Hensbergen, A. W.; van der Wal, S.; de Korne, C. M.; Welling, M. M.; van der Poel, H. G.; Hardwick, J. C. H.; van Leeuwen, F. W. B., Tracers for Fluorescence-Guided Surgery: How Elongation of the Polymethine Chain in Cyanine Dyes Alters the Pharmacokinetics of a Dual-Modality c[RGDyK] Tracer. *J Nucl Med* **2018,** 59, (6), 986-992.

49. Owens, E. A.; Hyun, H.; Dost, T. L.; Lee, J. H.; Park, G.; Pham, D. H.; Park, M. H.; Choi, H. S.; Henary, M., Near-Infrared Illumination of Native Tissues for Image-Guided Surgery. *J Med Chem* **2016,** 59, (11), 5311-23.

50. Deng, H.; Wang, H.; Wang, M.; Li, Z.; Wu, Z., Synthesis and Evaluation of 64Cu-DOTA-NT-Cy5.5 as a Dual-Modality PET/Fluorescence Probe to Image Neurotensin Receptor-Positive Tumor. *Mol Pharm* **2015,** 12, (8), 3054-61.

51. Tan, M.; Ye, Z.; Lindner, D.; Brady-Kalnay, S. M.; Lu, Z. R., Synthesis and evaluation of a targeted nanoglobular dual-modal imaging agent for MR imaging and image-guided surgery of prostate cancer. *Pharm Res* **2014,** 31, (6), 1469-76.

52.   Fernandez-Fernandez, A.; Manchanda, R.; Carvajal, D. A.; Lei, T.; Srinivasan, S.; McGoron, A. J., Covalent IR820-PEG-diamine nanoconjugates for theranostic applications in cancer. *Int J Nanomedicine* **2014,** 9, 4631-48.

53.   Liu, S.; Li, D.; Huang, C. W.; Yap, L. P.; Park, R.; Shan, H.; Li, Z.; Conti, P. S., Efficient construction of PET/fluorescence probe based on sarcophagine cage: an opportunity to integrate diagnosis with treatment. *Mol Imaging Biol* **2012,** 14, (6), 718-24.

54.   Frangioni, J. V., Image taken from: The John V. Frangioni Lab.

55.   Oushiki, D.; Kojima, H.; Terai, T.; Arita, M.; Hanaoka, K.; Urano, Y.; Nagano, T., Development and application of a near-infrared fluorescence probe for oxidative stress based on differential reactivity of linked cyanine dyes. *J Am Chem Soc* **2010,** 132, (8), 2795-801.

56.   Sekar, R. B.; Periasamy, A., Fluorescence resonance energy transfer (FRET) microscopy imaging of live cell protein localizations. *J Cell Biol* **2003,** 160, (5), 629-33.

57.   Ni, Z.; Mark, M. E.; Cai, X.; Mao, Q., Fluorescence resonance energy transfer (FRET) analysis demonstrates dimer/oligomer formation of the human breast cancer resistance protein (BCRP/ABCG2) in intact cells. *Int J Biochem Mol Biol* **2010,** 1, (1), 1-11.

58.   Wang, C.; Weiss, E. A., Accelerating FRET between Near-Infrared Emitting Quantum Dots Using a Molecular J-Aggregate as an Exciton Bridge. *Nano Lett* **2017,** 17, (9), 5666-5671.

59.   Storz, G.-Y. L. a. P., Reactive oxygen species in cancer. *NIH Public Access* **2014,** 44, (5).

60.   Zhang, X.; Lin, Y.; Gillies, R. J., Tumor pH and its measurement. *J Nucl Med* **2010,** 51, (8), 1167-70.

61.   Miki, K.; Kojima, K.; Oride, K.; Harada, H.; Morinibu, A.; Ohe, K., pH-Responsive near-infrared fluorescent cyanine dyes for molecular imaging based on pH sensing. *Chem Commun (Camb)* **2017,** 53, (55), 7792-7795.

62.   Statics by: National Cancer Institute (NCI) | National Institutes of Health (NIH)

63.   Roy, R.; Godavarty, A.; Sevick-Muraca, E. M., Fluorescence-enhanced three-dimensional lifetime imaging: a phantom study. *Phys Med Biol* **2007,** 52, (14), 4155-70.

64.   Liu, X.; Li, M.; Liu, M.; Yang, Q.; Chen, Y., From Tetraphenylfurans to Ring-Opening (Z)-1,4-Enediones: ACQ Fluorophores versus AIEgens with Distinct Responses to Mechanical Force and Light. *Chemistry* **2018**.

65.   Johnson, J., Global Photoacoustic Imaging Market Developments and Forecast 2018-2025. *TOP News Corner* **2018**.

66.   Okumura, K.; Yoshida, K.; Yoshioka, K.; Aki, S.; Yoneda, N.; Inoue, D.; Kitao, A.; Ogi, T.; Kozaka, K.; Minami, T.; Koda, W.; Kobayashi, S.; Takuwa, Y.; Gabata, T., Photoacoustic imaging of tumour vascular permeability with indocyanine green in a mouse model. *Eur Radiol Exp* **2018,** 2, (1), 5.

67.   Nagaoka, R.; Tabata, T.; Yoshizawa, S.; Umemura, S. I.; Saijo, Y., Visualization of murine lymph vessels using photoacoustic imaging with contrast agents. *Photoacoustics* **2018,** 9, 39-48.

68.   Gao, F. P.; Lin, Y. X.; Li, L. L.; Liu, Y.; Mayerhoffer, U.; Spenst, P.; Su, J. G.; Li, J. Y.; Wurthner, F.; Wang, H., Supramolecular adducts of squaraine and protein for noninvasive tumor imaging and photothermal therapy in vivo. *Biomaterials* **2014,** 35, (3), 1004-14.

69.   Zhou, Y. Q.; Liu, D. Q.; Chen, S. P.; Sun, J.; Zhou, X. R.; Rittner, H.; Mei, W.; Tian, Y. K.; Zhang, H. X.; Chen, F.; Ye, D. W., Reactive oxygen species scavengers ameliorate mechanical allodynia in a rat model of cancer-induced bone pain. *Redox Biol* **2018,** 14, 391-397.

70.   Zhou, Y. Q.; Liu, D. Q.; Chen, S. P.; Sun, J.; Zhou, X. R.; Rittner, H.; Mei, W.; Tian, Y. K.; Zhang, H. X.; Chen, F.; Ye, D. W., Corrigendum to "Reactive oxygen species scavengers ameliorate mechanical allodynia in a rat model of cancer-induced bone pain" [REDOX 14 (2017) 391-397]. *Redox Biol* **2018**.

71.   Zhang, C.; Bourgeade Delmas, S.; Fernandez Alvarez, A.; Valentin, A.; Hemmert, C.; Gornitzka, H., Synthesis, characterization, and antileishmanial activity of neutral N-heterocyclic carbenes gold(I) complexes. *Eur J Med Chem* **2018,** 143, 1635-1643.

72.   LLC, N., Photothermal Therapy *Gold Nanoparticles Cancer Treatment Blog* **2015-2018**.

73.   Berger, M., Plasmonic nanocrystals for combined photothermal and photodynamic cancer therapies. *Nano Werk* **2015**.

74.   O'Connor, A. E.; Gallagher, W. M.; Byrne, A. T., Porphyrin and nonporphyrin photosensitizers in oncology: preclinical and clinical advances in photodynamic therapy. *Photochem Photobiol* **2009,** 85, (5), 1053-74.

75.   Ryan Dosselli†, M. G., Erika Bolognini‡, Sandro Campestrini‡ and Elena Reddi*†, Porphyrin–Apidaecin Conjugate as a New Broad Spectrum Antibacterial Agent. *ACS Med. Chem. Lett.* **2010,** 1, (1), 35-38.

76.   Charara, M.; Tovmasyan, A.; Batinic-Haberle, I.; Craik, J.; Benov, L., Post-illumination cellular effects of photodynamic treatment. *PLoS One* **2017,** 12, (12), e0188535.

77.   Pushpan, S. K.; Venkatraman, S.; Anand, V. G.; Sankar, J.; Parmeswaran, D.; Ganesan, S.; Chandrashekar, T. K., Porphyrins in photodynamic therapy - a search for ideal photosensitizers. *Curr Med Chem Anticancer Agents* **2002,** 2, (2), 187-207.

78.   Bonnett, R., Photosensitizers of the Porphyrin and Phthalocyanine Series for Photodynamic Therapy. *Royal Society of Chemistry* **1995,** Chemical Society Reviews, (24).

79.   Atchison, J.; Kamila, S.; Nesbitt, H.; Logan, K. A.; Nicholas, D. M.; Fowley, C.; Davis, J.; Callan, B.; McHale, A. P.; Callan, J. F., Iodinated cyanine dyes: a new class of sensitisers for use in NIR activated photodynamic therapy (PDT). *Chem Commun (Camb)* **2017,** 53, (12), 2009-2012.

80.   Fang Guo, a. M. Y., a Jinping Wang,a Fengping Tan*a and Nan Li*a The mitochondria-targeted and IR780-regulated theranosomes for imaging and enhanced photodynamic/photothermal therapy *Royal Society of Chemistry* **2016,** RCS Advances, (14).

81.   Wang, K.; Zhang, Y.; Wang, J.; Yuan, A.; Sun, M.; Wu, J.; Hu, Y., Self-assembled IR780-loaded transferrin nanoparticles as an imaging, targeting and PDT/PTT agent for cancer therapy. *Sci Rep* **2016,** 6, 27421.

82.   Uthaman, S.; Mathew, A. P.; Park, H. J.; Lee, B. I.; Kim, H. S.; Huh, K. M.; Park, I. K., IR 780-loaded hyaluronic acid micelles for enhanced tumor-targeted photothermal therapy. *Carbohydr Polym* **2018,** 181, 1-9.

83.   Bhattacharya, D.; Svechkarev, D.; Souchek, J. J.; Hill, T. K.; Taylor, M. A.; Natarajan, A.; Mohs, A. M., Impact of structurally modifying hyaluronic acid on CD44 interaction. *J Mater Chem B* **2017,** 5, (41), 8183-8192.

84.   Thomas, A. P.; Palanikumar, L.; Jeena, M. T.; Kim, K.; Ryu, J. H., Cancer-mitochondria-targeted photodynamic therapy with supramolecular assembly of HA and a water soluble NIR cyanine dye. *Chem Sci* **2017,** 8, (12), 8351-8356.

2   SYNTHESIS AND OPTICAL PROPERTIES OF NEAR-INFRARED MESO-PHENYL SUBSTITUTED SYMMETRIC HEPTAMETHINE CYANINE DYES

Various cyanine dyes have been synthesized and large libraries have been generated; however, one point of modification that has not been thoroughly utilized or procedurally optimized is the *meso* carbon (central carbon) of heptamtehine dyes. Previous dyes made included a *meso*-chlorine atom which then substituted, this proved a difficult and inefficient procedure. The compounds synthesized in this publication incorporated carbon-based substituents which were introduced prior to the synthesis of the dye. This proved a more efficient method.

The introduction of the *meso*-phenyl substituent was aimed to increase the hydrophobicity of heptamethine dyes for human serum albumin (HSA). HSA is the most abundant blood protein, containing four hydrophobic binding pockets. This protein plays key roles in carrying various compounds throughout the body. The Henary lab previously synthesized various cyanine dyes with varying levels of hydrophobicity to further study HSA. Among the various dyes, the research did not include heptamethine dye which observes superior optical properties. The aim of this project was to enhance the synthetic process of the incorporation of carbon bases substituents pre-dye synthesis along with better-understanding HSA bonding beyond hydrophobicity.

This chapter was adapted from the following publication: Synthesis and Optical Properties of Near-Infrared *meso*-Phenyl-Substituted Symmetric Heptamethine Cyanine Dyes. Invited manuscript. This article belongs to the Special Issue of Heterocycles. [‡] Co-First authors. My contributions to the manuscript consisted of the synthetic, in silico and spectroscopic

experiments, analysis, figure and manuscript preparation and frequent discussions concerning the project.

2.1 Abstract

Heptamethine cyanine dyes are a class of near-infrared fluorescence (NIRF) probes are of great interest in bioanalytical and imaging applications due to their modifiability, allowing them to be tailored for particular applications. Generally, modifications at the *meso*-position of these dyes are achieved through Suzuki-Miyaura C-C coupling and $S_{RN}1$ nucleophilic substitution of the chlorine atom at the *meso*-position of the dye. Herein, a series of 15 *meso* phenyl-substituted heptamethine cyanines was synthesized utilizing a modified dianil linker. Their optical properties, including molar absorptivity, fluorescence, Stokes shift, and quantum yield were measured. The HSA binding affinities of two representative compounds were measured and compared to that of a series of trimethine cyanines previously synthesized by our lab. The results indicate that the binding of these compounds to HSA is not only dependent on hydrophobicity, but may also be dependent on steric interferences in the binding site and structural dynamics of the NIRF compounds.

Keywords: heptamethine cyanine dyes; absorbance; fluorescence; NIRF; physiochemical properties; HSA binding

2.2 Introduction

Heptamethine cyanine dyes are a class of near infared fluorescence (NIRF) probes that have shown great potential in numerous applications due to their versatility, low toxicity, narrow absorption band, and high extinction coefficients [8-13]. These dyes are comprised of two terminal nitrogen-containing heterocycles linked together by a conjugated polymethine chain. The

heterocycles act as both electron donors and acceptors creating an electron deficient system throughout the molecule, allowing for long wavelength absorption [14-17]. Heptamethine cyanines have been used in medical imaging targeting of: cartilage, bone, endocrine gland, biomolecular labeling and much more all serving as contrast agents to aid in surgical application [1, 12, 18-23]. Modifications to the cyanine dye scaffold can alter optical properties, solubility, and allow for specific tailoring of dyes for their desired application.

A main contributing factor in the successful application of heptamethine cyanine dyes is their modifiability. Most commonly cyanines are modified by the use of different heterocycles and with different substituents on the nitrogen atom of the heterocycle. One point of modification that has not been thoroughly investigated is the central (*meso*) carbon of the methine bridge. Many derivatives described in literature have been made by replacing the chlorine atom at this position via a $S_{RN}1$ mechanism [12–14]. The most common method of carbon-coupling at the *meso*-position thus far has been done by first synthesizing a heptamethine cyanine dye containing a chlorine atom at the *meso*-position followed by Suzuki-Miyaura coupling [24-26]. While this method is successful in synthesizing many scaffolds, it requires tedious purification and the use of an expensive palladium catalyst [12–14]. Although the phenyl-substituted dianil linker has been previously synthesized, it has not been thoroughly investigated for its effects on the optical properties on the NIRF dye [27, 28].

Many of these cyanine dyes are administered via IV injection in which the dyes are transported to their target through the bloodstream [29]. Human serum albumin (HSA) is the most abundant protein in human blood plasma, serving an important role of transporting substances throughout the body [29-31]. It is synthesized in the liver and has great binding capacity for hydrophobic compounds [29, 32]. HSA has been a widely studied protein because of its importance in drug

delivery [15]. HSA contains four binding pockets and does not require biomolecular ligand specificity, increasing its versatility and usefulness in medical research [29-32]. It is well described in literature that HSA binds to hydrophobic entities. A unique attribute of HSA is that it forms reversible covalent bonds with the binding agent, this allows for stable complex formation; however, since the bonds are reversible also allows for localization and deposit [33].

Our lab has previously designed and synthesized a series of trimethine dyes and studied their hydrophobicity and its effect on their interactions with HSA [34]. In this paper, a series of heptamethine cyanines with varying degrees of hydrophobicity containing a *meso*-phenyl substituent were synthesized through the use of a phenyl-substituted dianil linker. This method not only allows for a more facile synthesis, but a wider array of dyes can be made and can serve for various applications. The effect of the phenyl ring on the dyes hydrophobicity, optical properties, and binding to HSA was studied and compared to the results from our previous study [34].

2.3   Results and Discussion

2.3.1   *Synthesis*

As shown in Scheme 1, the synthesis began with a Fischer indole cyclization by refluxing 4-substituted phenylhydrazines **1** overnight with 3-methyl-2-butanone in glacial acetic acid. After cooling to room temperature, the reaction mixture was neutralized and the substituted indoles **2** were extracted with dichloromethane to give brown oils. The oils were dissolved in acetonitrile and refluxed overnight with various alkyl halides to yield quaternary ammonium salts **3**. In parallel to salt formation, a phenyl-substituted dianil compound was synthesized through a Vilsmeier Haack formylation with 1-phenylcyclohexene (**4**). The ends of the dianil linker were capped with aniline for stability to yield dianil compound **5** [27, 28]. Various quaternary ammonium salts **3** and dianil compound **5** are then condensed in a 2:1 ratio in acetic anhydride to yield the final phenyl

substituted heptamethine cyanines **6**. Pure compounds were obtained in good yield by simply washing with methanol.

The synthetic route described in Scheme 1 provided a new carbon-carbon linked substituent position at the *meso* center adding to the versatility of heptamethine cyanine. The phenyl group was added before the dye was made. This allowed for an efficient method of preparation of the dye, which required no catalysts or complex purification methods and allowed for a wider array hydrophobic compounds to be made.

Once the dyes have been successfully synthesized, the optical properties were measured, and representative dyes **6a** and **6k** were studied for their binding affinity to HSA. The optical properties were compared to commercially available heptamethine dyes **Cy-7** and **IR-780** due to the similar absorbance and emission wavelengths. The binding studies of compounds **6a** and **6k** were compared to **MHI-06,** a dye previously reported as a strong HSA binding agent [28]. Figure 1 shows the three dye structures of the standards used in this study.
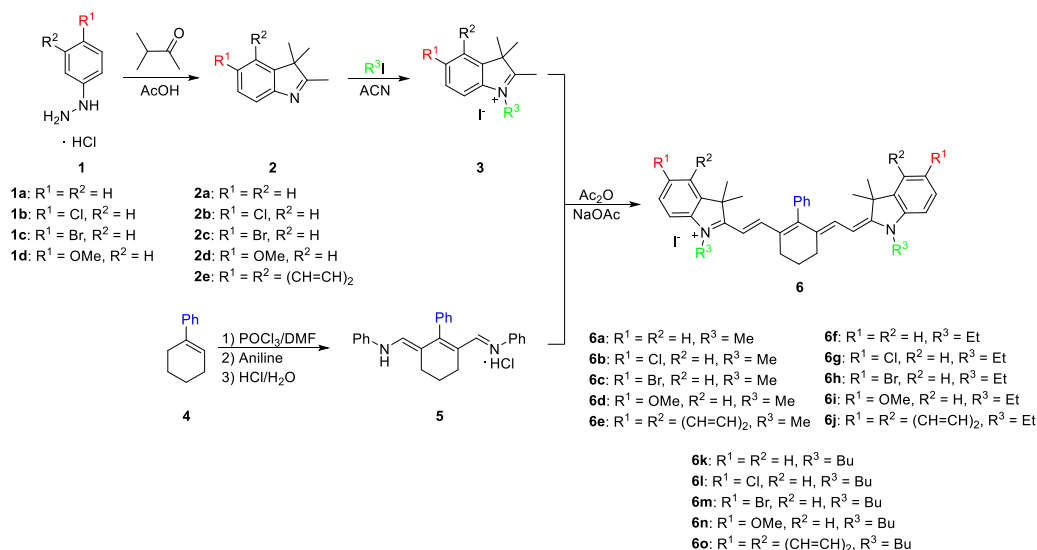
Scheme 2.**1.** Synthetic routes of heptamethine dyes containing a phenyl ring at the *meso*-position.
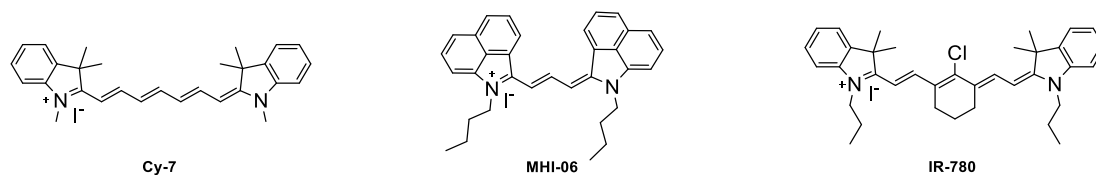
Figure 2.1 The structures of the three NIR standards used for the study.

2.3.2 *Optical Properties*

As described in Scheme 1, fifteen final NIRF contrast agents were synthesized using the dianil linker to yield symmetrical heptamethine cyanines 6a–o. The compounds are broken down to three sets of five. Dyes 6a–e all contain a methyl substituent off the nitrogen of the heterocycle with varying substitutions at the six position of the heterocyclic ring.

Table 2.1. Spectral Characteristics of dyes Cy-7, IR-780 and 6a–o. All optical properties of the dyes were measured in ethanol.

Dye	λ_{max} (nm)	$\lambda_{emission}$ (nm)	Stokes Shift (nm)	ε (L·mol^{-1}·cm^{-1})	Φ (%)	Molecular Brightness (M^{-1}· cm^{-1})
Cy-7	753	775	22	200,000	28	56,000
IR-780	779	799	20	274,000	8.0	20,800
6a	759	774	15	265,700	31	82,000
6b	765	780	15	261,000	34	88,700
6c	767	783	16	275,600	35	96,500
6d	782	802	20	249,500	10	25,000
6e	798	810	12	255,400	16	40,900

6f	760	781	21	263,900	39	102,300
6g	769	785	16	286,600	38	109,300
6h	770	786	16	282,900	42	119,200
6i	786	804	18	143,500	12	17,200
6j	797	810	13	231,800	17	39,400
6k	763	780	17	198,500	45	89,300
6l	772	787	15	123,400	47	58,000
6m	773	788	15	239,200	48	113,600
6n	789	805	16	249,900	11	27,100
6o	800	812	12	226,600	17	38,500

Dyes **6f–j** and **6k–o** contain ethyl and butyl *N*-alkyl substituents, respectively. In comparison to **Cy-7**, the optical properties of the new compounds were found to be superior (Table 1). The addition of the cyclohexene ring provided rigidity to the compounds, increasing the molar absorptivity and quantum yield by 60,000 $M^{-1} \cdot cm^{-1}$ and 5%, respectively, for **6a [35]**. To determine the effects the phenyl ring had on the optical properties, the dyes were compared to **IR-780** [36]. Although the molar absorptivity of the studied dyes were within the same range as the commercially available dye, the quantum yield was dramatically increased with the introduction of the electron rich phenyl ring, observing a 23–47% increase in quantum yield. The chlorine atom at the *meso*-position of dye IR-780 promotes intersystem crossing due to the heavy atom effect, and allows for the molecule to relax in non-radiative means and decreases the fluorescence [37].
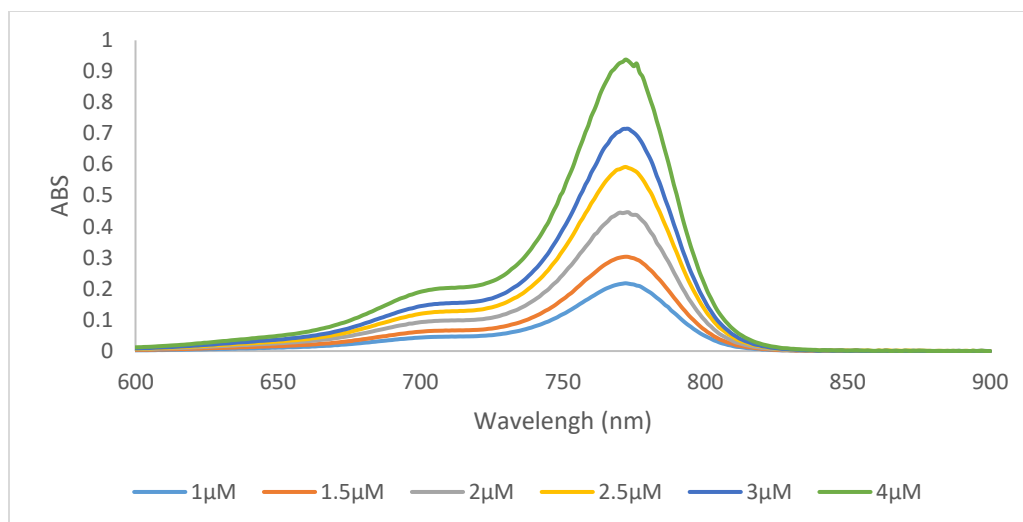
*Figure 2.2 Absorption spectra of dye **6m** in ethanol.*

Increasing the length of *N*-alkyl substituents from a methyl to ethyl did not result in any significant changes in optical properties, but an increase in size to the butyl group generally lowered the molar absorptivity. Dyes containing hydrogen **6a**,**f**,**k**, and halogens **6b**,**c**,**g**,**h**,**l**,**m** at the 6 position of the heterocycle displayed absorption λ_{max} values of 759–773 nm with redshifts from the hydrogen to the halogens from 6 nm to 10 nm which has previously been described [38]. Absorption spectra of representative compound **6m** was shown in Figure 2. All 15 compounds have Stokes shifts ranging from 12 to 21 with the benz[*e*]indolenine containing compounds **6e**,**j**,**o** having the shortest Stokes shifts. All three methoxy-substituted compounds **6d**,**i**,**n** had redshifted absorption λ_{max} values from 16 nm to 26 nm and lower quantum yields than the other compounds while dyes **6e**,**j**,**o** were redshifted 37–39 nm around 800 nm due to the increased conjugation of the benz[*e*]indolenine heterocycle.
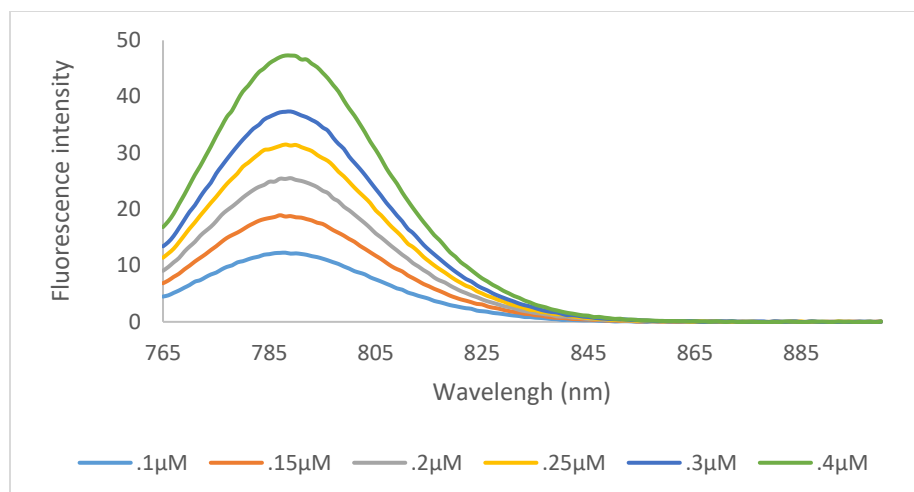
*Figure 2.3 Emission spectra of dye **6m** in ethanol with excitation wavelength of 750 nm.*

The emission data of all the dyes followed the same trends, whereby compounds containing the hydrogen **6a,f,k**, and halogen **6b,c,g,h,l,m** substituents had the highest quantum yields, and the longer *N*-alkyl chains increased the quantum yield by 4–8% from methyl to ethyl and 5–7% from ethyl to butyl. Emission spectra of representative compound **6m** was shown in Figure 3. There was no significant difference in quantum yield between the hydrogen and halogens within the same set. Compounds **6e,j,o** containing the benz[*e*]indolenine heterocycle and **6d,i,n** containing the methoxy substituent displayed lower quantum yields at 16–17% and 10–12%, respectively, which is consistent with previous reports [1].

Although molar absorptivity and quantum yield are important properties of fluorophores, in regards to application, the molecular brightness gives a more useful indication of the dye utility. Molecular brightness takes into account both molar absorptivity and quantum yield [39, 40]. Dyes that have high quantum yield, but do not absorb light efficiently (low molar absorptivity) are still not emitting as many photons and are less useful for fluorescent applications. *N*-alkyl substituents from a methyl to ethyl increased the molecular brightness by approximately 20,000 $M^{-1} \cdot cm^{-1}$ for the hydrogen- **6a,f,k**, and halogen- **6b,c,g,h,l,m** substituted compounds while the butyl compounds

showed lower molecular brightness. Due to the low quantum yield of the benz[*e*]indolenine heterocycle **6e,j,o** and the methoxy **6d,i,n** substituted compounds, the two sets showed the lowest molecular brightness of 38,000–40,000 $M^{-1} \cdot cm^{-1}$ and 17,000–20,000 $M^{-1} \cdot cm^{-1}$, respectively.

2.3.3 Physiochemical Properties

In our previous study of trimethine cyanine dyes it was shown that **MHI-06** (Figure 1) bound HSA with an affinity of 1.0×10^6 M^{-1} [28]. In that study of the binding affinity of trimethine cyanines, a trend was observed correlating hydrophobicity to the binding affinity. As the dyes became more hydrophobic greater binding affinity was observed. However, the correlation did not hold when the large *N*-phenylpropyl side chain was introduced in the trimethine series [28]. It was hypothesized that the binding affinity decreased due to the increased size of the *N*-phenylpropyl side chain hindering the dye from entering the HSA binding pocket. The heptamethine cyanines **6a**–**o** synthesized in this work were tailored to be hydrophobic in order to observe if binding increases due to increase of hydrophobicity or decreases due to the size and steric hindrance.

*Table 2.2 Physicochemical properties (*in silico*) of dyes **MHI-06** and **6a**–**o** calculated using ChemAxon. The data calculated (at pH 7.4) include: logD, polarizability, dipole moment (debye), number of rotatable bonds, volume ($Å^3$), molecular surface area ($Å^3$), and molar mass (g/mol).*

Dye	log D	Polarizab ility	Dipole Moment	Rot. Bonds	Volu me	Molec. Surface Area	Molar Mass
MHI-06	4.9 7	59.45	2.48	8	441.4 4	693.216	584.54
6a	6.0 7	65.57	8.35	4	519.8 5	814.001	652.66

6b	7.28	69.15	12.3	4	547.45	845.982	721.55
6c	7.61	70.67	13.02	4	556.15	854.732	810.46
6d	5.75	70.51	27.66	6	569.71	907.778	712.72
6e	8.05	80.82	11.87	4	604.27	936.392	752.78
6f	6.75	69.26	3.2	6	552.14	874.685	680.72
6g	7.99	72.84	4.81	6	579.48	906.491	749.6
6h	8.32	74.35	4.97	6	588.47	915.629	838.51
6i	6.47	74.2	25.29	8	603.83	969.908	740.77
6j	8.76	84.51	4.59	6	638.63	999.272	7803.84
6k	8.72	76.65	2.85	10	620.01	996.744	736.81
6l	9.92	80.23	4.63	10	647.91	1029.597	805.71

6m	10.25	81.71	4.96	10	656.64	1038.143	894.62
6n	8.40	81.59	26.66	12	672.63	1094.66	796.88
6o	10.69	91.9	3.96	10	708.29	1124.8	836.95

The physicochemical properties were calculated using ChemAxon for the 15 heptamethine dyes synthesized and compared to our pervious reported compound **MHI-06** (Table 2) [28]. Physicochemical trends were observed in each series with the same heterocyclic substituents as well as with the same *N*-alkyl side chain. Compounds **6d,i,n** with the methoxy substituent showed the lowest log*D*, due to its ability to form hydrogen bonds. Slightly higher values were observed for compounds with the hydrogen-substitued **6a,f,k**. A 1.2 and 1.5 increase of log*D* was observed from the hydrogen to the chloro-and bromo-substituted compounds, respectively. As expected, the series with the benz[*e*]indolenine heterocycle **6e,j,o** had the highest log*D* values due to the addition of another phenyl ring. All heptamethine cyanines **6a–o** had significantly higher log*D* values compared to that of **MHI-06** due to the presence of the phenyl substituent at the *meso*-position and the increased size of the hydrocarbon skeleton. The dipole moments decreased as the length of the alkyl chain increased from methyl to butyl, with methoxy-substituted dyes having significantly higher values. In comparison to **MHI-06** most of the compounds, especially that of the methyl series **6a–e**, had a higher dipole moment, but for **6k** which had fairly similar results to **MHI-06** at 2.85 and 2.48, respectively. The number of rotatable bonds increased by 2 from methyl to ethyl and by 4 from ethyl to butyl. Only the methoxy heterocyclic substitution affected the number of

rotatable bonds with an additional rotatable bond for each methoxy in compounds **6d,i,n**. **MHI-06** had eight rotatable bonds. All of the dyes with the exception of those containing the methoxy substituent had a total polar surface area (TPSA) of 6.25, 0 hydrogen bond donors, and 1 hydrogen bond acceptor (ChemAxon). Dyes **6d,i,n** containing the methoxy substituent had higher TPSA at 24.71 and three hydrogen bond acceptors. The presence of the polar oxygen increases the TPSA, and increases the number of hydrogen bond that can form by two.

In summary, the newly synthesized heptamethine dyes **6a–o** were significantly more hydrophobic then **MHI-06**, but had a much larger volume. Although hydrophobicity plays a key role in binding to HSA, reversibly the size of the compound could inhibit the ability of its binding to HSA pocket. Compounds **6a** and **6k** were tested for their ability to bind to HSA, to further determine if other factors than hydrophobicity, play an important role in HSA binding allowing a better understanding of binding nature of the larger heptamethine cyanines to HSA. The HSA binding spectra for **6a** is shown below (Figure 4) and binding data of **6k** is shown in the supplemental information (**6k** HSA binding).
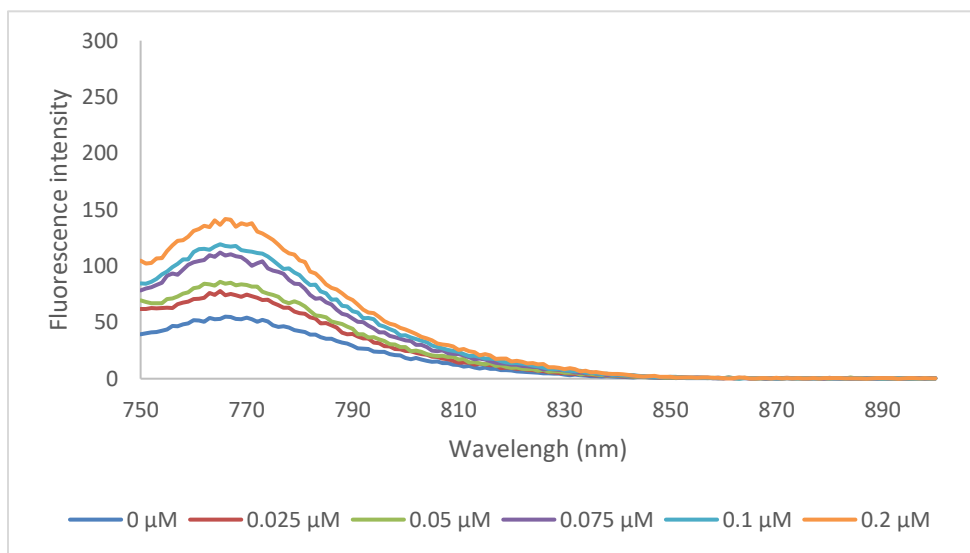
*Figure 2.4 The emission specra of **6a** (0.2 μM) binding with various concentration of HSA, in PBS buffer at excitation wavelength of 740 nm.*

2.3.4   HSA Bidning

The formation of a dye/substrate conjugate was studied with HSA in phosphate buffered saline

(PBS), pH 7.4. Previous research by Kim et al. suggested that cyanine dyes bind HSA in with a

1:1 stoichiometry which was confirmed by our and other research groups using trimethine cyanine

dyes [10, 34, 41-43]. The binding interactions were studied by measuring the changes in emission

intensities at a fixed concentration of dye with varying micromolar concentrations of HSA and

using a double reciprocal plot of $[HSA]^{-1}$ vs. ΔF^{-1}, where ΔF is the change in emission intensity

of the Dye/HSA conjugate, that should give a linear relationship. The binding affinity is then

calculated by dividing the intercept by the slope of the line. Our lab has previously shown that

both the *N*-alkyl substituents and the heterocyclic ring of the cyanines have profound effects on

overall conjugation with the biomolecule [20]. It has also previously been shown that cyanine dyes

aggregate in polar solvents such as PBS buffer due to strong intermolecular van der Waals

interactions between the heterocycles that cause the dyes to form H-aggregates [44]. Generally,

organic solvents are used to disrupt this aggregate formation, but organic solvents cannot be used

in the presence of HSA due to their ability to denature the biomolecule. Conjugate formation with

HSA disrupts the aggregation increasing monomer formation and thereby increasing fluorescence

emission of the dyes. It was determined that heptamethine dye **6a** binds HSA with an affinity of 8

$\times 10^1$ M^{-1}. This is 5 orders of magnitude lower than the previously tested trimethine cyanines,

MHI-06, which bound on the order of 1×10^6 M^{-1} [28]. This further confirms our previous

hypothesis that the binding affinity of the dyes is not only hydrophobicity dependent, but

dependent on steric interferences in the HSA binding site. It also confirms that the delocalized

cationic nature of the dyes may has no electrostatic interference with the binding cavity as this

heptamethine cyanine displays increased delocalization over the previously tested trimethine

cyanines. Albumin is known to bind a variety of compounds including fatty acids, nucleic acids, and oligoproteins therefore this information on the steric specificity of these binding sites is of potential interest when developing methods to study them [34].

2.4 Experimental Section

2.4.1 General Information

All chemicals and solvents were of American Chemical Society grade or HPLC purity and were used as received. HPLC grade ethanol *were purchased from Sigma-Aldrich (St. Louis, MO, USA). All other chemicals were purchased from Fisher Scientific (Pittsburgh, PA, USA) or Acros Organics (Pittsburgh, PA, USA). The reactions were followed using silica gel 60 F254 thin layer chromatography plates (Merck EMD Millipore, Darmstadt, Germany). The 1H-NMR and 13C-NMR spectra were obtained using high quality Kontes NMR tubes (Kimble Chase, Vineland, NJ, USA) rated to 500 MHz and were recorded on an Avance spectrometer (Bruker, Billerica, MA; 400 MHz for 1H and 100 MHz for 13C) in* DMSO-d6, acetone-d6 *CD3Cl-d3. High-resolution accurate mass spectra (HRMS) were obtained at the Georgia State University Mass Spectrometry Facility using a Q-TOF micro (ESI-Q-TOF) mass spectrometer (Waters, Milford, MA, USA). All compounds tested were >95% pure. Infrared spectra (FT-IR) were obtained using a Spectrum 100 spectrometer (PerkinElmer, Duluth, GA, USA) (see Supplementary Materials). UV-Vis/NIR absorption spectra were recorded on a Cary 50 spectrophotometer (Varian, Palo Alto, CA, USA) interfaced with Cary WinUV Scan Application v3.00 using VWR disposable polystyrene cuvettes with a 1 cm pathlength. Laser Induced Fluorescence (LIF) emission spectra were acquired using Shimadzu RF-5301 Spectroflurophotometer (Shimadzu Corporation Analytical Instruments Division, Duisburg, Germany) interfaced to a PC with RF-5301PC software using Sigma-Aldrich disposable polystyrene fluorimeter cuvettes with a 1 cm pathlength. All spectral measurements*

were recorded at room temperature. The data analysis and calculations were carried out using

Microsoft Excel (Microsoft Corporation, Redmond, WA, USA).

2.4.2   Synthetic Procedure

A solution of POCl3 (11 mL, 117.66 mmol) in dichloromethane (10 mL) was added

dropwise to a solution of DMF (13 mL, 167.89 mmol) in dichloromethane (13 mL) at 0 °C for

30 min under inert conditions. Then 1-phenylcyclohexene (4, 5.5 mL, 32.81 mmol) was

dissolved in dry dichloromethane (5 mL) and added dropwise to the solution which was then

refluxed for 3 h. The solution was allowed to cool to room temperature and then poured over 500

mL of ice/water. Aniline (9 mL, 98.57 mmol) in ethanol (9 mL) was added to cap the ends. The

crude solid was collected and washed with diethyl ether and hexanes. Resulting in the dianil

linker 5 as a pure compound and used without further purification.

In parallel, substituted hydrazines 1 (4.0 g, 22.25 mmol) were reacted with 3-

methylbutanone (3 mL, 28.04 mmol) in acetic acid and heated to a 100 °C for 24 h. The solution

was then neutralized using sodium bicarbonate and extracted using dichloromethane; affording

substituted indolenine heterocycles 2 which was dried under reduced pressure. The heterocycles

2 were then reacted with an alkyl halide in acetonitrile at 100 °C for 12–18 h. The quaternary

ammonium salts 3 were precipitated with diethyl ether, and collected.

The various salts 3 (2 molar eq), the dianil linker 5 (1 molar eq), and sodium acetate (2

molar eq) were dissolved in acetic anhydride and heated to 60 °C for 2–3 h. The crude product

was then precipitated with diethyl ether, collected, and washed with methanol to yield

heptamethine dyes 6 as pure sample.

2.4.3   Characterization

1,3,3-Trimethyl-2-((E)-2-((E)-6-(2-((E)-1,3,3-trimethylindolin-2-ylidene)ethylidene)-3,4,5,6-tetrahydro-[1,1'-biphenyl]-2-yl)vinyl)-3H-indol-1-ium iodide, **6a**: Yield 77%; m.p. > 260 °C; ^{1}H-NMR (CDCl$_3$) **δ** 1.11 (s, 12H), 1.95 (m, 2H), 2.68 (t, *J* = 6.0 Hz, 4H), 3.58 (s, 6H), 6.17 (d, *J* = 14.0 Hz, 2H), 7.16 (m, 4H), 7.25 (d, *J* = 8.4 Hz, 2H), 7.34 (m, 4H), 7.46 (d, *J* = 7.6 Hz, 2H), 7.62 (m, 3H). ^{13}C-NMR (CDCl$_3$) **δ** 21.3, 24.5, 27.3, 31.5, 48.5, 100.7, 111.3, 122.7, 124.9, 128.5, 128.8, 129.0, 129.6, 131.0, 139.1, 140.9, 143.3, 147.3, 161.5, 172.1. HRMS (ESI) *m/z*: calcd. for C$_{38}$H$_{41}$N$_2$$^+$ 525.3264, obsd 525.3241.

5-Chloro-2-((E)-2-((E)-6-(2-((E)-5-chloro-1,3,3-trimethylindolin-2-ylidene)ethylidene)-3,4,5,6-tetrahydro-[1,1'-biphenyl]-2-yl)vinyl)-1,3,3-trimethyl-3H-indol-1-ium iodide, **6b**: Yield 78%; m.p. > 260 °C; ^{1}H-NMR (CDCl$_3$) **δ** 1.17 (s, 12H), 2.07 (m, 2H), 2.74 (t, *J* = 6.4 Hz, 4H), 3.65 (s, 6H), 6.12 (d, *J* = 14.0 Hz, 2H), 7.05 (d, *J* = 8.4 Hz, 2H), 7.17 (m, 6H), 7.30 (t, *J* = 8.4 Hz, 2H), 7.56 (m, 3H); ^{13}C-NMR (CDCl$_3$) **δ** 21.1, 25.0, 27.5, 32.5, 48.5, 100.8, 111.3, 122.5, 128.2, 128.5, 128.7, 129.4, 130.2, 133.0, 138.7, 141.5, 142.1, 148.2, 163.0, 171.4. HRMS (ESI) *m/z*: calcd. for C$_{38}$H$_{39}$Cl$_2$N$_2$$^+$ 593.2485, obsd 593.2475.

5-Bromo-2-((E)-2-((E)-6-(2-((E)-5-bromo-1,3,3-trimethylindolin-2-ylidene)ethylidene)-3,4,5,6-tetrahydro-[1,1'-biphenyl]-2-yl)vinyl)-1,3,3-trimethyl-3H-indol-1-ium iodide, **6c**: Yield 75%; m.p. > 260 °C; ^{1}H-NMR (CDCl$_3$) **δ** 1.12 (s, 12H), 2.08 (m, 2H), 2.76 (t, *J* = 6.4 Hz, 4H), 3.66 (s, 6H), 6.15 (d, *J* = 14.0 Hz, 2H), 6.99 (d, *J* = 8.4 Hz, 2H), 7.15 (d, *J* = 14.0 Hz, 2H), 7.21 (dd, *J* = 7.6 Hz, 2H), 7.46 (dd, *J* = 8.4 Hz, 2H), 7.56 (m, 3H). ^{13}C-NMR (CDCl$_3$) **δ** 21.0, 25.0, 27.5, 32.5, 48.4, 100.9, 111.7, 117.7, 125.3, 128.2, 128.5, 129.4, 131.5, 133.2, 138.7, 142.0, 142.4, 148.1, 162.9, 171.2. HRMS (ESI) *m/z*: calcd. for C$_{38}$H$_{39}$Br$_2$N$_2$$^+$ 681.1475, obsd 681.1475.

5-Methoxy-2-((E)-2-((E)-6-(2-((E)-5-methoxy-1,3,3-trimethylindolin-2-ylidene)ethylidene)-3,4,5,6-tetrahydro-[1,1'-biphenyl]-2-yl)vinyl)-1,3,3-trimethyl-3H-indol-1-ium iodide, **6d**: Yield 73%; m.p. 238–240 °C; ^{1}H-NMR (CDCl$_3$) **δ** 1.17 (s, 12H), 2.06 (m, 2H), 2.70 (t, J = 6.4 Hz, 4H), 3.61 (s, 6H), 3.82 (s, 6H), 6.03 (d, J = 14.0 Hz, 2H), 6.76 (s, 2H), 6.86 (d, J = 8.8 Hz, 2H), 7.04 (d, J = 8.4 Hz, 2H), 7.10 (d, J = 14.0 Hz, 2H), 7.21 (d, J = 6.8 Hz, 2H), 7.55 (m, 3H); ^{13}C-NMR (CDCl$_3$) **δ** 21.2, 24.9, 27.5, 32.2, 48.5, 55.9, 99.8, 109.1, 110.9, 112.8, 128.0, 128.4, 129.5, 131.4, 136.5, 139.1, 142.2, 146.8, 157.8, 161.3, 171.0. HRMS (ESI) m/z: calcd. for $C_{40}H_{75}N_2O_2^+$ 585.3476, obsd 585.3469.

1,1,3-Trimethyl-2-((E)-2-((E)-6-((E)-2-(1,1,3-trimethyl-1,3-dihydro-2H-benzo[e]indol-2-ylidene)ethylidene)-3,4,5,6-tetrahydro-[1,1'-biphenyl]-2-yl)vinyl)-1H-benzo[e]indol-3-ium iodide, **6e**: Yield 63%; m.p. > 260 °C; ^{1}H-NMR (CDCl$_3$) **δ** 1.50 (s, 12H), 2.11 (m, 2H), 2.79 (t, J = 6.4 Hz, 4H), 3.77 (s, 6H), 6.16 (d, J = 14.0 Hz, 2H), 7.30 (m, 2H), 7.44 (m, 4H), 7.55 (t, J = 7.6 Hz, 2H), 7.66 (m, 3H), 7.92 (m, 6H); ^{13}C-NMR (CDCl$_3$) **δ** 21.2, 25.0, 27.1, 32.5, 50.2, 99.9, 110.5, 121.9, 124.7, 127.5, 128.0, 128.3, 128.6, 129.5, 130.1, 130.5, 131.7, 132.2, 132.9, 139.0, 140.2, 147.1, 162.0, 173.3. HRMS (ESI) m/z: calcd. for $C_{46}H_{45}N_2^+$ 625.3577, obsd 625.3570.

1-Ethyl-2-((E)-2-((E)-6-(2-((E)-1-ethyl-3,3-dimethylindolin-2-ylidene)ethylidene)-3,4,5,6-tetrahydro-[1,1'-biphenyl]-2-yl)vinyl)-3,3-dimethyl-3H-indol-1-ium iodide, **6f**; Yield: 70%; m.p. > 260 °C; ^{1}H-NMR (acetone-d$_6$) **δ** 1.11 (s, 12H), 1.24 (t, J = 7.2 Hz, 6H), 1.96 (m, 2H), 2.97 (t, 4H), 4.14 (m, 4H) 6.20 (d, J = 14 Hz, 2H), 7.18 (m, 4H), 7.35 (m, 4H), 7.47 (d, J = 7.6 Hz, 2H), 7.61 (m, 3H); ^{13}C NMR (100 MHz, CDCl$_3$) **δ** 12.3, 21.2, 25.0, 27.6, 39.7, 48.6, 99.8, 110.2, 122.1, 124.8, 128.2, 128.6, 128.7, 129.5, 132.2, 138.9, 140.8, 141.9, 148.2, 162.6, 170.9; ^{13}C-NMR (acetone-d$_6$) **δ** 12.5, 21.3, 24.6, 27.4, 39.8, 40.0, 40.2, 48.7, 100.2, 111.2, 123.0, 125.0, 128.6,

129.0, 129.1, 129.6, 131.1, 141.1, 142.1, 147.7, 171.2. HRMS (ESI) *m/z*: calcd. for $C_{40}H_{45}N_2^+$ 553.3577, obsd 553.1566.

5-Chloro-2-((E)-2-((E)-6-(2-((E)-5-chloro-1-ethyl-3,3-dimethylindolin-2-ylidene)ethylidene)-3,4,5,6-tetrahydro-[1,1'-biphenyl]-2-yl)vinyl)-1-ethyl-3,3-dimethyl-3H-indol-1-ium iodide, **6g**; Yield 64%; m.p. > 260 °C; ¹H-NMR (CDCl₃) **δ** 1.16 (s, 12H), 1.38 (t, *J* = 7.2 Hz, 6H), 2.07 (t, *J* = 5.6, 2H), 2.73 (t, *J* = 6.0 Hz, 4H), 4.142 (m, 4H), 6.10 (d, *J* = 14.0 Hz, 2H), 7.07 (d, *J* = 8.4 Hz, 2H), 7.28 (m, 8H) 7.59 (m, 3H); ¹³C-NMR (CDCl₃) **δ** 12.2, 21.1, 25.0, 27.5, 40.7, 48.6, 100.1, 111.4, 122.6, 128.3, 128.7, 128.8, 129.4, 130.3, 132.6, 138.7, 140.5, 142.4, 148.3, 163.1, 170.5. HRMS (ESI) *m/z*: calcd. for $C_{40}H_{43}Cl_2N_2^+$ 621.2798, obsd 621.2788.

5-Bromo-2-((E)-2-((E)-6-(2-((E)-5-chloro-1-ethyl-3,3-dimethylindolin-2-ylidene)ethylidene)-3,4,5,6-tetrahydro-[1,1'-biphenyl]-2-yl)vinyl)-1-ethyl-3,3-dimethyl-3H-indol-1-ium iodide, **6h**; Yield 71%; m.p. > 260 °C; ¹H-NMR (CDCl₃) **δ** 1.18 (s, 12H), 1.41 (t, *J* = 7.2 Hz, 6H), 2.10 (t, *J* = 6.4 Hz, 2H), 2.75 (t, 5.6 Hz, 4H), 4.16 (m, 4H), 6.13 (d, *J* = 14.4 Hz, 2H), 7.22 (m, 10H), 7.59 (m, 3H); ¹³C-NMR (CDCl₃) **δ** 12.2, 21.1, 25.1, 27.5, 40.1, 48.6, 100.3, 111.7, 117.7, 125.5, 128.3, 128.6, 129.4, 131.6, 133.0, 138.8, 141.0, 142.7, 148.2, 162.9, 170.3. HRMS (ESI) *m/z*: calcd. for $C_{40}H_{43}Br_2N_2^+$ 709.1788, obsd 709.1780.

1-Ethyl-2-((E)-2-((E)-6-(2-((E)-1-ethyl-5-methoxy-3,3-dimethylindolin-2-ylidene)ethylidene)-3,4,5,6-tetrahydro-[1,1'-biphenyl]-2-yl)vinyl)-5-methoxy-3,3-dimethyl-3H-indol-1-iumiodide, **6i**; Yield 61%; m.p. > 260 °C; ¹H-NMR (acetone-d₆) **δ** 1.22 (s; 12H), 1.34 (t, *J* = 7.2 Hz, 6H), 2.02 (m, 2H), 2.73 (t, *J* = 6.0 Hz 4H), 3.84 (s, 6H), 4.21 (m, 4H), 6.23 (d, *J* = 14 Hz 2H), 6.23 (d, *J* = 2.8 Hz 2H) 6.94 (d, *J* = 2.4 Hz 2H) 7.22 (s, 2H) 7.28 (m, 6H) 7.66 (m, 3H); ¹³C-NMR (acetone-d₆) **δ** 11.6, 21.3 24.5, 26.8, 39.0, 48.8, 55.4, 99.1, 109.0, 111.2, 113.4, 128.0, 128.7, 129.5, 130.3,

135.5, 139.4, 142.8, 145.0, 158.1, 161.0, 170.6. HRMS (ESI) *m/z*: calcd. for $C_{42}H_{49}N_2O_2^+$ 613.3789, obsd 613.3777.

3-Ethyl-2-((E)-2-((E)-6-((E)-2-(3-ethyl-1,1-dimethyl-1,3-dihydro-2H-benzo[e]indol-2-ylidene)ethylidene)-3,4,5,6-tetrahydro-[1,1'-biphenyl]-2-yl)vinyl)-1,1-dimethyl-1H-benzo[e]indol-3-ium iodide, **6j**; Yield 65%; m.p. > 260 °C; ^{1}H-NMR (CDCl₃) **δ** 1.46 (t, *J* = 6.8 Hz, 6H), 1.51 (s, 12H), 2.13 (t, *J* = 5.6 Hz, 2H), 2.79 (t, *J* = 6.0 Hz, 4H), 4.28 (m, 4H), 6.17 (d, *J* = 14.0 Hz, 2H), 7.45 (m, 13H), 7.94 (m, 6H); ^{13}C-NMR (CDCl₃) **δ** 99.3, 110.4, 122.0, 124.8, 127.6, 128.1, 128.3, 128.7, 129.5, 130.1, 130.7, 131.7, 132.0, 133.3, 139.1, 139.3, 147.3, 162.0, 172.4. HRMS (ESI) *m/z*: calcd. for $C_{48}H_{49}Cl_2N_2^+$ 593.2485, obsd 593.2475.

1,3,3-Trimethyl-2-((E)-2-((E)-6-(2-((E)-1,3,3-trimethylindolin-2-ylidene)ethylidene)-3,4,5,6-tetrahydro-[1,1'-biphenyl]-2-yl)vinyl)-3H-indol-1-ium iodide, **6k**; yield 68%; m.p. > 260 °C; ^{1}H-NMR (CDCl₃) **δ** 1.04 (t, *J* = 7.2 Hz, 6H), 1.23 (s, 12H), 1.49 (m, 4H), 1.80 (m, 4H), 2.11 (t, *J* = 6.0 Hz, 2H), 2.745 (s, 4H), 4.04 (t, *J* = 7.2 Hz, 4H), 6.10 (d, *J* = 14 Hz, 2H), 7.07 (d, *J* = 11.6 Hz, 2H), 7.22 (m, 6H), 7.33 (t, *J* = 7.2 Hz, 2H), 7.61 (m, 3H)); ^{13}C-NMR (CDCl₃) 14.0, 20.5, 21.3,25.0, 27.7, 29.4, 110.4, 122.1, 124.8, 128.2, 128.6, 129.6, 140.8, 142.3. HRMS (ESI) *m/z*: calcd. for $C_{44}H_{53}N_2^+$ 609.4203, obsd 609.4198.

1-Butyl-2-((E)-2-((E)-6-(2-((E)-1-butyl-5-chloro-3,3-dimethylindolin-2-ylidene)ethylidene)-3,4,5,6-tetra-hydro-[1,1'-biphenyl]-2-yl)vinyl)-5-chloro-3,3-dimethyl-3H-indol-1-ium iodide, **6l**: Yield 67%; m.p. > 260; ^{1}H-NMR (CDCl₃) **δ** 1.03 (t, *J* =7.2 Hz, 6H), 1.191 (s, 12H), 1.47 (m, 4H), 1.78 (t, *J* = 6.8 Hz, 4H), 2.12 (s, 2H), 2.75 (s, 4H), 4.02 (s, 4H), 6.09 (d, *J* = 12.4 Hz, 2H), 6.98 (d, *J* = 8.0 Hz, 2H), 7.28 (m, 8H), 7.86 (m, 3H); ^{13}C-NMR (CDCl₃) **δ** 14.0, 20.4, 21.3, 25.0, 27.7, 29.3, 44.7, 48.6, 100.4, 111.3, 122.7, 128.3, 128.6, 129.6, 130.2, 138.7, 141.0, 142.4, 148.5, 171.0. HRMS (ESI) *m/z*: calcd. for $C_{44}H_{51}Cl_2N_2^+$ 677.3424, obsd 677.3421.

1-Butyl-2-((E)-2-((E)-6-(2-((E)-1-butyl-3,3-dimethylindolin-2-ylidene)ethylidene)-3,4,5,6-tetrahydro-[1,1'-biphenyl]-2-yl)vinyl)-3,3-dimethyl-3H-indol-1-ium iodide, **6m**: Yield 65%; m.p. > 260 °C; ^{1}H-NMR (CDCl$_3$), **δ** 1.04 (t, J =7.2 Hz, 6H), 1.20 (s, 12H), 1.51 (m, 4H), 1.81 (m, 4H), 2.13 (t, J = 5.2 Hz, 2H), 2.75 (s, 4H), 4.04 (t, J =7.2 Hz, 4H), 6.10 (d, J = 14.0 Hz, 2H), 7.07 (d, J = 8 Hz, 2H), 7.20 (m, 8H), 7.61 (m, 3H); ^{13}C-NMR (CDCl$_3$) **δ** 14.0, 20.5, 21.3, 25.0, 27.7, 29.4, 44.4, 48.6, 100.0, 110.3, 122.1, 124.7, 128.2, 128.6, 129.6, 132.1, 138.8, 140.8, 142.3, 148.4, 162.9, 171.4. HRMS (ESI) m/z: calcd. for C$_{44}$H$_{51}$Br$_2$N$_2^+$ 765.2414, obsd 765.2422.

1-Butyl-2-((E)-2-((E)-6-(2-((E)-1-butyl-5-methoxy-3,3-dimethylindolin-2-ylidene)ethylidene)-3,4,5,6-tetrahydro-[1,1'-biphenyl]-2-yl)vinyl)-5-methoxy-3,3-dimethyl-3H-indol-1-ium iodide, **6n**: Yield 66%; m.p. > 260 °C; ^{1}H-NMR (CDCl$_3$) **δ** 1.01 (t, J = 6.8 Hz, 6H), 1.17 (s,12H), 1.46 (m, 4H), 1.80 (m, 4H), 2.07 (s, 2H), 2.68 (s, 4H), 3.82 (s, 6H), 4.03 (t, J = 7.2 Hz, 4H), 6.00 (d, J = 14.0 Hz, 2H) 6.78 (s, 2H), 6.88 (d, J = 8.4 Hz, 2H), 7.03 (d, J = 8.8 Hz, 2H), 7.11 (d, J = 14.0 Hz, 2H), 7.21 (d, J = 6.8 Hz, 2H), 7.57 (m, 3H); ^{13}C-NMR (CDCl$_3$) **δ** 13.9, 20.4, 21.3, 24.8, 27.7, 29.4, 44.6, 48.7, 56.0, 99.4, 109.1, 111.1, 113.1, 128.1, 128.6, 129.4, 130.9, 135.9, 139.0, 142.4, 146.9, 157.9, 161.4, 170.6. HRMS (ESI) m/z: calcd. for C$_{46}$H$_{57}$N$_2$O$_2^+$ 669.4415, obsd 669.4404.

3-Butyl-2-((E)-2-((E)-6-((E)-2-(3-butyl-1,1-dimethyl-1,3-dihydro-2H-benzo[e]indol-2-ylidene)ethylidene)-3,4,5,6-tetrahydro-[1,1'-biphenyl]-2-yl)vinyl)-1,1-dimethyl-1H-benzo[e]indol-3-ium iodide, **6o**: Yield 70%; m.p. >260 °C; ^{1}H-NMR (CDCl$_3$) **δ** 1.03 (t, J = 7.2 Hz, 6H), 1.52 (m, 16H), 1.86 (m, 4H), 2.16 (t, J = 6.0 Hz, 2H), 2.79 (s, 4H), 4.17 (s, 4H), 6.15 (d, J = 14.4 Hz, 2H), 7.34 (m, 6H), 7.45 (d, J = 7.6 Hz, 2H), 7.53 (m, 2H), 7.68 (t, J = 2.8 Hz, 3H), 7.93 (m, 6H); ^{13}C-NMR (CDCl$_3$) **δ** 14.0, 20.4, 21.4, 25.0, 27.2, 29.7, 44.6, 50.4, 99.6, 110.6, 122.0, 124.8, 127.6, 128.1, 128.4, 128.7, 129.6, 130.1, 130.6, 131.7, 133.2, 139.0, 139.7, 147.3, 172.8. HRMS (ESI) m/z: calcd. for C$_{52}$H$_{57}$N$_2^+$ 709.4516, obsd 709.4540.

2.4.4 Stock Solution

Stock solutions of the dyes and standard were prepared by weighing the solid on a 5-digit analytical balance in an amber vial and adding solvent via a class A volumetric pipette to a final concentration of 1.0 mM. The vials were vortexed for 20 s and then sonicated for 15 min to ensure complete dissolution. The stock solutions were stored in a dark freezer at 4 °C when not in use. Working solutions were prepared just prior to use by dilution of the stock to final concentrations.

2.4.5 Method of Determining Molar Absorptivity and Fluorescence Quantum Yield

Stock solutions were used to prepare six dilutions of dyes in ethanol and the standard with concentrations ranging from 1 μM to 4 μM using a class A volumetric pipette in order to maintain absorption between 0.1 and 1.0. The dye solutions were diluted ten-fold for fluorescence in order to minimize inner filter effect. The absorbance spectra of each sample was measured in triplicate from 400nm to 900 nm. The emission spectrum of each sample was measured in triplicate with a 750 nm excitation wavelength.

For molar absorptivity, the absorbance at the wavelength of maximum absorbance (λ_{max}) was determined and the absorbance of each sample at λ_{max} was plotted as a function of dye concentration. The linear regression equation was computed using Microsoft Excel.

The fluorescence quantum yields were determined relative to the indocyanine green standard utilizing the gradient from the plot of integrated fluorescence intensity vs. absorbance (Grad) and the published quantum yield of the standard (φ_S, 13.2% [35]) as per Equation (1):

$$\varphi_D = \varphi_S * Grad_D/Grad_S * \eta^2_S/\eta^2_D \tag{1}$$

2.4.6   HSA Binding Study

A stock solution of **6a** (4×10^{-5} M) and HSA (4×10^{-5} M; Sigma Aldrich, St. Louis, MO, USA) were prepared in PBS buffer. Fluorescence titration with HSA concentrations (0–2 µM) were made by mixing 35 µL dye solution with PBS buffer solution with and without HSA to a total volume of 4000 µL in a fluorescence cuvette to make working solutions of 2 µM dye. Fluorescence spectra were measured in duplicate with excitation at 740 nm and slit widths of 5 nm for both excitation and emission.

2.5   Conclusion

A series of 15 phenyl-substituted heptamethine cyanines was synthesized in good yields and characterized by ^{1}H- and ^{13}C-NMR. Their optical properties including molar absorptivity, fluorescence, Stokes shift, and quantum yield were measured. The optical properties followed similar trends to previously published cyanine dye **MHI-06**. The binding affinity of one of these heptamethine cyanine dyes to HSA was measured to be 5 orders of magnitude lower than our previous synthesized trimethine cyanines further confirming the hypothesis that the binding affinity of the dyes is not only hydrophobicity dependent, but dependent on steric interferences in the binding site [34]. Because albumin is known to bind a variety of compounds, this information on the steric specificity of these binding sites is of potential interest when developing methods to study them.

2.6   Acknowledgment

2.7 References

1. Hyun, H.; Owens, E. A.; Wada, H.; Levitz, A.; Park, G.; Park, M. H.; Frangioni, J. V.; Henary, M.; Choi, H. S., Cartilage-Specific Near-Infrared Fluorophores for Biomedical Imaging. *Angew Chem Int Ed Engl* **2015,** 54, (30), 8648-52.
2. Choi, H. S.; Gibbs, S. L.; Lee, J. H.; Kim, S. H.; Ashitate, Y.; Liu, F.; Hyun, H.; Park, G.; Xie, Y.; Bae, S.; Henary, M.; Frangioni, J. V., Targeted zwitterionic near-infrared fluorophores for improved optical imaging. *Nat Biotechnol* **2013,** 31, (2), 148-53.
3. Ye, Y.; Akers, W.; Xu, B.; Bloch, S.; Odonkor, C.; Achilefu, S., Near-infrared fluorescent divalent RGD ligand for integrin alphavbeta(3)-targeted optical imaging. *Bioorg Med Chem Lett* **2012,** 22, (17), 5405-9.
4. Guosong Hong, A. L. A., and Hongjie Dai, Near-Infrared fluorophores for biomedical imaging *Nature* **2017**, (Optical imaging for diagnostics).
5. Schols, R. M.; Bouvy, N. D.; van Dam, R. M.; Stassen, L. P., Advanced intraoperative imaging methods for laparoscopic anatomy navigation: an overview. *Surg Endosc* **2013,** 27, (6), 1851-9.
6. Mallidi, S.; Luke, G. P.; Emelianov, S., Photoacoustic imaging in cancer detection, diagnosis, and treatment guidance. *Trends Biotechnol* **2011,** 29, (5), 213-21.
7. Yang, X.; Wang, L. V., Photoacoustic tomography of a rat cerebral cortex with a ring-based ultrasonic virtual point detector. *J Biomed Opt* **2007,** 12, (6), 060507.
8. Flanagan, J. H., Jr.; Khan, S. H.; Menchen, S.; Soper, S. A.; Hammer, R. P., Functionalized tricarbocyanine dyes as near-infrared fluorescent probes for biomolecules. *Bioconjug Chem* **1997,** 8, (5), 751-6.
9. George, A.; Patonay, G., Fluorescence studies of carbocyanines using AOTF. *Talanta* **1997,** 45, (2), 285-9.
10. Patonay, G.; Salon, J.; Sowell, J.; Strekowski, L., Noncovalent labeling of biomolecules with red and near- infrared dyes. *Molecules* **2004,** 9, (3), 40-9.
11. Yang, X.; Shi, C.; Tong, R.; Qian, W.; Zhau, H. E.; Wang, R.; Zhu, G.; Cheng, J.; Yang, V. W.; Cheng, T.; Henary, M.; Strekowski, L.; Chung, L. W., Near IR heptamethine cyanine dye-mediated cancer imaging. *Clin Cancer Res* **2010,** 16, (10), 2833-44.
12. Shi, C.; Wu, J. B.; Pan, D., Review on near-infrared heptamethine cyanine dyes as theranostic agents for tumor imaging, targeting, and photodynamic therapy. *J Biomed Opt* **2016,** 21, (5), 50901.
13. Dali Qiu, Y. L., Mengnan Li, Hongbiao Chen, Huaming Li, Near-infrared chemodosimetric probes based on heptamethine cyanine dyes for the "naked-eye" detection of cyanide in aqueous media. *Journal of Luminescence* **2017,** 185, 286-291.
14. Soriano, E.; Holder, C.; Levitz, A.; Henary, M., Benz[c,d]indolium-containing Monomethine Cyanine Dyes: Synthesis and Photophysical Properties. *Molecules* **2015,** 21, (1), E23.
15. Atanas Kurutosa, O. R., Ulyana Tarabara, Valeriya Trusovab, Galyna Gorbenko, Nikolai Gadjev, Todor Deligeorgiev, Novel synthetic approach to near-infrared heptamethine cyanine dyes and spectroscopic characterization in presence of biological molecules. *Journal of Photochemistry and Photobiology A: Chemistry* **2016,** 328, 87-96.
16. Ernst, L. A.; Gupta, R. K.; Mujumdar, R. B.; Waggoner, A. S., Cyanine dye labeling reagents for sulfhydryl groups. *Cytometry* **1989,** 10, (1), 3-10.

17. Honig, B.; Greenberg, A. D.; Dinur, U.; Ebrey, T. G., Visual-pigment spectra: implications of the protonation of the retinal Schiff base. *Biochemistry* **1976,** 15, (21), 4593-9.

18. Ashitate, Y.; Levitz, A.; Park, M. H.; Hyun, H.; Venugopal, V.; Park, G.; El Fakhri, G.; Henary, M.; Gioux, S.; Frangioni, J. V.; Choi, H. S., Endocrine-specific NIR fluorophores for adrenal gland targeting. *Chem Commun (Camb)* **2016,** 52, (67), 10305-8.

19. Hyun, H.; Park, M. H.; Owens, E. A.; Wada, H.; Henary, M.; Handgraaf, H. J.; Vahrmeijer, A. L.; Frangioni, J. V.; Choi, H. S., Structure-inherent targeting of near-infrared fluorophores for parathyroid and thyroid gland imaging. *Nat Med* **2015,** 21, (2), 192-7.

20. Hyun, H.; Wada, H.; Bao, K.; Gravier, J.; Yadav, Y.; Laramie, M.; Henary, M.; Frangioni, J. V.; Choi, H. S., Phosphonated near-infrared fluorophores for biomedical imaging of bone. *Angew Chem Int Ed Engl* **2014,** 53, (40), 10668-72.

21. Kim, S. H.; Park, G.; Hyun, H.; Lee, J. H.; Ashitate, Y.; Choi, J.; Hong, G. H.; Owens, E. A.; Henary, M.; Choi, H. S., Near-infrared lipophilic fluorophores for tracing tissue growth. *Biomed Mater* **2013,** 8, (1), 014110.

22. Owens, E. A.; Henary, M.; El Fakhri, G.; Choi, H. S., Tissue-Specific Near-Infrared Fluorescence Imaging. *Acc Chem Res* **2016,** 49, (9), 1731-40.

23. Valeriy E. Shershov, M. A. S., Viktoriya E. Kuznetsova, Edward N. Timofeev, Olga A. Ivashkina, Ivan S. Abramov, Tatyana V. Nasedkina, Alexander S. Zasedatelev, Alexander V. Chudinov, Near-infrared heptamethine cyanine dyes. Synthesis, spectroscopic characterization, thermal properties and photostability. *Dyes and Pigments* **2013,** 97, (2), 353-360.

24. Lee, H.; Berezin, M. Y.; Tang, R.; Zhegalova, N.; Achilefu, S., Pyrazole-substituted near-infrared cyanine dyes exhibit pH-dependent fluorescence lifetime properties. *Photochem Photobiol* **2013,** 89, (2), 326-31.

25. Lee, H.; Mason, J. C.; Achilefu, S., Heptamethine cyanine dyes with a robust C-C bond at the central position of the chromophore. *J Org Chem* **2006,** 71, (20), 7862-5.

26. Lee, H.; Mason, J. C.; Achilefu, S., Synthesis and spectral properties of near-infrared aminophenyl-, hydroxyphenyl-, and phenyl-substituted heptamethine cyanines. *J Org Chem* **2008,** 73, (2), 723-5.

27. Mohammad, I.; Stanford, C.; Morton, M. D.; Zhu, Q.; Smith, M. B., Structurally modified indocyanine green dyes. Modification of the polyene linker. *Dyes and Pigments* **2013,** 99, (2), 275-283.

28. Jozef Salon, E. W., Aldona Raszkiewicz, Gabor Patonay and Lucjan Strekowski, Synthesis of Benz[e]indolium Heptamethine Cyanines Containing

C-Substituents at the Central Portion of the Heptamethine Moiety. *Journal of Heterocyclic Chemistry* **2005,** 42, 959.

29. Theodore Peters, J., *All About Albumin: Biochemistry, Genetics, and Medical Applications*. Academic: San Diego, California 1995; Vol. 1.

30. Larsen, M. T.; Kuhlmann, M.; Hvam, M. L.; Howard, K. A., Albumin-based drug delivery: harnessing nature to cure disease. *Mol Cell Ther* **2016,** 4, 3.

31. Bernardi, M.; Maggioli, C.; Zaccherini, G., Human albumin in the management of complications of liver cirrhosis. *Crit Care* **2012,** 16, (2), 211.

32. Fasano, M.; Curry, S.; Terreno, E.; Galliano, M.; Fanali, G.; Narciso, P.; Notari, S.; Ascenzi, P., The extraordinary ligand binding properties of human serum albumin. *IUBMB Life* **2005,** 57, (12), 787-96.

33. Ghuman, J.; Zunszain, P. A.; Petitpas, I.; Bhattacharya, A. A.; Otagiri, M.; Curry, S., Structural basis of the drug-binding specificity of human serum albumin. *J Mol Biol* **2005,** 353, (1), 38-52.

34. Beckford, G.; Owens, E.; Henary, M.; Patonay, G., The solvatochromic effects of side chain substitution on the binding interaction of novel tricarbocyanine dyes with human serum albumin. *Talanta* **2012,** 92, 45-52.

35. Rurack, K.; Spieles, M., Fluorescence quantum yields of a series of red and near-infrared dyes emitting at 600-1000 nm. *Anal Chem* **2011,** 83, (4), 1232-42.

36. Chapman, G.; Henary, M.; Patonay, G., The effect of varying short-chain alkyl substitution on the molar absorptivity and quantum yield of cyanine dyes. *Anal Chem Insights* **2011,** 6, 29-36.

37. Caldwell, R. A.; Jacobs, L. D.; Furlani, T. R.; Nalley, E. A.; Laboy, J., Conformationally Dependent Heavy Atom Effect of Chlorine on Alkene Triplet Lifetimes. Experimental and ab Initio Calculations *Journa of the American Chemical Society* **1991,** 144, 1623-1625.

38. Dost, T. L.; Gressel, M. T.; Henary, M., Synthesis and Optical Properties of Pentamethine Cyanine Dyes With Carboxylic Acid Moieties. *Anal Chem Insights* **2017,** 12, 1177390117711938.

39. Toseland, C. P., Fluorescent labeling and modification of proteins. *J Chem Biol* **2013,** 6, (3), 85-95.

40. Waggoner, A., Covalent labeling of proteins and nucleic acids with fluorophores. *Methods Enzymol* **1995,** 246, 362-73.

41. Patonay, G.; Kim, J. S.; Kodagahally, R.; Strekowski, L., Spectroscopic study of a novel bis(heptamethine cyanine) dye and its interaction with human serum albumin. *Appl Spectrosc* **2005,** 59, (5), 682-90.

42. Zhang, Y.; Du, H.; Tang, Y.; Xu, G.; Yan, W., Spectroscopic investigation on the interaction of J-aggregate with human serum albumin. *Biophys Chem* **2007,** 128, (2-3), 197-203.

43. Berezin, M. Y.; Lee, H.; Akers, W.; Nikiforovich, G.; Achilefu, S., Ratiometric analysis of fluorescence lifetime for probing binding sites in albumin with near-infrared fluorescent molecular probes. *Photochem Photobiol* **2007,** 83, (6), 1371-8.

44. Kim, J. S.; Kodagahally, R.; Strekowski, L.; Patonay, G., A study of intramolecular H-complexes of novel bis(heptamethine cyanine) dyes. *Talanta* **2005,** 67, (5), 947-54.

3   THE INCORPORATION OF THE QUINOLINE HETEROCYCLE TO PENTAMETHINE AND HEPTAMETHINE CYANINE DYES

3.1   Introduction

Photodynamic therapy (PDT), as introduced earlier, has raised a great deal of interest as a new and innovative method for treating cancers and other skin diseases. The current PTD methods have shown some success but have left room for improvement. Through the work done by Dr. Grant and other research groups, it has been determined that cyanine dyes are strong candidates in this field. Cyanine dyes act as a contrast agent that induces apoptosis via reactive oxygen species (ROS) generation [1-4]. Although some dyes have shown effective DNA cleavage in preliminary studies there is much room for optimization and the need for large library generation.

Recent work by the Henary and Grant lab have shown that quinoline-based pentamethine dyes are effective for PDT application [5]. The main compounds that proved effective were 4-methyl quinoline-based pentamethine cyanine dyes and bromine substituted 2-methyl pentamethine cyanine dyes. Due to the effectivity of these compounds, it initiated a great deal of interest to further develop these two compound via the introduction of different substituents.

The 2-methyl quinoline heterocycle enables a great deal optimization due to the fact it halogen substituents can be incorporated onto the heterocycle. Since the bromine atom at the 6-position proved effective in previous work, fluorine was introduced into the heterocycle due to the lipophilicity, electronegativity, and small size of the fluorine atom [6]. Along with chemical and physical characteristics of the fluorine atom, it has shown great success upon to its introduction in various other medical application. With the reasons presented, a project was

generated in aims to study the effects of fluorine on the quinoline heterocycle in PDT application.

Although the substituents have proven to be effective at altering the results, the counter-ion can play a vital role in prolonging the triplet state, ultimately making the contrast agent more effective. A relatively common counter-ion for cyanine dyes is the iodine atom, which is a triplet state quencher [7]. The iodine atom is introduced into the dye upon alkylation of heterocycle during the salt synthesis. In order to study the effects of the counter-ion, different alkylating agents and methods were used to study the effects iodine versus other counter-ions to determine the effects the counter ion has on the effectivity of the contrast agent in PDT application.

The quinoline heterocycle yield dyes that are non-fluorescent, it allows the dyes to be used for other application. Due to its structure of the heterocycle, a second double bond contributes to the conjugation, this extra double bond, in comparison the 2,3,3-trimethyl-3H-indole heterocycle, enable the heterocycle to extend the conjugation red-shifting the compounds 50 nm, and 100 nm in the 2-methyl based quinoline cyanine dyes and 4-methyl quinoline cyanine dyes; respectively. Many pentamethine dyes have been made using these dyes; however, the introduction of these heterocycles to heptamethine cyanine dyes is new. The benefits of synthesizing quinoline-based heptamethine dyes are the far red-shift that is observed pushing these dyes to the near-infrared II window (1000 nm-1700 nm) range. These dyes offer a great contrast with respect to endogenous tissue in a biological application and unveil a largely untapped field in the cyanine dye field. These compounds can be used for various application and offer a great deal variance due to the many the points of modifications they provide.

3.2 Introduction References

1. James, N. S.; Chen, Y.; Joshi, P.; Ohulchanskyy, T. Y.; Ethirajan, M.; Henary, M.; Strekowsk, L.; Pandey, R. K., Evaluation of polymethine dyes as potential probes for near infrared fluorescence imaging of tumors: part - 1. Theranostics 2013, 3, (9), 692-702.
2. James, N. S.; Ohulchanskyy, T. Y.; Chen, Y.; Joshi, P.; Zheng, X.; Goswami, L. N.; Pandey,R. K., Comparative tumor imaging and PDT Efficacy of HPPH conjugated in the mono- and di-forms to various polymethine cyanine dyes: part - 2. Theranostics 2013, 3, (9), 703-18.
3. Lu, M.; Kang, N.; Chen, C.; Yang, L.; Li, Y.; Hong, M.; Luo, X.; Ren, L.; Wang, X., Plasmonic enhancement of cyanine dyes for near-infrared light-triggered photodynamic/photothermal therapy and fluorescent imaging. Nanotechnology 2017, 28, (44), 445710.
4. Noh, I.; Lee, D.; Kim, H.; Jeong, C. U.; Lee, Y.; Ahn, J. O.; Hyun, H.; Park, J. H.; Kim, Y. C., Enhanced Photodynamic Cancer Treatment by Mitochondria-Targeting and Brominated Near-Infrared Fluorophores. Adv Sci (Weinh) 2018, 5, (3), 1700481.
5. Holder, C., Synthetic development and investigation of cyanine dyes and their interaction with duplex dna. 2016.
6. Shah, P.; Westwell, A. D., The role of fluorine in medicinal chemistry. J Enzyme Inhib Med Chem 2007, 22, (5), 527-40.
7. Nilsson, R.; Merkel, P. B.; Kearns, D. R., Kinetic properties of the triplet states of methylene blue and other photosensitizing dyes. Photochem Photobiol 1972,16,(2),109-16.

3.3 Experimental Section

3.3.1 Materials

All chemicals and solvents were of American Chemical Society grade or HPLC purity and were used as received. HPLC grade ethanol *was purchased from Sigma-Aldrich (St. Louis, MO, USA). All other chemicals were purchased from Fisher Scientific (Pittsburgh, PA, USA) or Acros Organics (Pittsburgh, PA, USA). The reactions were followed using silica gel 60 F254 thin layer chromatography plates (Merck EMD Millipore, Darmstadt, Germany). The 1H-NMR and 13C-NMR spectra were obtained using high-quality Kontes NMR tubes (Kimble Chase, Vineland, NJ, USA) rated to 500 MHz and were recorded on an Avance spectrometer (Bruker, Billerica, MA; 400 MHz for 1H and 100 MHz for 13C) in* DMSO-d6, acetone-d6 *CD3Cl-d3. High-resolution accurate mass spectra (HRMS) were obtained at the Georgia State University Mass Spectrometry Facility using a Q-TOF micro (ESI-Q-TOF) mass spectrometer (Waters, Milford, MA, USA). All compounds tested were >95% pure. Infrared spectra (FT-IR) were obtained using a Spectrum 100 spectrometer (PerkinElmer, Duluth, GA, USA) (see Supplementary Materials). UV-Vis/NIR absorption spectra were recorded on a Cary 50 spectrophotometer (Varian, Palo Alto, CA, USA) interfaced with Cary WinUV Scan Application v3.00 using VWR disposable polystyrene cuvettes with a 1 cm pathlength.. All spectral measurements were recorded at room temperature. The data analysis and calculations were carried out using Microsoft Excel (Microsoft Corporation, Redmond, WA, USA).*

3.3.2   Scheme of the pentamethine fluorinated quinoline-based cyanine dyes
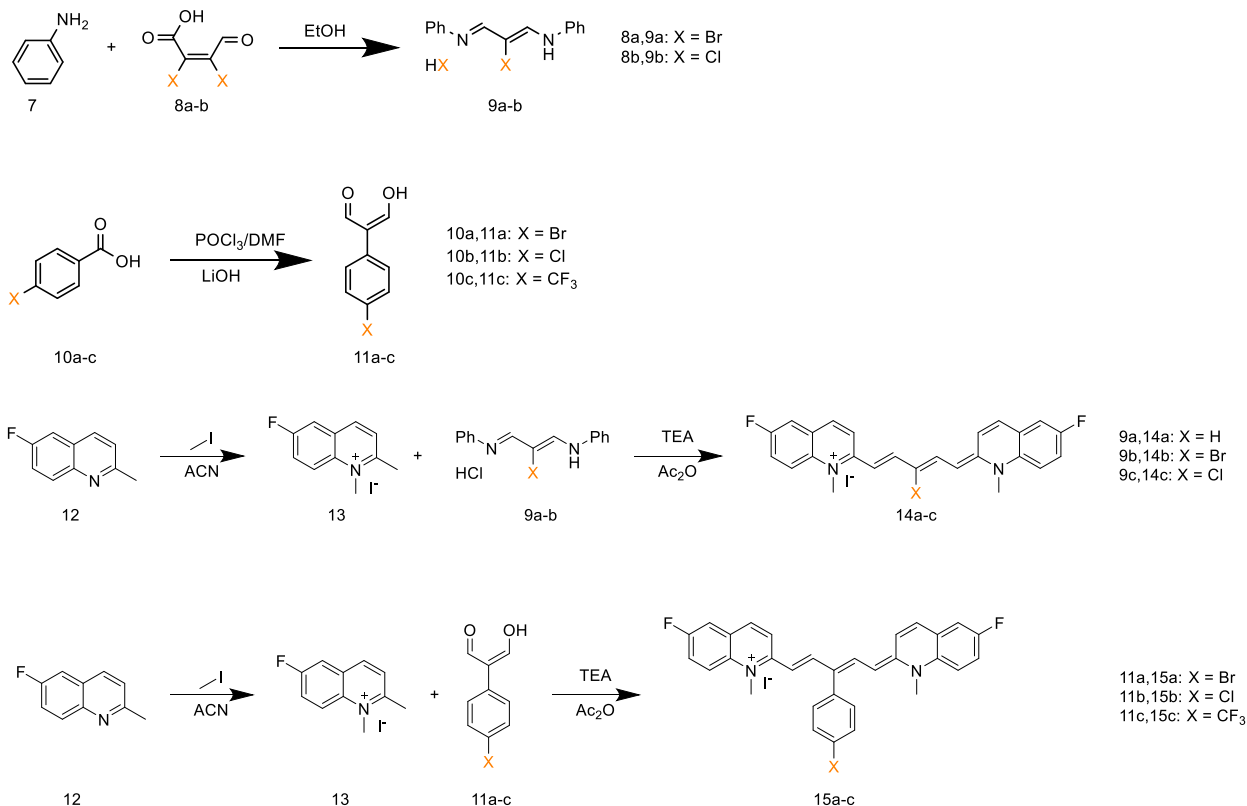
3.3.3   The synthesis of the pentamethine fluorinated quinoline-based cyanine dyes

Linkers (9a-b) were prepared following the procedure published by the Henary lab []. A

solution of a 2.5 molar equivalence of aniline (7) dissolved in ethanol was added dropwise to a 1

molar equivalence of 2,3-dichloro-4-oxo-but-2-enoic acid dissolved in ethanol solution. The

mixture was heated for 5 h at 60 °C. The reaction was monitored using a reverse phase thin layer

chromatography (TLC) (mobile phase: DCM), upon completion of the reaction, the mixture was

poured into an excess of ethyl ether and. The precipitate was vacuum filter and dried under

reduced pressure. A golden precipitate was assumed pure and used without further purification.

Linkers (11a-c) were prepared by reacting a solution of DMF dissolved in DCM, POCl$_3$

was then added dropwise at 0 °C. Substituted benzoic acid was then added dropwise and the

reaction was refluxed for 4 h. The reaction was monitored using TLC (mobile phase: Ethyl

acetate/hexanes). The solution was allowed to cool and poured over ice. Lithium hydroxide was added, precipitating the product. The solid was vacuumed filtered, allowed dry overnight and used without further purification.

The synthesis of the fluorinated quinoline salt was prepared with respect to how many other heterocyclic salts. The 6-fluoro quinoline heterocycle (12) was purchased and used without further purification. A 1 molar equivalence of the fluorinated heterocycle and an excess of methyl iodide was dissolved in acetonitrile and heated to 100 °C in a sealed tube for 12 h. The reaction was allowed to cool, poured over chilled ethyl ether and vacuum filtered. A yellow precipitate (13) was afforded and used without further purification.

The synthesis of the dyes (14a-c and 15a-c) were attempted using conventional heat which resulted in no reaction. Next, the reaction was done using microwave radiation. A 2 molar equivalence of the fluorinated heterocyclic salt (13), a 2 molar equivalence of triethylamine (TEA), and a 1 molar equivalence of linkers (9a-c, 11a-c) were reacted in a microwave reactor (100 °C, 115 W, 5 min). The reaction was monitored using UV-Vis spectroscopy. The reaction mixture was precipitated using ethyl ether and vacuum filtered. The crude product was recrystallized in ethanol and filtered again yielding dyes (14a-c, 15a-c).

3.3.4   *Scheme of the pentamethine quinoline-based cyanine dyes with varying counter-ions*
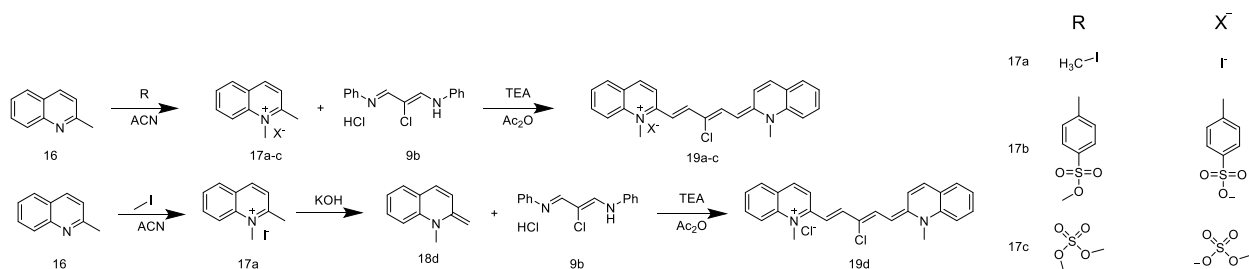
3.3.5 The synthesis of the pentamethine quinoline-based cyanine dyes with varying counter-ions

The 2-methyl quinoline (16) heterocycle was methyl alkylated using four different synthetic procedures to obtain varying counter-ions. In a 1:1 molar equivalence the heterocycle was reacted with methyl iodide, methyl 4-methylbenzenesulfonate, and dimethyl sulfoxide. The reaction was done using acetonitrile as solvent and heated to 100 °C for 12-24 h. Upon completion, ethyl ether was added to the reaction mixture yielding 1,2-dimethyl quinoline heterocyclic salts 17a-c and assumed pure with no further purification. In a 2:1:2 molar equivalence, salts 17a-c, linker 9b, and trimethylamine were dissolved in acetic anhydride and heated to 80 °C for 1 h. The reaction was monitored using UV-Vis spectroscopy, and upon completion was allowed to cool to room temperature and poured into an excess amount of ethyl ether. The crude precipitate was collected by vacuum filtration and recrystallized, affording pure product 19a-c. In order to obtain compound 19d, salt 17a was deprotonated in an aqueous solution of KOH, vacuum filtered and allowed to dry overnight yielding compound 18d. The same synthetic procedure for dyes 19a-c was followed to synthesize compound 19d.

3.3.6 Scheme of heptamethine quinoline-based cyanine dyes
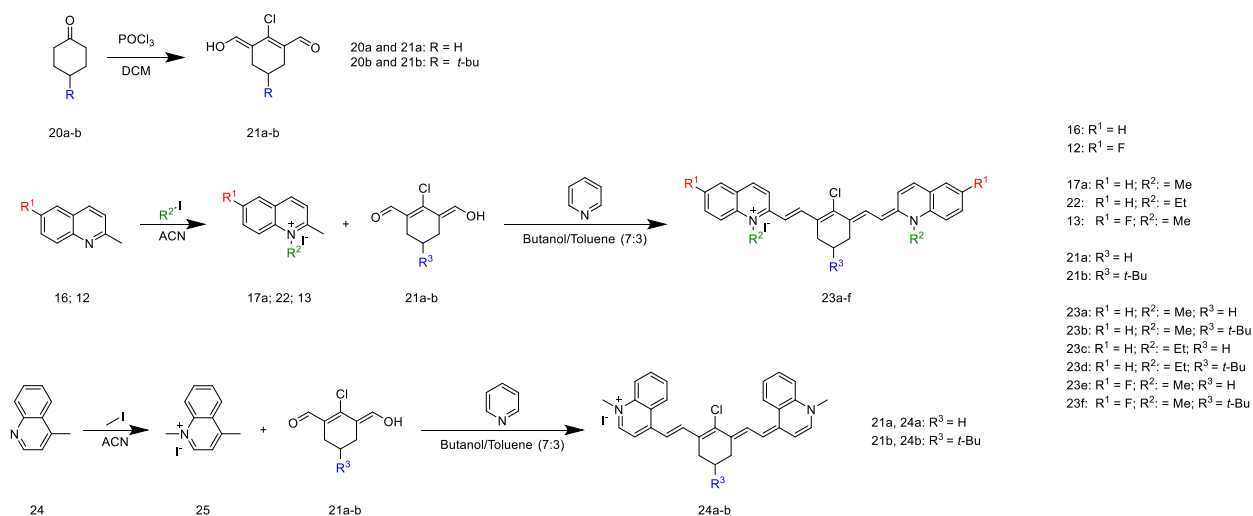
3.3.7 *The synthesis of heptamethine quinoline-based cyanine dyes*

The synthetic procedures for the bis-aldehyde linkers 20a-b were done using the procedures proposed by the Henary lab. First, a solution of DMF dissolved in DCM was allowed to cool to 0 °C. POCl₃ was then added to the solution dropwise over a course of 30 min. cyclohexone (20a) or *t*-butyl cyclohexone (20b) was added dropwise over a course 15 min, while the temperature was maintained at 0 °C. The reaction mixture was allowed to stir for 15 min then refluxed for 4 h. The reaction mixture was poured over ice and remained in the aqueous solution for 12 h, affording a yellow precipitate (21a-b). The linkers were used without further purification.

The heterocyclic salts previously used (17a and 13) were utilized again for the heptamethine cyanine dye series. 2-methyl quinoline (16) and 4-methyl quinoline (24) was reacted with ethyl iodide and methyl iodide, respectively. The reaction mixture was dissolved in acetonitrile and heated to 100 °C for 12 h. The reaction was allowed to cool and poured into an excess of ethyl ether yielding a crude yellow precipitate which was then collected using vacuum filtration. The ethyl alkylated heterocyclic salt (22) and methyl alkulated heterocyclic salt (25) was used without further purification.

 The heptamethine quinoline-based cyanine dye synthetic procedure is new but followed similar procedures previously used in the synthesis of squarine dyes. 1 molar equivalence of heterocyclic salts (17a, 22, 13 and 25) was added to a 1 molar equivalence of vilsmier linkers (21a-b) and dissolved in a 7:3 volumetric equivalence of toluene and butanol. The reaction vessel was equipped with a Dean-Stark apparatus filled with toluene and condenser. The reaction mixture was heated to 130 °C for 4 h. Another 1 molar equivalence of the same salts and a 2 molar equivalence pyridine was added to the reaction mixture and heated for another 3 h. The

reaction was monitored under UV-Vis spectroscopy. Upon completion, the reaction mixture was allowed to cool and added to an excess of ethyl ether yielding the crude precipitate which was collected using vacuum filtration. The crude compound was recrystallized using ethanol and washed with water, acetone, and methanol yielding pure compounds 23a-f and 24a-b.

3.3.8 Characterization

6-fluoro-2-((1*E*,3*E*)-5-((*E*)-6-fluoro-1-methylquinolin-2(1*H*)-ylidene)penta-1,3-dien-1-yl)-1-methylquinolin-1-ium iodide, 14a; Yield 69%; mp: > 260 °C; ^{1}H NMR (400 MHz, DMSO) δ 4.01 (s, 6 H), 6.30 (d, *J* = 12 Hz, 2 H), 7.23 (m, 2 H), 7.78 (dd, 2 H), 7.80 (t, 1 H), 7.98 (d, *J* = 9.2 Hz 2 H), 8.08 (dd, 2 H), 8.17 (d, *J* = 9.2 Hz 2 H), 8.31 (d, *J* = 12.8 Hz 2 H); ^{19}F NMR (376 MHz, DMSO/HFB) δ 163.46.

2-((1*E*,3*Z*)-3-bromo-5-((*E*)-6-fluoro-1-methylquinolin-2(1*H*)-ylidene)penta-1,3-dien-1-yl)-6-fluoro-1-methylquinolin-1-ium iodide, 14b, Yield 22%; mp: > 260 °C; ^{1}H NMR (400 MHz, DMSO) δ 3.98 (s, 6 H), 6.27 (d, *J* = 12.8 Hz, 2 H), 7.69 (m, 2 H), 7.77 (dd, 2 H), 7.96 (d, *J* = 9.6 Hz, 2 H), 8.05 (dd, 2 H), 8.14 (d, *J* = 9.6 Hz, 2 H), 8.28 (d, *J* = 12.8 Hz, 2 H)); ^{19}F NMR (376 MHz, DMSO/HFB) δ 162.91.

2-((1*E*,3*Z*)-3-chloro-5-((*E*)-6-fluoro-1-methylquinolin-2(1*H*)-ylidene)penta-1,3-dien-1-yl)-6-fluoro-1-methylquinolin-1-ium iodide, 14c, Yield 75%; mp: > 260 °C; ^{1}H NMR (400 MHz, DMSO) δ 4.00 (s, 6 H), 6.32 (d, *J* = 13.2 Hz, 2 H), 7.71 (m, 2 H), 7.79 (dd, 2 H), 7.96 (d, *J* = 9.6 Hz, 2 H), 8.07 (dd, 2 H), 8.19 (m, 2 H); ^{19}F NMR (376 MHz, DMSO/HFB) δ 163.01.

2-((1*E*,3*Z*)-3-(4-bromophenyl)-5-((*E*)-6-fluoro-1-methylquinolin-2(1*H*)-ylidene)penta-1,3-dien-1-yl)-6-fluoro-1-methylquinolin-1-ium iodide, 15a, Yield 65%; mp: > 260 °C; ^{1}H NMR (400 MHz, DMSO) δ 3.71 (s, 6 H), 5.86 (d, *J* = 14 Hz, 2 H), 7.36 (d, *J* = 8.4 Hz, 2 H), 7.63 (d, *J* = 3.2

Hz, 2 H), 7.67 (m, 4 H), 7.75 (m, 2 H), 7.93 (dd, 2 H), 8.06 (m, 4 H), 8.20 (d, J = 14 Hz, 2 H); [19]F

NMR (376 MHz, DMSO/HFB) δ 162.88.

6-fluoro-2-((1E,3Z)-5-((E)-6-fluoro-1-methylquinolin-2(1H)-ylidene)-3-(4-

(trifluoromethyl)phenyl)penta-1,3-dien-1-yl)-1-methylquinolin-1-ium iodide, 15b, Yield 42%;

mp: > 260 °C; ^{1}H NMR (400 MHz, DMSO) δ 3.68 (s, 6 H), 5.82 (d, J = 13.6 Hz, 2 H), 7.59 (dd,

2 H), 7.64 (dd, 2 H), 7.79 (m, 4 H), 7.91 (s, 4 H), 8.22 (d, J = 14 Hz, 2 H); ^{19}F NMR (376 MHz,

DMSO/HFB) δ 162.84, 162.78.

2-((1E,3Z)-3-chloro-5-((E)-6-fluoro-1-methylquinolin-2(1H)-ylidene)penta-1,3-dien-1-yl)-6-

fluoro-1-methylquinolin-1-ium iodide, 14c, Yield 65%; mp: > 260 °C; ^{1}H NMR (400 MHz,

DMSO) δ 3.98 (s, 6 H), 6.29 (d, J = 12.8 Hz, 2 H), 7.73 (m, 2 H), 7.77 (dd, 2 H), 7.99 (d, J = 9.6

Hz, 2 H), 8.15 (dd, 2 H), 8.19 (d, J = 9.6 Hz, 2 H), 8.32 (d, J = 12.8 Hz, 2 H)); ^{19}F NMR (376

MHz, DMSO/HFB) δ 163.91.

2-((1E,3Z)-3-chloro-5-((E)-1-methylquinolin-2(1H)-ylidene)penta-1,3-dien-1-yl)-1-

methylquinolin-1-ium iodide, 17a, yield 70%, mp: 218-220 °C; ^{1}H NMR (400 MHz, DMSO) δ

3.98 (s, 6 H), 6.32 (d, J = 14.8 Hz, 2 H), 7.53 (t, J = 8 Hz, 2 H), 7.81 (t, J = 7.2 Hz, 2 H), 7.91 (

dd, 4 H), 8.00 (d, J = 8 Hz, 2 H), 8.21 (dd, 4 H).

2-((1E,3Z)-3-chloro-5-((E)-1-methylquinolin-2(1H)-ylidene)penta-1,3-dien-1-yl)-1-

methylquinolin-1-ium 4-methylbenzenesulfonate, 17b, yield 67%, mp: 219-221 °C; ^{1}H NMR

(400 MHz, DMSO) δ 2.29 (s, 3 H), 3.99 (s, 6 H), 6.30 (d, J = 12.8 Hz, 2 H), 7.11 (d, J = 7.6 Hz,

2 H), 7.493 (dd, 4 H), 7.84 (m, 8 H), 7.99 (dd, 4 H).

2-((1E,3Z)-3-chloro-5-((E)-1-methylquinolin-2(1H)-ylidene)penta-1,3-dien-1-yl)-1-

methylquinolin-1-ium methyl sulfate, 17c, yield 66%, mp: 217-219 °C; ^{1}H NMR (400 MHz,

DMSO) δ 3.38 (s, 3 H), 4.00 (s, 6 H), 6.32 (d, *J* = 13.2 Hz, 2 H), 7.51 (t, *J* = 7.2 Hz, 2 H), 7.79 (t, *J* = 13.2 Hz, 2 H), 7.89 (dd, 4 H), 7.92 (d, 2 H), 8.01 (dd, 4 H).

2-((1*E*,3*Z*)-3-chloro-5-((*E*)-1-methylquinolin-2(1*H*)-ylidene)penta-1,3-dien-1-yl)-1-methylquinolin-1-ium chloride, 17d, yield 58%, mp: 218-219 °C; ^{1}H NMR (400 MHz, DMSO) δ 4.01 (s, 6 H), 6.33 (d, *J* = 14.8 Hz, 2 H), 7.54 (t, *J* = 8 Hz, 2 H), 7.82 (t, *J* = 7.2 Hz, 2 H), 7.92 (dd, 4 H), 8.03 (d, *J* = 8 Hz, 2 H), 8.21 (dd, 4 H).

4-((E)-2-((E)-2-chloro-3-(2-((Z)-1-methylquinolin-4(1H)-ylidene)   ethylidene)cyclohex-1-en-1-yl)vinyl)-1-methylquinolin-1-ium iodide, 24a, yields 75%, mp: >220 °C; ^{1}H NMR (400 MHz, DMSO) δ 1.86 (t, *J* = , 2 H), 2.78 (t, *J* =, 4 H), 3.94 (s, 6 H), 6.94 (d, *J* =, 2 H), 7.30 (d, *J* =, 2 H), 7.57 (t, *J* = , 2 H), 7.80 (m, 4 H), 7.96 (d, *J* =, 2 H), 8.03 (d, *J* =, 2 H), 8.42 (d, *J* =, 2 H); HRMS (ESI) *m*/*z*: calcd. for $C_{30}H_{28}ClN_2^+$ 451.1925, obsd 451.1946.

4-((E)-2-((E)-5-(tert-butyl)-2-chloro-3-(2-((Z)-1-methylquinolin-4(1H)-ylidene)ethylidene)cyclohex-1-en-1-yl)vinyl)-1-methylquinolin-1-ium iodide, 24b, yields 77%, mp: >220 °C; ^{1}H NMR (400 MHz, DMSO) δ 1.11 (s, 9 H), 1.50 (t, 1 H), 2.24 (t, *J* = , 2 H), 3.05 (d, 4 H), 4.00 (s, 6 H), 7.03 (d, *J* =, 2 H), 7.36 (d, *J* =, 2 H), 7.63 (t, *J* = , 2 H), 7.84 (m, 4 H), 8.00 (d, *J* =, 2 H), 8.03 (d, *J* =, 2 H), 8.53 (d, *J* =, 2 H); HRMS (ESI) *m*/*z*: calcd. for $C_{34}H_{36}ClN_2^+$ 508.1255 obsd 254.1307 Z=2.

2-((E)-2-((E)-2-chloro-3-(2-((E)-1-methylquinolin-2(1H)-ylidene)ethylidene)cyclohex-1-en-1-yl)vinyl)-1-methylquinolin-1-ium iodide, 23a, yields 72%, mp: >220 °C; ^{1}H NMR (400 MHz, DMSO) δ 1.86 (t, *J* = , 2 H), 2.78 (t, *J* =, 4 H), 3.94 (s, 6 H), 6.31 (d, *J* =, 2 H), 7.45 (t, *J* =, 2 H), 7.74 (t, *J* = , 2 H), 7.88 (m, 6 H), 8.03 (m, 4 H) HRMS (ESI) *m*/*z*: calcd. for $C_{30}H_{28}ClN_2^+$ 452.0175, obsd 452.1949.

2-((E)-2-((E)-5-(tert-butyl)-2-chloro-3-(2-((E)-1-methylquinolin-2(1H)-ylidene)ethylidene)cyclohex-1-en-1-yl)vinyl)-1-methylquinolin-1-ium iodide 23b, yields 77%, mp: >220 °C; ^{1}H NMR (400 MHz, DMSO) δ 1.11 (s, 9 H), 1.50 (t, 1 H), 2.24 (t, J = , 2 H), 3.05 (d, 4 H), 4.00 (s, 6 H), 7.03 (d, J =, 2 H), 7.36 (d, J =, 2 H), 7.63 (t, J = , 2 H), 7.84 (m, 4 H), 8.00 (d, J =, 2 H), 8.03 (d, J =, 2 H), 8.53 (d, J =, 2 H); HRMS (ESI) m/z: calcd. for $C_{34}H_{36}ClN_2^+$ 508.1255 obsd 254.1306 (z=2).

2-((E)-2-((E)-2-chloro-3-(2-((E)-1-ethylquinolin-2(1H)-ylidene)ethylidene)cyclohex-1-en-1-yl)vinyl)-1-ethylquinolin-1-ium iodide, 23c, yields 66%, mp: >220 °C; ^{1}H NMR (400 MHz, DMSO) δ 1.06 (t, J = , 6 H), 1.83 (t, 2 H) 2.63 (m, 4 H), 4.37 (m, 4 H), 6.24 (d, J =, 2 H), 7.45 (t, J =, 2 H), 7.85 (t, J =, 2 H), 7.89 (m, 6 H), 8.03 (d, J =, 2 H), 8.11 (d, J =, 2 H); HRMS (ESI) m/z: calcd. for $C_{32}H_{32}ClN_2^+$ 480.0715 obsd 479.2234.

2-((E)-2-((E)-5-(tert-butyl)-2-chloro-3-(2-((E)-1-ethylquinolin-2(1H)-ylidene)ethylidene)cyclohex-1-en-1-yl)vinyl)-1-ethylquinolin-1-ium iodide, 23d, yields 67%, mp: >220 °C; ^{1}H NMR (400 MHz, DMSO) δ 1.08 (s, 9H), 1.41 (t, 6 H), 1.44 (t, 1 H), 2.22 (t, J = , 2 H), 2.91 (d, 2 H), 4.56 (m, 4 H), 6.28 (d, J =, 2 H), 7.46 (t, J =, 2 H), 7.61 (t, J =, 2 H), 7.91 (m, 6 H), 8.05 (m, 4 H); HRMS (ESI) m/z: calcd. for $C_{36}H_{40}ClN_2^+$ 536.1795 obsd 268.1462 (z=2).

2-((E)-2-((E)-2-chloro-3-(2-((E)-6-fluoro-1-methylquinolin-2(1H)-ylidene)ethylidene)cyclohex-1-en-1-yl)vinyl)-6-fluoro-1-methylquinolin-1-ium iodide 23e, yields 55%, mp: >220 °C; ^{1}H NMR (400 MHz, DMSO) δ 1.86 (br, 2 H), 2.69 (br, 4 H), 3.91 (s, 6 H), 6.24 (d, J =, 2 H), 7.58 (t, J =, 2 H), 7.70 (d, J =, 2 H), 7.95 (m, 8 H); ^{19}F NMR (376 MHz, DMSO/HFB) δ 116.84.

2-((E)-2-((E)-5-(tert-butyl)-2-chloro-3-(2-((E)-6-fluoro-1-methylquinolin-2(1H)-ylidene)ethylidene)cyclohex-1-en-1-yl)vinyl)-6-fluoro-1-methylquinolin-1-ium iodide 23f, yields 55%, mp: >220 °C; ^{1}H NMR (400 MHz, DMSO) δ 1.08 (s, 9 H), 1.49 (br, 1 H), 2.91 (br, 2 H),

3.92 (s, 6 H), 6.25 (d, $J =$, 2 H), 7.57 (br, 2 H), 7.70 (br, 2 H), 8.00 (m, 8 H)); ^{19}F NMR (376 MHz, DMSO/HFB) δ 162.77.

3.3.9   Optical Properties

Stock solutions of the dyes and standard were prepared by weighing the solid on a 5-digit analytical balance in an amber vial and adding solvent via a class A volumetric pipette to a final concentration of 1.0 mM. The vials were vortexed for 20 s and then sonicated for 15 min to ensure complete dissolution. The stock solutions were stored in a dark freezer at 4 °C when not in use. Working solutions were prepared just prior to use by dilution of the stock to final concentrations.

Stock solutions were used to prepare six dilutions of dyes in ethanol and the standard with concentrations ranging from 1 μM to 4 μM using a class A volumetric pipette in order to maintain absorption between 0.1 and 1.0. The dye solutions were diluted ten-fold for fluorescence in order to minimize the inner filter effect. The absorbance spectra of each sample were measured in triplicate from 400nm to 900 nm. The emission spectrum of each sample was measured in triplicate with a 750 nm excitation wavelength.

For molar absorptivity, the absorbance at the wavelength of maximum absorbance ($λ_{max}$) was determined and the absorbance of each sample at $λ_{max}$ was plotted as a function of dye concentration. The linear regression equation was computed using Microsoft Excel.

3.4   Results and Discussion

3.4.1   Optical Properties

Table 3.1: Absorbance data of the fluorinated quinoline-based pentamthine dyes

Dyes	λ_{abs} (nm)	ε (L·mol^{-1} · cm^{-1})
14a	718	161,000
14b	701	188,000
14c	703	191,000
15a	709	110.000
15b	711	111,000
15c	709	222,000

Quinoline based pentamethine cyanine dyes absorb at 715 nm with a molar absorptivity value of 141,000 (L · mol^{-1} · cm^{-1}) [14]. Upon introduction of fluorine to the heterocycle, a 100 nm increase to the absorbance wavelength and an increase of 20,000 (L · mol^{-1} · cm^{-1}) to the molar absorptivity was observed. The introduction of a bromine and chlorine atom to the central carbon of the polymethine bridge, to the fluorine-substituted quinoline-based pentamethine cyanine dyes, decreased the absorbance value by 19 nm and 15 nm, respectively; however, increases the molar absorptivity by 26,000 (L · mol^{-1} · cm^{-1}) and 30,000 (L · mol^{-1} · cm^{-1}), respectively. Phenyl bromide and phenyl chloride substituents incorporated to the polymethine bridge has little variance in comparison to each other, but with respect to the unsubstituted straight chain linker 14a, observed a 9 nm and 7 nm decreases to absorbance values, as well as a 51,000 (L · mol^{-1} · cm^{-1}) and 50,000 (L · mol^{-1} · cm^{-1}) decrease to the molar absorptivity, respectively. Unsuspectedly, however, the introduction of (trifluoromethyl) benzene increased the molar absorptivity by 61,000 (L · mol^{-1} · cm^{-1}) in comparison to 14a. This could be due to the decreased aggregation of the compounds due to three fluorine atoms, along with increase

electron withdrawing ability of the fluorine atoms from the phenyl ring, leading it to donate even

more electrons to polymethine bridge.

Table 3.2 Absorbance data of the quinoline-based heptamthine dyes

Dyes	λ_{abs} (nm)	ε (L $\cdot$ mol^{-1} $\cdot$ cm^{-1})
24a	953	119,000
24b	954	133,000
23a	847	111,000
23b	849	170,000
23c	851	215,000
23d	855	217,000
23e	856	100,000
23f	859	125,000

Quinoline based cyanine dyes observe 100 nm shift based on the position of the methyl

group of the heterocycle. 4-methyl quinoline dyes have absorbance values approximately 100 nm

more (redshifted) versus the dyes that contain 2-methyl quinoline heterocycles due to the extra

double bond adding to the conjugation. Compounds 63 and 64 both incorporated the 4-methyl

quinoline heterocycles and had absorbance values in the 953 and 954 nm range. The addition of

the *t*-butyl group to the bisaldehyde vilsmier heptamethine linker increases the absorbance by 1-2

nm throughout the series of dyes. Compounds with 2-methyl quinoline that contained a methyl

substituent of the nitrogen atom of the heterocycle absorbed at 847 nm, increasing the methyl to

an ethyl increased the absorbance to 851 nm. Again the introduction of the fluorine substituent

redshifted the absorbance to 859 nm. Molar absorptivity was enhanced upon the introduction of

the *t*-butyl group by 14,000 (L $\cdot$ mol^{-1} $\cdot$ cm^{-1}), 59,000 (L $\cdot$ mol^{-1} $\cdot$ cm^{-1}), 2,000 (L $\cdot$ mol^{-1} $\cdot$

cm^{-1}), and 25,000 (L $\cdot$ mol^{-1} $\cdot$ cm^{-1}) for the 4-methyl quinoline, 2-methyl quinoline with methyl

substituent off the nitrogen of the heterocycle, 2-methyl quinoline with ethyl substituent off the

nitrogen of the heterocycle, and the fluorinated compound, respectively. With respect to the

compounds without the *t*-butyl group, compound (ethyl) observed a significantly higher

absorptivity in comparison to the 4-methyl quinoline, 2-methyl quinoline with the methyl group,

and the fluorinated series. This trend is parallel with previously synthesized series.

3.4.2   *Photodynamic therapy data*

Photodynamic therapy (PDT) preliminary data determines the degree of reactive oxygen

species generation and ultimately the effectiveness of certain contrast agents for the application

by using plasmid DNA in solution with the contrast agent. The data results determine multiple

aspects of the dye, laser, and solution. To determine if the contrast agent alone is cytotoxic,

which is an undesirable results; the dye is introduced to the DNA without a laser radiation

("dark" slots). The absence of laser prevents the dye from going into the excited state and

prevents the dye from ROS generation. The other control groups are the laser without the dye to

determine that the laser is not inducing the DNA damage (control light: not seen in the diagram),

and finally, control dark state to assure that the buffer solution is not damaging DNA ("control

dark" slot). Testing the effectivity of the compounds is determined by quantifying the degree of

cleavage of the plasmid DNA. The two types of cleavage observed is linear cleavage (blot with

largest RF) where the plasmid DNA is completely cleaved and nicked where the one strand is

nicked. Although linear cleavage is more effective, the accumulation of enough nicked DNA

(middle plot) is sufficient in leading the cells to apoptosis.

A few of the fluorinated quinoline-based pentamethine dyes with varying linkers that is

substituted at the central carbon with bromine, bromobenzene, and trifluoro methyl benzene were

tested for their ability to cleave plasmid DNA.
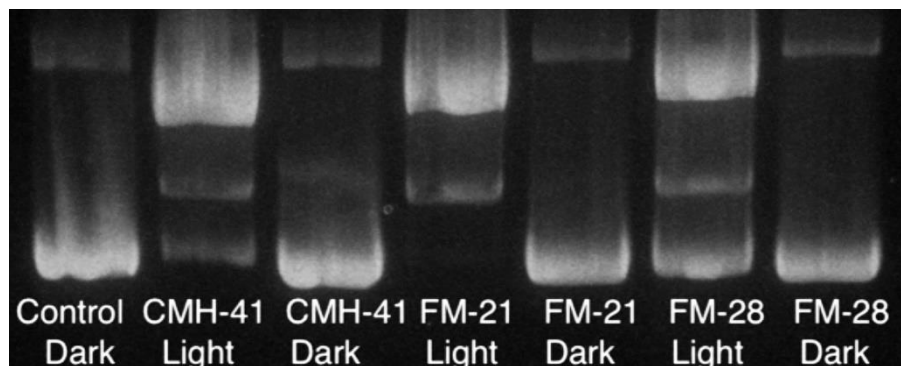
Figure 3.1 PDT gel image (FM-21=14b; FM 29=15a). 38 μM b.p of pUC19 plasmid, 25 μM dye, 30 min irradiation 638 nm. CMH-41 was syneyhsized by Cory Holder (see: Holder thesis) Data Obtained by Dr. Grant's laboratory
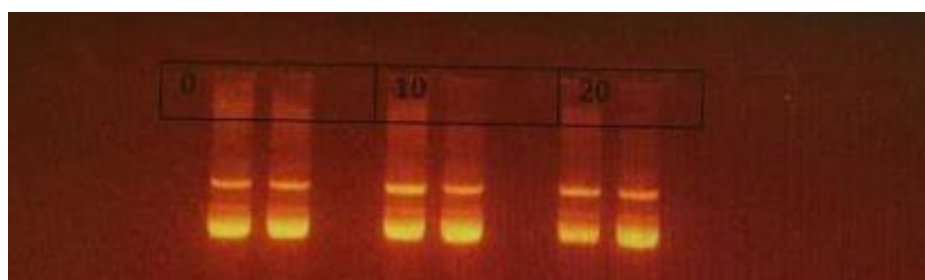
Figure 3.2 PDT gel image of 15c with varying concentrations. Data obtained by Dr. Grant's laboratory.

The varying counter-ions pentamethine dyes were tested as well. Cuvette samples of

bromine (14b) in comparison to bromobenzene (15a) show that the bromide substituent is more

effective with a greater deal of nicked cleavage. The trifluoro methyl benzene (15c) results

indicated that the compound yielded insufficient DNA cleavage. The dyes with differing

counter-ions continuously showed the chloride counter-ion (19d) is most effective that iodide

which is more effective than the organic counter-ions (19b-c). This demonstrates the versatility

of cyanine dyes due to their multiple sites of modifications, which allows for optimization for the

respected application.

1	2	3	4	5	6	7	8
17a	17a	19d	19d	17b	17b	17c	17c
Light	Dark	Light	Dark	Light	Dark	Light	Dark
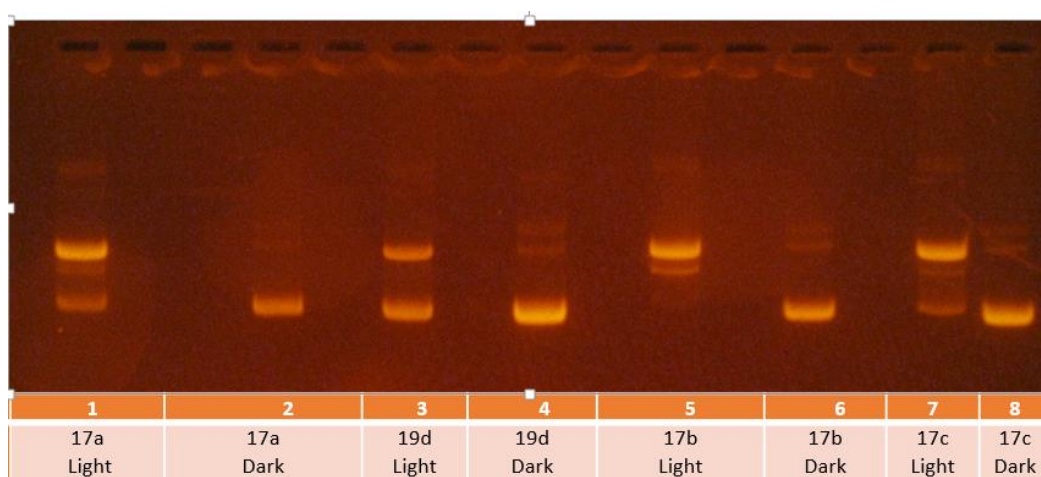
3.5   Conclusion

The quinoline heterocycle has proven to be an effective addition to the cyanine dyes scaffold

due to the effects it has on the optical properties. The structure of the heterocycle contributes an

extra double bond to the conjugation of the dye yielding a further red-shifted compound. The

lack fluoresces enables it to be used in PDT application. The versatility of the dyes enables the

addition of substituents to multiple locations on the dye which allows for the synthesis of

multiple derivatives and tailoring for the desired use. Here the focus was to introduce a fluorine

atom into the heterocycle for PDT application due to the pharmacological benefits fluorine has

had in previous research. Next, the effects of iodide, a common counter-ion of cyanine dyes, was

studied due to the triplet state quenching it provides. This quenching is an undesirable factor for

PDT   *Figure 3.3 PDT gel image for the iodine counterion (17a) and chlorine counterion (19d). Data Obtained by Dr. Grant's Lab (Kanchan).*

application, and due to the modifiability of cyanine dyes, this was overcome by the use of different alkylating agents and synthetic procedures. Finally, the quinoline heterocycle was introduced to the heptamethine dyes allowing the dyes to be far red-shifted into the NIR II region which a hugely untapped field for cyanine dyes. The compounds were studied for the optical properties and some were tested for their effectivity in PDT application, proving that the fluorine atom slightly enhances DNA cleavage while the chloride counter-ion enhances the cleavage in comparison to the common iodide.

4   RESEARCH OVERVIEW

My research entails the design and the synthesis of biologically relevant cyanine dyes. Cyanine dyes are a class of near-infrared (NIR) contrast agents that have shown great potential in medical application. These dyes are versatile and modifiable allowing for specific tailoring and optimization sites; as well as, absorb light at a longer wavelength which is both safer and optimal for contrast due to the low absorption of endogenous tissue in NIR spectral region. The projects that I have taken on include synthesis of photosynthesizing agents for photodynamic therapy (PDT), synthesis of contrast agents for optoacoustic imaging modalities (OAI), and the design and execution of an optimized procedure for the synthesis of highly hydrophobic fluorescent compounds for human serum albumin (HSA) studies.

As a medicinal organic chemist both synthetic and biological theories must be utilized in order to yield compounds with medicinal relevancy. Tailoring weakly fluorescent photosynthesizing agents that, upon NIR laser excitation, interact with singlet oxygen and undergo intersystem crossing into the triplet state is ideal for PDT application. This quantum phenomenon leads to the generation of reactive oxygen species (ROS) which ultimately leads the cell to an apoptotic state. PDT utilizes these agents as guidance systems for cancer therapy. Although PDT currently uses alternative contrast agents (such as porphyrins), in comparison to cyanine dyes, these are unfavorable due to synthetic and solubility issues, shorter wavelength absorption reducing the penetration depth, and poor clearance leading to major side effects and poorer quality of life. The dyes I currently synthesize are as effective and improve on these factors. I aim to further optimize these compounds for PDT application in the field of cancer therapeutics.

Molecular imaging (MI) facilitates early detection of disease which has proven to be among the most effective ways of treating cancers. There are various studies which have shown much correlation relating survival rate to early-stage detection. OAI is a new and innovative MI technique that incorporates contrast agents with ultrasound imaging technology. Upon the introduction of the NIR contrast agent and NIR light, the dye goes into an excited state where it observes various relaxation pathways to the ground state. Among those pathways, dyes that exhibit high levels of vibration relaxation induces molecular thermal expansion leading to an acoustic signal generation which is detectable by ultrasound sensors. Once again NIR contrast agents enhance this imaging modality by providing better signal generation that acts as a targeting tool; while they too are enhanced by increasing their depth penetration in comparison to their fluorescence signal. Some cyanine dyes have been tested and proven to be effective;

however, are far from optimal. Due to the novelty of this technique, not much is known for of

what constitutes as optimal characteristics for the contrast agents. Herein I systemically aim to

further develop a large library of compounds for screening to better understand and optimize

OAI techniques.

HSA is the most abundant blood protein in the human body and plays a crucial role in the

delivery of various molecules. It has been well established that the protein contains four

hydrophobic binding pockets, which led to my design of hydrophobic contrast agents. Here I

aimed to better understand the hindrances and binding properties of HSA which than can be used

in coherence with other studies. Along with the design of the compounds, I successfully optimize

the synthetic procedure for these compound, allowing for an alternative synthetic method that

resulted in superior yields and allowed for an easier purification method.

APPENDICES

Appendix Chapter 2

Table of content:

^{1}H and ^{13}C NMR spectra of all cyanines synthesized in this study

Absorbance, fluorescence spectra and Beer-Lambert plots of all cyanines synthesized in this study

^{1}H and ^{13}C NMR spectra of all cyanines synthesized in this study
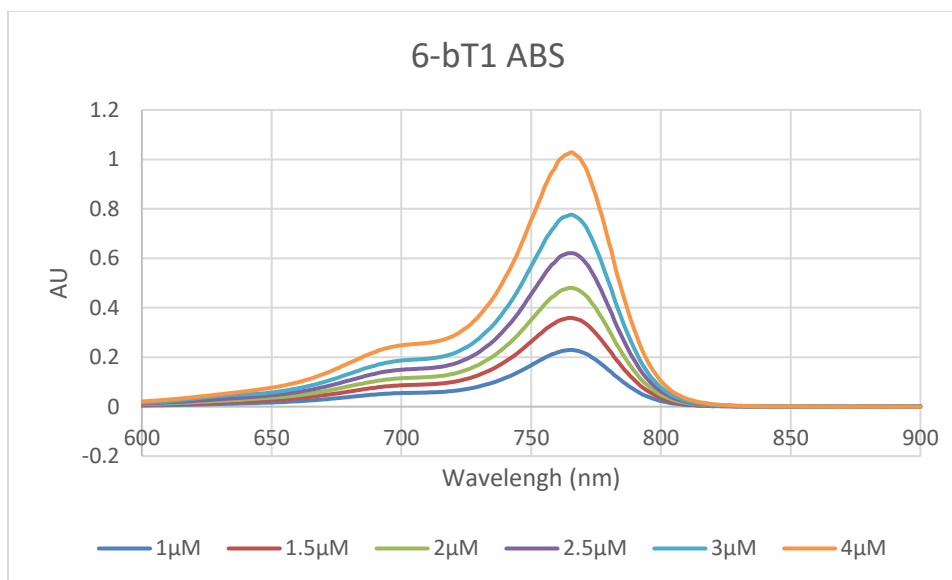
*30f-30j correspond to 6a-e and were synthesized by Dr. Andrew Levitz (See: Levitz dissertation)

AL_167_DMSO_13C

172.17, 161.52, 147.36, 143.31, 140.98, 139.10, 131.06, 129.62, 129.08, 128.85, 128.57, 124.98, 122.75, 111.30, 100.73, 48.53, 31.54, 27.34, 24.57, 21.38

30f

Current Data Parameters
NAME   AL_167_DMSO_13C
EXPNO   1
PROCNO   1

F2 - Acquisition Parameters
Date_   20160205
Time   23.53
INSTRUM   spect
PROBHD   5 mm PABBO BB-
PULPROG   jmod
TD   65536
SOLVENT   DMSO
NS   11153
DS   4
SWH   24038.461 Hz
FIDRES   0.366798 Hz
AQ   1.3631488 sec
RG   203
DW   20.800 usec
DE   6.50 usec
TE   298.0 K
CNST2   145.0000000
CNST11   1.0000000
D1   2.00000000 sec
D20   0.00689655 sec
TD0   1

======== CHANNEL f1 ========
SFO1   100.6253446 MHz
NUC1   13C
P1   9.00 usec
P2   18.00 usec
PLW1   62.00000000 W

======== CHANNEL f2 ========
SFO2   400.1416006 MHz
NUC2   1H
CPDPRG[2   waltz16
PCPD2   90.00 usec
PLW2   16.00000000 W
PLW12   0.36267000 W

F2 - Processing parameters
SI   32768
SF   100.6152830 MHz
WDW   EM
SSB   0
LB   1.00 Hz
GB   0
PC   1.40

AL_190_CDCl3_1H

7.568, 7.550, 7.526, 7.221, 7.204, 7.125, 7.090, 7.052, 7.031, 6.877, 6.855, 6.769, 6.047, 6.012, 3.822, 3.619, 2.709, 2.062, 1.172

30g

Current Data Parameters
NAME   AL_190_CDCl3_1H
EXPNO   1
PROCNO   1

F2 - Acquisition Parameters
Date_   20160420
Time   14.12
INSTRUM   spect
PROBHD   5 mm PABBO BB-
PULPROG   zg30
TD   65536
SOLVENT   CDCl3
NS   27
DS   2
SWH   8012.820 Hz
FIDRES   0.122266 Hz
AQ   4.0894465 sec
RG   203
DW   62.400 usec
DE   6.50 usec
TE   298.0 K
D1   1.00000000 sec
TD0   1

======== CHANNEL f1 ========
SFO1   400.1424710 MHz
NUC1   1H
P1   13.55 usec
PLW1   16.00000000 W

F2 - Processing parameters
SI   65536
SF   400.1400000 MHz
WDW   EM
SSB   0
LB   0.30 Hz
GB   0
PC   1.00

AL_190_CDC13_13C

BRUKER

Current Data Parameters
NAME   AL_190_CDC13_13C
EXPNO   1
PROCNO   1

F2 - Acquisition Parameters
Date_   20160424
Time   23.29
INSTRUM   spect
PROBHD   5 mm PABBO BB-
PULPROG   jmod
TD   65536
SOLVENT   CDC13
NS   10074
DS   4
SWH   24038.461 Hz
FIDRES   0.366798 Hz
AQ   1.3631488 sec
RG   203
DW   20.800 usec
DE   6.50 usec
TE   298.1 K
CNST2   145.0000000
CNST11   1.0000000
D1   2.00000000 sec
D20   0.00689655 sec
TD0   1

======== CHANNEL f1 ========
SFO1   100.6253446 MHz
NUC1   13C
P1   9.00 usec
P2   18.00 usec
PLW1   62.00000000 W

======== CHANNEL f2 ========
SFO2   400.1416006 MHz
NUC2   1H
CPDPRG[2   waltz16
PCPD2   90.00 usec
PLW2   16.00000000 W
PLW12   0.36267000 W

F2 - Processing parameters
SI   32768
SF   100.6152830 MHz
WDW   EM
SSB   0
LB   1.00 Hz
GB   0
PC   1.40

AL_181_CDC13_1H

BRUKER

Current Data Parameters
NAME   AL_181_CDC13_1H
EXPNO   1
PROCNO   1

F2 - Acquisition Parameters
Date_   20160301
Time   13.45
INSTRUM   spect
PROBHD   5 mm PABBO BB-
PULPROG   zg30
TD   65536
SOLVENT   CDC13
NS   9
DS   2
SWH   8012.820 Hz
FIDRES   0.122266 Hz
AQ   4.0894465 sec
RG   203
DW   62.400 usec
DE   6.50 usec
TE   298.0 K
D1   1.00000000 sec
TD0   1

======== CHANNEL f1 ========
SFO1   400.1424710 MHz
NUC1   1H
P1   13.55 usec
PLW1   16.00000000 W

F2 - Processing parameters
SI   65536
SF   400.1400000 MHz
WDW   EM
SSB   0
LB   0.30 Hz
GB   0
PC   1.00

AL_181_CDC13_13C

BRUKER

Current Data Parameters
NAME   AL_181_CDC13_13C
EXPNO   1
PROCNO   1

F2 - Acquisition Parameters
Date_   20160306
Time   22.44
INSTRUM   spect
PROBHD   5 mm PABBO BB-
PULPROG   jmod
TD   65536
SOLVENT   CDCl3
NS   11500
DS   4
SWH   24038.461 Hz
FIDRES   0.366798 Hz
AQ   1.3631488 sec
RG   203
DW   20.800 usec
DE   6.50 usec
TE   298.1 K
CNST2   145.0000000
CNST11   1.0000000
D1   2.00000000 sec
D20   0.00689655 sec
TD0   1

======== CHANNEL f1 ========
SFO1   100.6253446 MHz
NUC1   13C
P1   9.00 usec
P2   18.00 usec
PLW1   62.00000000 W

======== CHANNEL f2 ========
SFO2   400.1416006 MHz
NUC2   1H
CPDPRG[2   waltz16
PCPD2   90.00 usec
PLW2   16.00000000 W
PLW12   0.36267000 W

F2 - Processing parameters
SI   32768
SF   100.6152830 MHz
WDW   EM
SSB   0
LB   1.00 Hz
GB   0
PC   1.40

30h

AL_188_CDC13_1H

BRUKER

Current Data Parameters
NAME   AL_188_CDC13_1H
EXPNO   2
PROCNO   2

F2 - Acquisition Parameters
Date_   20160404
Time   15.09
INSTRUM   spect
PROBHD   5 mm PABBO BB-
PULPROG   zg30
TD   65536
SOLVENT   CDCl3
NS   16
DS   2
SWH   8012.820 Hz
FIDRES   0.122266 Hz
AQ   4.0894465 sec
RG   161
DW   62.400 usec
DE   6.50 usec
TE   298.0 K
D1   1.00000000 sec
TD0   1

======== CHANNEL f1 ========
SFO1   400.1424710 MHz
NUC1   1H
P1   13.55 usec
PLW1   16.00000000 W

F2 - Processing parameters
SI   65536
SF   400.1400000 MHz
WDW   EM
SSB   0
LB   0.30 Hz
GB   0
PC   1.00

AL_188_CDC13_13C

BRUKER

Current Data Parameters
NAME   AL_188_CDC13_13C
EXPNO   1
PROCNO   1

F2 - Acquisition Parameters
Date_   20160404
Time   15.39
INSTRUM   spect
PROBHD   5 mm PABBO BB-
PULPROG   jmod
TD   65536
SOLVENT   CDCl3
NS   679
DS   4
SWH   24038.461 Hz
FIDRES   0.366798 Hz
AQ   1.3631488 sec
RG   203
DW   20.800 usec
DE   6.50 usec
TE   298.2 K
CNST2   145.0000000
CNST11   1.0000000
D1   2.00000000 sec
D20   0.00689655 sec
TD0   1

======== CHANNEL f1 ========
SFO1   100.6253446 MHz
NUC1   13C
P1   9.00 usec
P2   18.00 usec
PLW1   62.00000000 W

======== CHANNEL f2 ========
SFO2   400.1416006 MHz
NUC2   1H
CPDPRG[2   waltz16
PCPD2   90.00 usec
PLW2   16.00000000 W
PLW12   0.36267000 W

F2 - Processing parameters
SI   32768
SF   100.6152830 MHz
WDW   EM
SSB   0
LB   1.00 Hz
GB   0
PC   1.40

AL_184_CDC13_1H

Current Data Parameters
NAME   AL_184_CDC13_1H
EXPNO   1
PROCNO   1

F2 - Acquisition Parameters
Date_   20160304
Time   14.18
INSTRUM   spect
PROBHD   5 mm PABBO BB-
PULPROG   zg30
TD   65536
SOLVENT   CDCl3
NS   7
DS   2
SWH   8012.820 Hz
FIDRES   0.122266 Hz
AQ   4.0894465 sec
RG   203
DW   62.400 usec
DE   6.50 usec
TE   298.0 K
D1   1.00000000 sec
TD0   1

======== CHANNEL f1 ========
SFO1   400.1424710 MHz
NUC1   1H
P1   13.55 usec
PLW1   16.00000000 W

F2 - Processing parameters
SI   65536
SF   400.1400000 MHz
WDW   EM
SSB   0
LB   0.30 Hz
GB   0
PC   1.00

AL_184_CDC13_13C

Current Data Parameters
NAME   AL_184_CDC13_13C
EXPNO   1
PROCNO   1

F2 - Acquisition Parameters
Date_   20160306
Time   0.09
INSTRUM   spect
PROBHD   5 mm PABBO BB-
PULPROG   jmod
TD   65536
SOLVENT   CDCl3
NS   12500
DS   4
SWH   24038.461 Hz
FIDRES   0.366798 Hz
AQ   1.3631488 sec
RG   203
DW   20.800 usec
DE   6.50 usec
TE   298.2 K
CNST2   145.0000000
CNST11   1.0000000
D1   2.00000000 sec
D20   0.00689655 sec
TD0   1

======== CHANNEL f1 ========
SFO1   100.6253446 MHz
NUC1   13C
P1   9.00 usec
P2   18.00 usec
PLW1   62.00000000 W

======== CHANNEL f2 ========
SFO2   400.1416006 MHz
NUC2   1H
CPDPRG[2   waltz16
PCPD2   90.00 usec
PLW2   16.00000000 W
PLW12   0.36267000 W

F2 - Processing parameters
SI   32768
SF   100.6152830 MHz
WDW   EM
SSB   0
LB   1.00 Hz
GB   0
PC   1.40

AC_7_CDC13_1H

Current Data Parameters
NAME   AC_7_CDC13_1H
EXPNO   1
PROCNO   1

F2 - Acquisition Parameters
Date_   20160329
Time   15.06
INSTRUM   spect
PROBHD   5 mm PABBO BB-
PULPROG   zg30
TD   65536
SOLVENT   CDC13
NS   6
DS   2
SWH   8012.820 Hz
FIDRES   0.122266 Hz
AQ   4.0894465 sec
RG   128
DW   62.400 usec
DE   6.50 usec
TE   298.0 K
D1   1.00000000 sec
TD0   1

======= CHANNEL f1 =======
SFO1   400.1424710 MHz
NUC1   1H
P1   13.55 usec
PLW1   16.00000000 W

F2 - Processing parameters
SI   65536
SF   400.1400000 MHz
WDW   EM
SSB   0
LB   0.30 Hz
GB   0
PC   1.00

AC_7_CDC13_13C

Current Data Parameters
NAME   AC_7_CDC13_13C
EXPNO   1
PROCNO   1

F2 - Acquisition Parameters
Date_   20160331
Time   23.37
INSTRUM   spect
PROBHD   5 mm PABBO BB-
PULPROG   jmod
TD   65536
SOLVENT   CDC13
NS   690
DS   4
SWH   24038.461 Hz
FIDRES   0.366798 Hz
AQ   1.3631488 sec
RG   203
DW   20.800 usec
DE   6.50 usec
TE   298.2 K
CNST2   145.0000000
CNST11   1.0000000
D1   2.00000000 sec
D20   0.00689655 sec
TD0   1

======= CHANNEL f1 =======
SFO1   100.6253446 MHz
NUC1   13C
P1   9.00 usec
P2   18.00 usec
PLW1   62.00000000 W

======= CHANNEL f2 =======
SFO2   400.1416006 MHz
NUC2   1H
CPDPRG[2   waltz16
PCPD2   90.00 usec
PLW2   16.00000000 W
PLW12   0.36267000 W

F2 - Processing parameters
SI   32768
SF   100.6152830 MHz
WDW   EM
SSB   0
LB   1.00 Hz
GB   0
PC   1.40

AC_5_CDC13_1H

6-h

AC_5_CDC13_13C

6-h

AC_8_CDC13_1H

6-i

Peak list (¹H, ppm):
7.606, 7.588, 7.570, 7.543, 7.526, 7.257, 7.239, 7.140, 7.128, 7.005, 6.988, 6.889, 6.868, 6.795, 6.003, 4.061, 3.833, 2.724, 2.095, 1.413, 1.396, 1.378, 1.188

Current Data Parameters
NAME   AC_8_CDC13_1H
EXPNO   3
PROCNO   3

F2 - Acquisition Parameters
Date_   20160408
Time   13.12
INSTRUM   spect
PROBHD   5 mm PABBO BB-
PULPROG   zg30
TD   65536
SOLVENT   CDC13
NS   22
DS   2
SWH   8012.820 Hz
FIDRES   0.122266 Hz
AQ   4.0894465 sec
RG   203
DW   62.400 usec
DE   6.50 usec
TE   298.0 K
D1   1.00000000 sec
TD0   1

-------- CHANNEL f1 --------
SFO1   400.1424710 MHz
NUC1   1H
P1   13.55 usec
PLW1   16.00000000 W

F2 - Processing parameters
SI   65536
SF   400.1400000 MHz
WDW   EM
SSB   0
LB   0.30 Hz
GB   0
PC   1.00

Integrals: 3.14, 2.02, 1.94, 2.08, 1.99, 2.03, 2.04, 3.88, 5.93, 4.04, 2.04, 5.92, 12.00

Peak list (¹³C, ppm):
129.46, 128.60, 128.22, 113.24, 110.96, 109.33, 77.43, 77.11, 76.80, 65.84, 56.11, 48.80, 28.68, 27.66, 15.27, 12.58, -0.01

6-i

Current Data Parameters
NAME   ac8-cdc13-13C
EXPNO   1
PROCNO   1

F2 - Acquisition Parameters
Date_   20170802
Time   13.25
INSTRUM   spect
PROBHD   5 mm PABBO BB-
PULPROG   zgpg30
TD   65536
SOLVENT   CDC13
NS   410
DS   4
SWH   24038.461 Hz
FIDRES   0.366798 Hz
AQ   1.3631488 sec
RG   203
DW   20.800 usec
DE   6.50 usec
TE   297.3 K
D1   2.00000000 sec
D11   0.03000000 sec
TD0   1

======= CHANNEL f1 =======
SFO1   100.6253441 MHz
NUC1   13C
P1   9.25 usec
PLW1   62.00000000 W

======= CHANNEL f2 =======
SFO2   400.1416006 MHz
NUC2   1H
CPDPRG[2   waltz16
PCPD2   90.00 usec
PLW2   16.00000000 W
PLW12   0.36267000 W
PLW13   0.29376000 W

F2 - Processing parameters
SI   32768
SF   100.6152830 MHz
WDW   EM
SSB   0
LB   1.00 Hz
GB   0
PC   1.40

FM_4_CDC13_1H

Current Data Parameters
NAME   FM_4_CDC13_1H
EXPNO   1
PROCNO   1

F2 - Acquisition Parameters
Date_   20160315
Time   13.41
INSTRUM   spect
PROBHD   5 mm PABBO BB-
PULPROG   zg30
TD   65536
SOLVENT   CDc13
NS   12
DS   2
SWH   8012.820 Hz
FIDRES   0.122266 Hz
AQ   4.0894465 sec
RG   203
DW   62.400 usec
DE   6.50 usec
TE   298.0 K
D1   1.00000000 sec
TD0   1

-------- CHANNEL f1 --------
SFO1   400.1424710 MHz
NUC1   1H
P1   13.55 usec
PLW1   16.00000000 W

F2 - Processing parameters
SI   65536
SF   400.1400000 MHz
WDW   EM
SSB   0
LB   0.30 Hz
GB   0
PC   1.00

FM_4_CDC13_13C

Current Data Parameters
NAME   FM_4_CDC13_13C
EXPNO   1
PROCNO   1

F2 - Acquisition Parameters
Date_   20160504
Time   0.41
INSTRUM   spect
PROBHD   5 mm PABBO BB-
PULPROG   jmod
TD   65536
SOLVENT   CDC13
NS   9573
DS   4
SWH   24038.461 Hz
FIDRES   0.366798 Hz
AQ   1.3631488 sec
RG   203
DW   20.800 usec
DE   6.50 usec
TE   298.2 K
CNST2   145.0000000
CNST11   1.0000000
D1   2.00000000 sec
D20   0.00689655 sec
TD0   1

-------- CHANNEL f1 --------
SFO1   100.6253446 MHz
NUC1   13C
P1   9.00 usec
P2   18.00 usec
PLW1   62.00000000 W

-------- CHANNEL f2 --------
SFO2   400.1416006 MHz
NUC2   1H
CPDPRG[2   waltz16
PCPD2   90.00 usec
PLW2   16.00000000 W
PLW12   0.36267000 W

F2 - Processing parameters
SI   32768
SF   100.6152830 MHz
WDW   EM
SSB   0
LB   1.00 Hz
GB   0
PC   1.40

7.607
7.590
7.572
7.545
7.469
7.448
7.234
7.216
7.170
7.135
6.989
6.968
6.176
6.141

4.126
4.108
4.090
2.756
2.744
2.729
2.092
1.811
1.794
1.774
1.757
1.737
1.507
1.489
1.471
1.451
1.433
1.168
1.029
1.011
0.993

6-m

FM_Dye1_CDC13_1H

BRUKER

Current Data Parameters
NAME   FM_Dye1_CDC13_1H
EXPNO   1
PROCNO   1

F2 – Acquisition Parameters
Date_   20160306
Time   22.28
INSTRUM   spect
PROBHD   5 mm PABBO BB-
PULPROG   zg30
TD   65536
SOLVENT   CDCl3
NS   14
DS   2
SWH   8012.820 Hz
FIDRES   0.122266 Hz
AQ   4.0894465 sec
RG   203
DW   62.400 usec
DE   6.50 usec
TE   298.0 K
D1   1.00000000 sec
TD0   1

-------- CHANNEL f1 --------
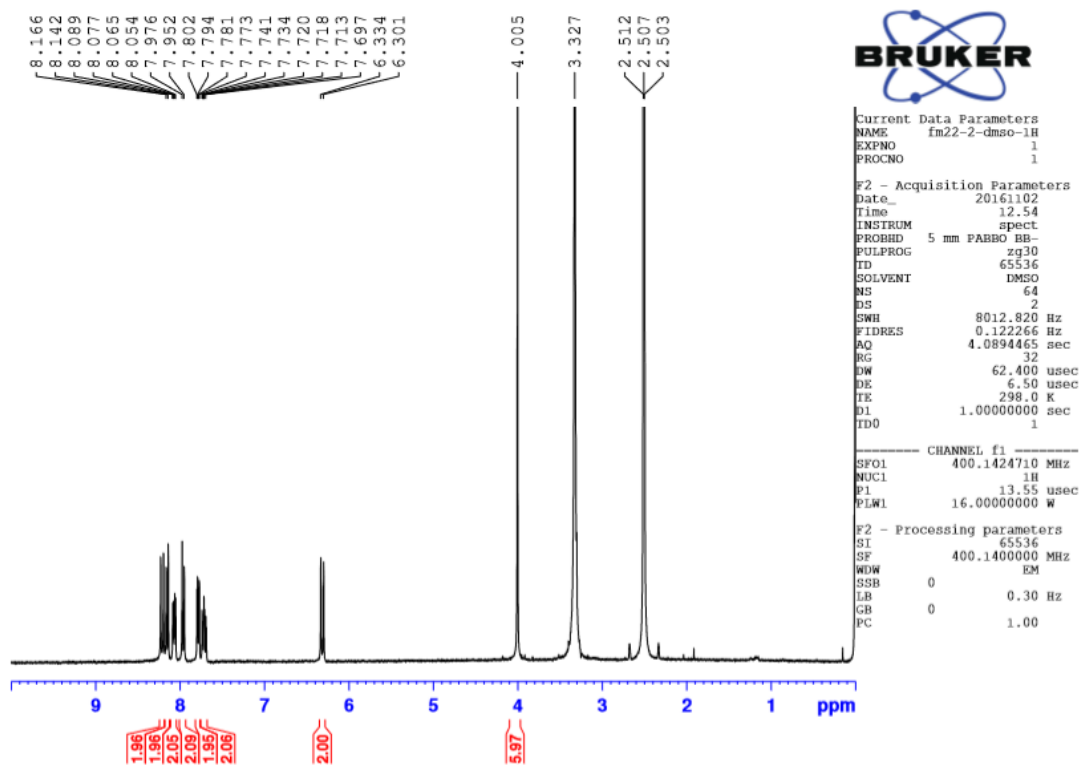SFO1   400.1424710 MHz
NUC1   1H
P1   13.55 usec
PLW1   16.00000000 W
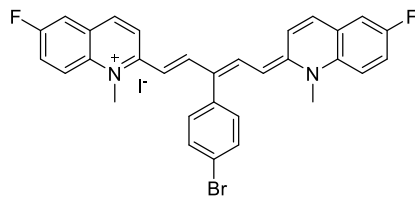
F2 – Processing parameters
SI   65536
SF   400.1400000 MHz
WDW   EM
SSB   0
LB   0.30 Hz
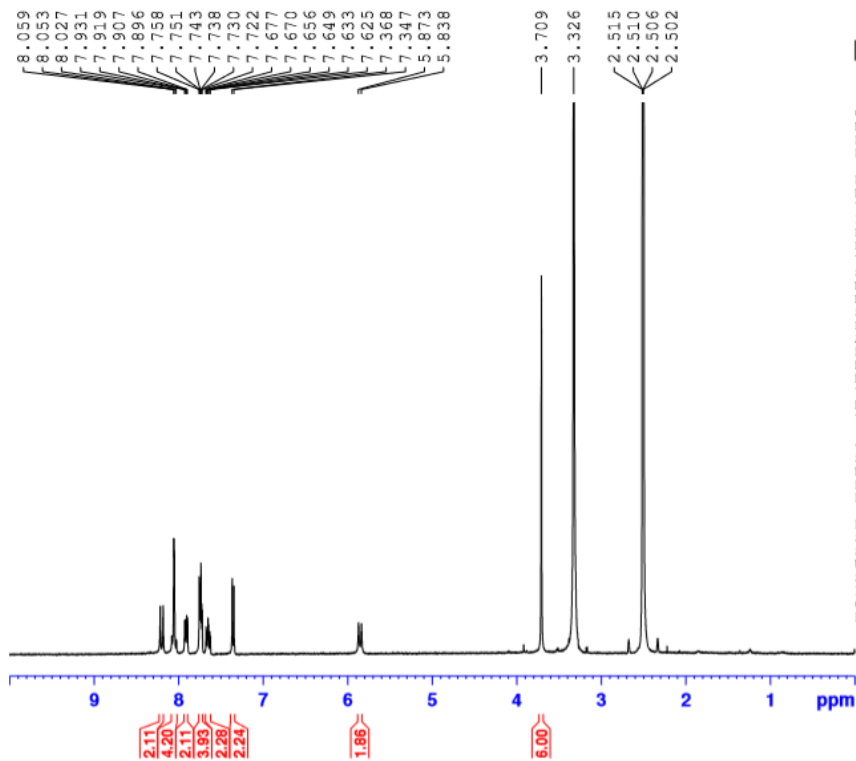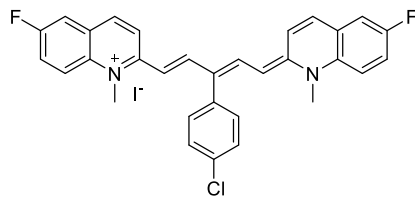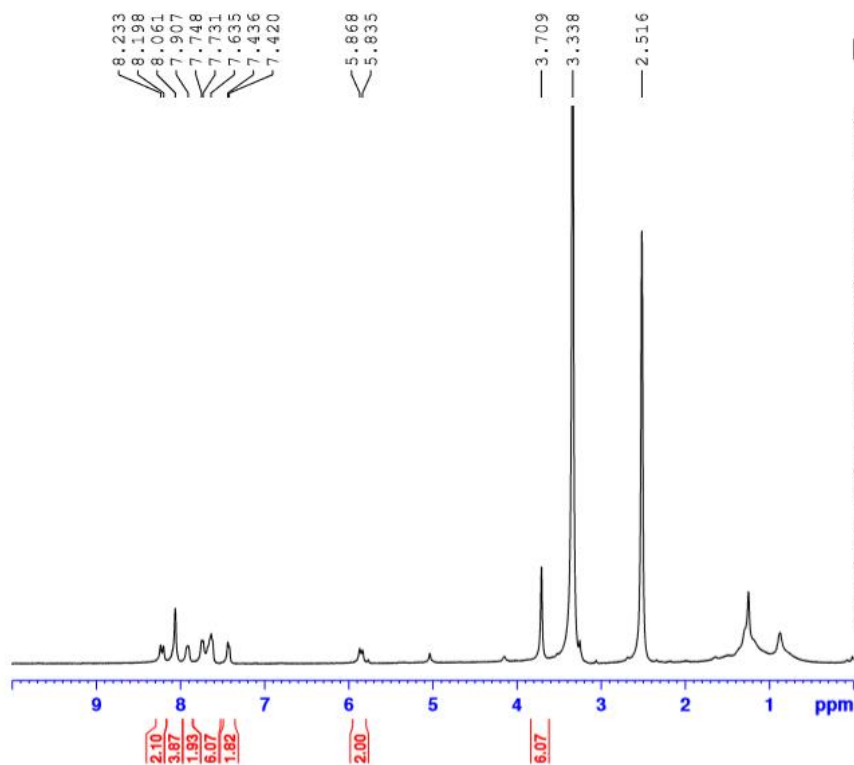GB   0
PC   1.00

3.13 2.05 2.08 2.03 2.01 2.04   4.00   3.98 1.97 4.04 3.92 11.98 6.12

6-h

Absorbance, fluorescence spectra and Beer-Lambert plots of all cyanines synthesized in this study

$y = 266800x + 0.0005$
$R^2 = 0.9956$

6-aT1 ABS

$y = 266800x + 0.0005$
$R^2 = 0.9956$

6-a7T1 ABS

6-aT1 ABS

6-aT2 ABS

6-aT1FL

y = 23133x + 1076.8
R² = 0.9983

6-aT2FL

y = 25076x + 1562
R² = 0.9936

6-aT1 FL

6-aT2 FL

6-bT1 abs

y = 260571x - 0.022
R² = 0.998

6-bT2 abs

y = 261476x + 0.0012
R² = 0.9992

6-bT1 ABS

6-bT2 ABS

6-bT1FL

y = 24548x + 1071
R^2 = 0.9889

6-bT2FL

$y = 26927x + 1612.5$
$R^2 = 0.9921$

6-bT2 FL

AU

Wavelengh

.1μM   .15μM   .2μM   .25μM   .3μM   .4μM

6-bT2 FL

6-c T1 ABS

$y = 275238x - 0.0239$
$R^2 = 0.9972$

6-c T2 ABS

$y = 275952x - 0.001$
$R^2 = 0.9986$

6-cT1 ABS

6-cT2 ABS

6-cT1FL

y = 25629x + 753.32
R² = 0.9985

6-cT2FL

y = 27660x + 1552
R² = 0.988

6-cT1 FL

6-c T2 FL

6-dT1 abs

$y = 245739x - 0.0068$
$R^2 = 0.9998$

6-d t2 abs

$y = 254000x - 0.0076$
$R^2 = 0.9989$

6-d T1 ABS

6-d T2 ABS

6-d0FL

$y = 7591.5x + 6.6843$
$R^2 = 0.9989$

6-dT2FL

$y = 7604.9x + 176.41$
$R^2 = 0.9955$

6-dT1 FL

6-dT2 FL

6-et1 abs

y = 251057x + 0.0006
R² = 0.9996

6-eT2 abs

y = 259686x - 0.0091
R² = 0.9977

6-eT1 ABS

6-eT2 ABS

6-et2 FL

y = 10607x + 137.93
R² = 0.9984

6-et1 FL

y = 10723x + 173.81
R² = 0.9986

6-eT1 FL

6-eFL

6-f t1 abs

$y = 275000x - 0.0045$
$R^2 = 0.9973$

6-f t2 abs

$y = 262800x - 0.007$
$R^2 = 0.996$

6-f T1 ABS

6-f T2 ABS

6-f t1 Fl

y = 34291x + 46.992
R² = 0.9998

6-f T2 Fl

y = 33411x + 314.09
R² = 0.9995

6-f T1 FL

6-f T2 FL

6-gT2 abs

y = 282143x - 0.0183
R² = 0.9964

6-gT1 ABS

1µm   1.5µm   2µm   2.5µm   3µm   4µm

6-gT2 ABS

6-gt1Fl

$y = 30066x + 1407.1$
$R^2 = 0.9913$

6-gT2Fl

$y = 31208x + 1159$
$R^2 = 0.9984$

6-gT1 FL

6-gT2 FL

6-h T1 abs

y = 291057x - 0.0089
R² = 0.9993

6-h T2 abs

y = 274657x - 0.0049
R² = 0.9994

6-h T1 ABS

6-h T2 ABS

6-h T1 Fl

$y = 36069x + 475.57$
$R^2 = 0.9952$

6-h T2 Fl

$y = 37098x + 437.62$
$R^2 = 0.9999$

6-h T1 FL

6-h T2 FL

6-i T2 abs

y = 147190x - 0.0178
R² = 0.9952

6-i T1 ABS

6-i T2 ABS

6-i T1FL

$y = 8189.5x + 62.958$
$R^2 = 0.9952$

6-i T2FL

$y = 9576.1x + 7.0045$
$R^2 = 0.9905$

6-i T1 FL

6-i T2 FL

6-j T1 abs

$y = 232732x - 0.0069$
$R^2 = 0.9912$

6-j T2 abs

$y = 230810x - 0.012$
$R^2 = 0.9994$

6-jT1 ABS

6-j T2 ABS

6-j T1FL

y = 12358x - 4.1389
R² = 0.9973

6-j T2FL

y = 13515x + 26.306
R² = 0.9995

6-j T1 FL

6-j T2 FL

6-k T1 abs

y = 202381x - 0.0009
R² = 0.9989

6-k T2 abs

y = 196952x - 0.0016
R² = 0.9996

6-k T1 ABS

6-k T2 ABS

6-k T1 Fl

y = 39480x + 567.62
R² = 0.9997

6-k T2 Fl

y = 39495x + 583.23
R² = 0.9996

6-k T1 Fl

6-k T2 Fl

y = 127381x - 0.0039
R² = 0.9971

6-l T1 ABS

y = 119381x - 0.0195
R² = 0.9909

6-l T2 ABS

6-l T1 ABS

6-l T2 ABS

y = 37939x + 285.28
R² = 0.9987

6-l T1 FL

y = 37870x + 1649.4
R² = 0.9893

6-l T2 FL

6-l T1 FL

6-l T2 FL

y = 239810x - 0.0205
R² = 0.9961

6-m T1 ABS

y = 238619x - 0.0027
R² = 0.999

6-m T2 ABS

6-m T1 ABS

6-m T2 ABS

6-m T1 Fl

y = 36806x + 877.1
R² = 0.9929

6-m T2 FL

y = 37767x + 447.91
R² = 0.9961

6-nT1 ABS

$y = 246657x - 0.0134$
$R^2 = 0.996$

6-nT2 ABS

$y = 253086x - 0.0256$
$R^2 = 0.9947$

6-nT1 ABS

6-nT2 ABS

y = 8449.2x + 62.987
R² = 0.9943

6-nT1 FL

y = 8592.7x + 69.994
R² = 0.9981

6-nT2 FL

y = 230048x - 0.0142
R² = 0.9981

6-oT1 ABS

y = 223238x - 0.0235
R² = 0.9952

6-oT2 ABS

6-oT1 ABS

6-oT2 ABS

y = 11029x + 90.3
R² = 0.997

6-oT1FL

y = 10908x + 133.91
R² = 0.997

6-oT2FL

Appendix Chapter 3

Chemical Formula: $C_{25}H_{21}F_2IN_2$
Molecular Weight: 514.3583

14a

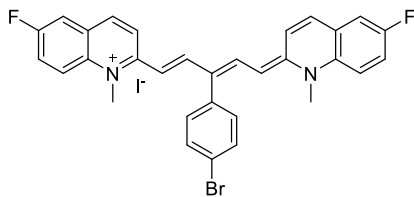Chemical Formula: $C_{25}H_{20}ClF_2IN_2$
Molecular Weight: 548.8003

14b
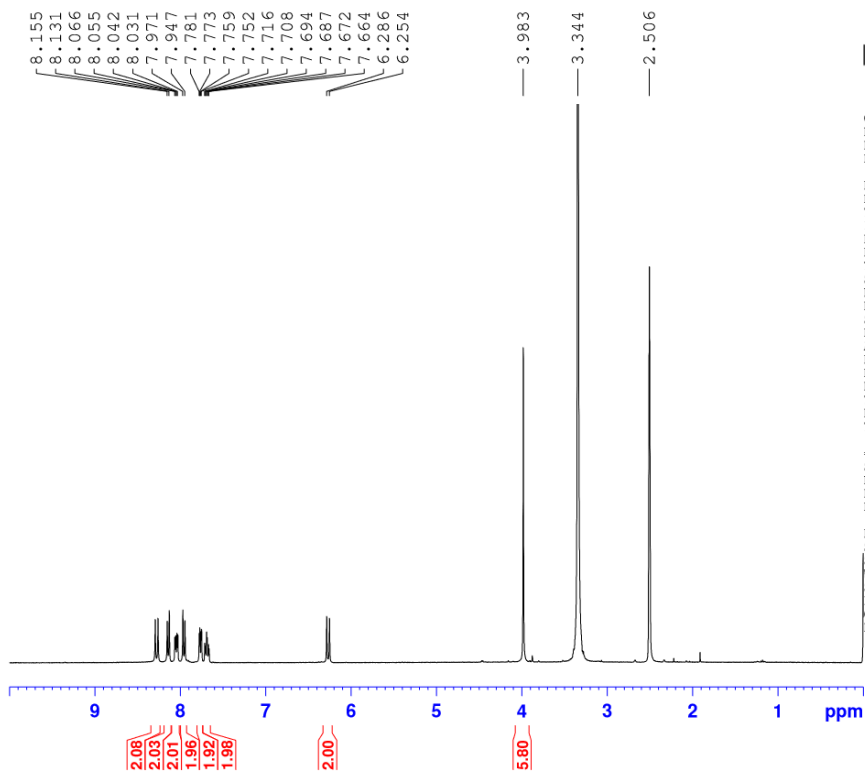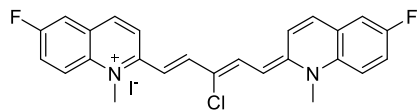
Chemical Formula: $C_{25}H_{20}ClF_2IN_2$
Molecular Weight: 548.8003

14c

Chemical Formula: $C_{31}H_{24}BrF_2IN_2$
Molecular Weight: 669.3523

15a

Chemical Formula: $C_{31}H_{24}ClF_2IN_2$
Molecular Weight: 624.8983

15b

Chemical Formula: C$_{32}$H$_{24}$F$_5$IN$_2$
Molecular Weight: 658.4545

15c

8.241
8.206
8.056
7.918
7.896
7.884
7.871
7.860
7.728
7.721
7.707
7.700
7.645
7.636
7.623
7.599
7.592
5.869
5.835
3.392
2.511
2.506
2.502

Current Data Parameters
NAME   6-f-2meq-cf3-dmso-1H
EXPNO   1
PROCNO   1

F2 - Acquisition Parameters
Date_   20170328
Time   17.25
INSTRUM   spect
PROBHD   5 mm PABBO BB-
PULPROG   zg30
TD   65536
SOLVENT   DMSO
NS   64
DS   2
SWH   8012.820 Hz
FIDRES   0.122266 Hz
AQ   4.0894465 sec
RG   32
DW   62.400 usec
DE   6.50 usec
TE   298.0 K
D1   1.00000000 sec
TD0   1

======== CHANNEL f1 ========
SFO1   400.1424710 MHz
NUC1   1H
P1   13.55 usec
PLW1   16.00000000 W

F2 - Processing parameters
SI   65536
SF   400.1400000 MHz
WDW   EM
SSB   0
LB   0.30 Hz
GB   0
PC   1.00

2.07 3.93 4.03 2.03 3.95   1.93   6.00

Chemical Formula: C$_{25}$H$_{21}$F$_2$IN$_2$
Molecular Weight: 514.3583

14a

F19

−162.91
−163.46

−158   −160   −162   −164   −166   −168   −170   ppm

Chemical Formula: $C_{25}H_{20}BrF_2IN_2$
Molecular Weight: 593.2543

14b

F19

−162.81
−162.91

−148 −150 −152 −154 −156 −158 −160 −162 −164 −166 −168   ppm
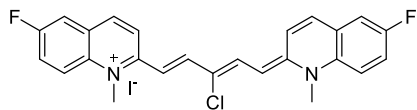
Chemical Formula: C$_{25}$H$_{20}$ClF$_2$IN$_2$
Molecular Weight: 548.8003

F19

14c

BRUKER

-162.91
-163.01

−161.5   −162.0   −162.5   −163.0   −163.5   ppm
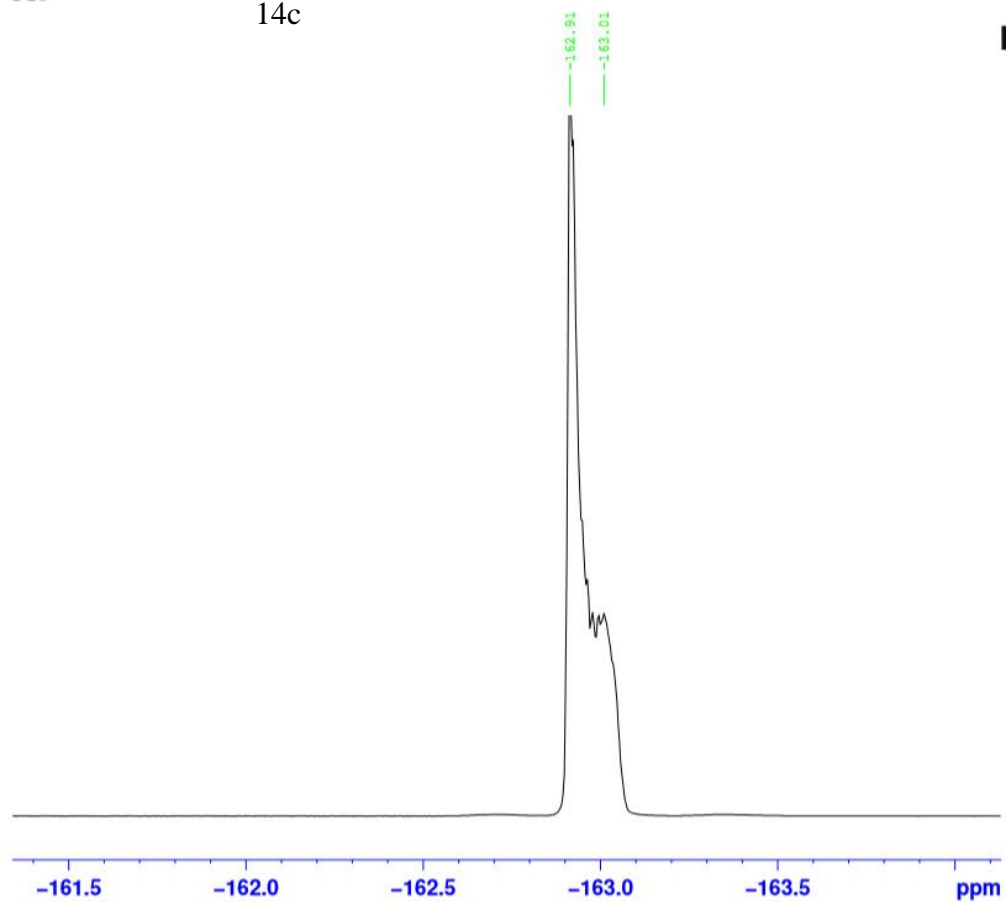
Chemical Formula: C$_{31}$H$_{24}$BrF$_2$IN$_2$
Molecular Weight: 669.3523

F19   15a

−162.77
−162.88

BRUKER

Current Data Parameters
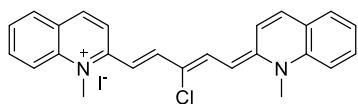NAME   FM28-DMSO-19F
EXPNO   1
PROCNO   1

F2 - Acquisition Parameters
Date_   20180417
Time   10.19
INSTRUM   spect
PROBHD   5 mm PABBO BB-
PULPROG   zgflqn
TD   131072
SOLVENT   DMSO
NS   16
DS   4
SWH   89285.711 Hz
FIDRES   0.681196 Hz
AQ   0.7340032 sec
RG   203
DW   5.600 usec
DE   6.50 usec
TE   295.9 K
D1   1.00000000 sec
TD0   1

======== CHANNEL f1 ========
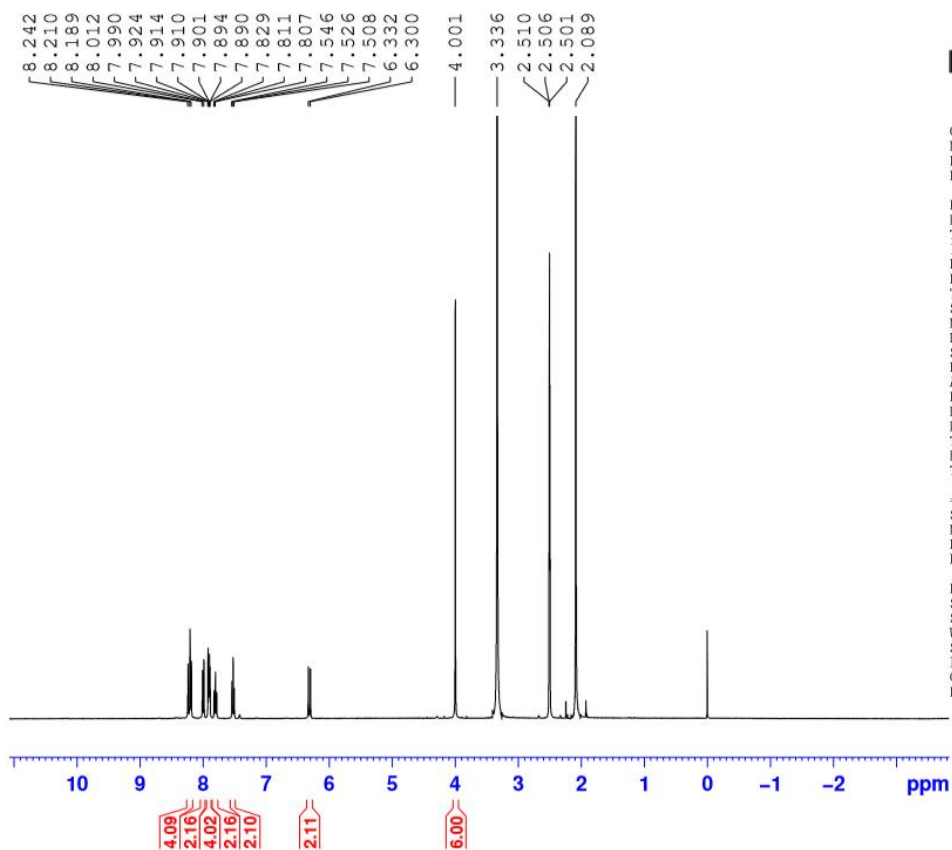SFO1   376.4701248 MHz
NUC1   19F
P1   14.00 usec
PLW1   20.00000000 W

F2 - Processing parameters
SI   65536
SF   376.5077760 MHz
WDW   EM
SSB   0
LB   0.30 Hz
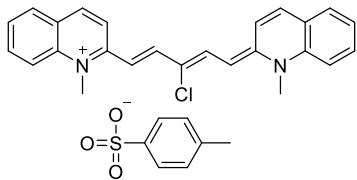GB   0
PC   1.00

−156 −157 −158 −159 −160 −161 −162 −163 −164 −165 −166 −167   ppm
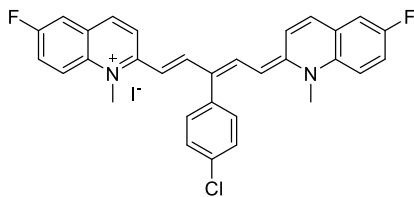
Chemical Formula: C$_{31}$H$_{24}$ClF$_2$IN$_2$
Molecular Weight: 624.8983

15b

F19

-162.74
-162.78
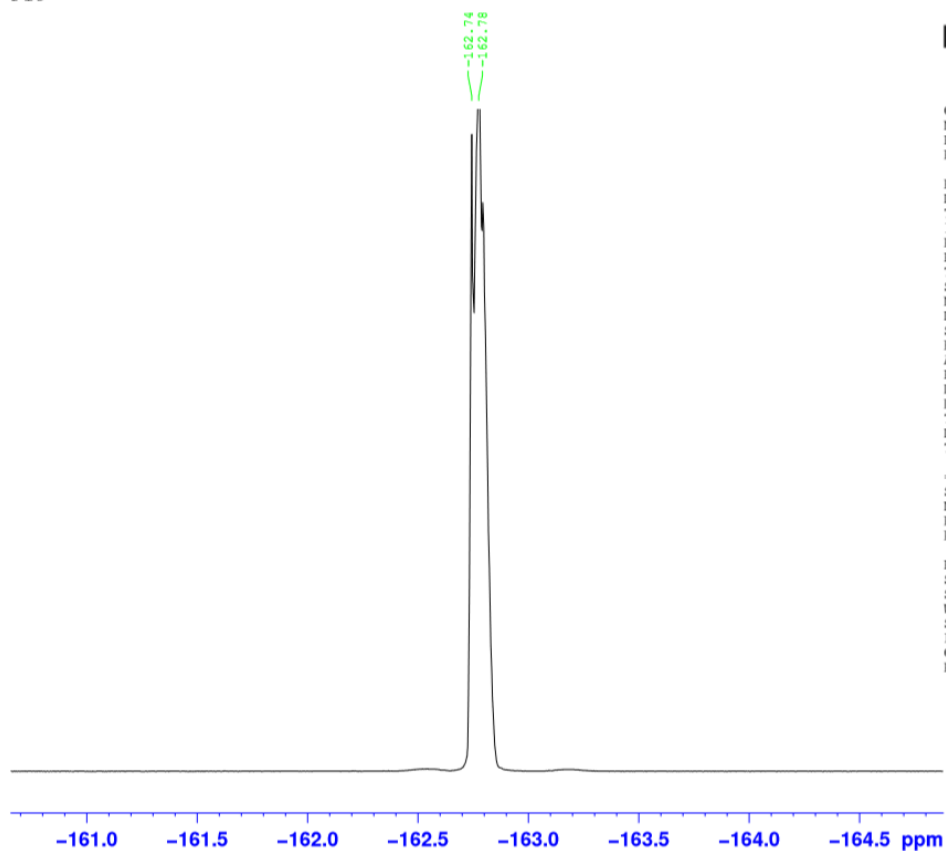
Current Data Parameters
NAME   FM25-DMSO-19F
EXPNO   1
PROCNO   1

F2 - Acquisition Parameters
Date_   20180417
Time   10.23
INSTRUM   spect
PROBHD   5 mm PABBO BB-
PULPROG   zgflqn
TD   131072
SOLVENT   DMSO
NS   16
DS   4
SWH   89285.711 Hz
FIDRES   0.681196 Hz
AQ   0.7340032 sec
RG   90.5
DW   5.600 usec
DE   6.50 usec
TE   296.0 K
D1   1.00000000 sec
TD0   1

======== CHANNEL f1 ========
SFO1   376.4701248 MHz
NUC1   19F
P1   14.00 usec
PLW1   20.00000000 W

F2 - Processing parameters
SI   65536
SF   376.5077760 MHz
WDW   EM
SSB   0
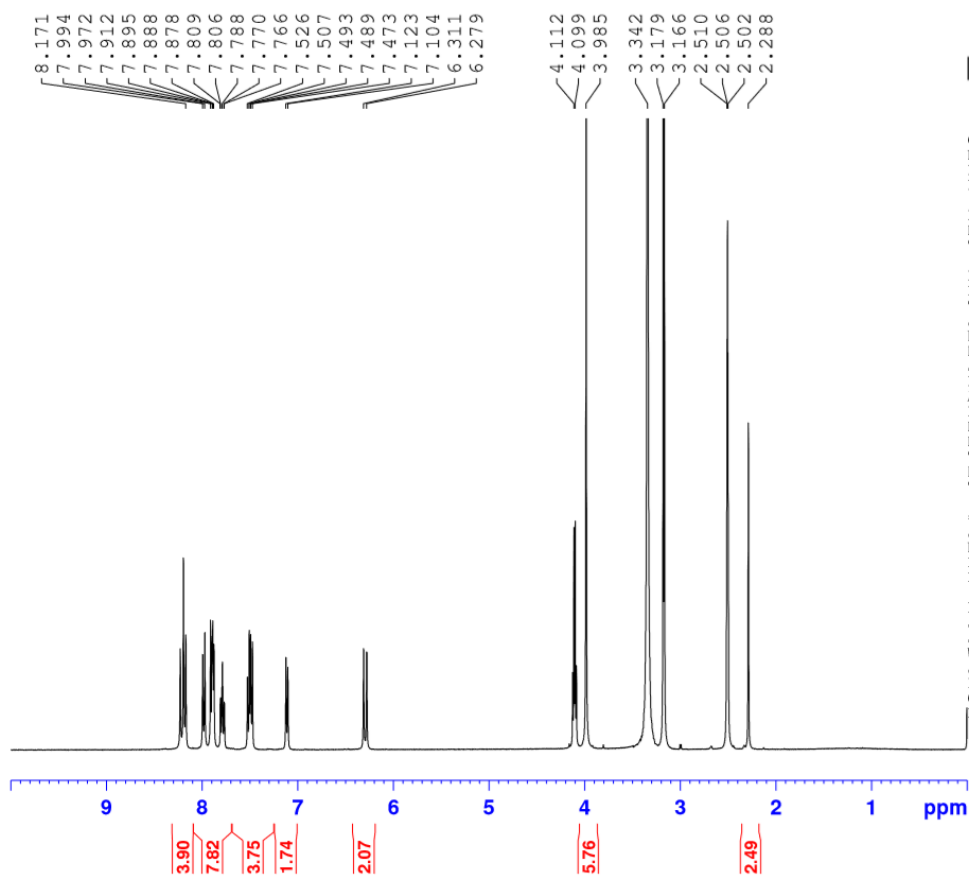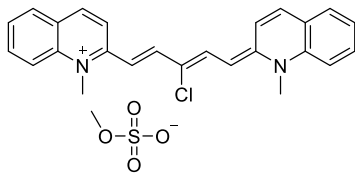LB   0.30 Hz
GB   0
PC   1.00

-161.0 -161.5 -162.0 -162.5 -163.0 -163.5 -164.0 -164.5 ppm
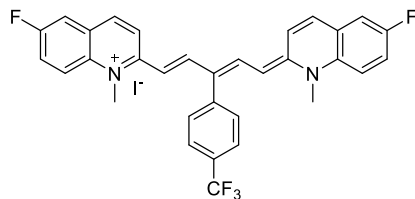
Chemical Formula: $C_{32}H_{24}F_5IN_2$
Molecular Weight: 658.4545

F19   15c

-162.77
-162.78
-162.84
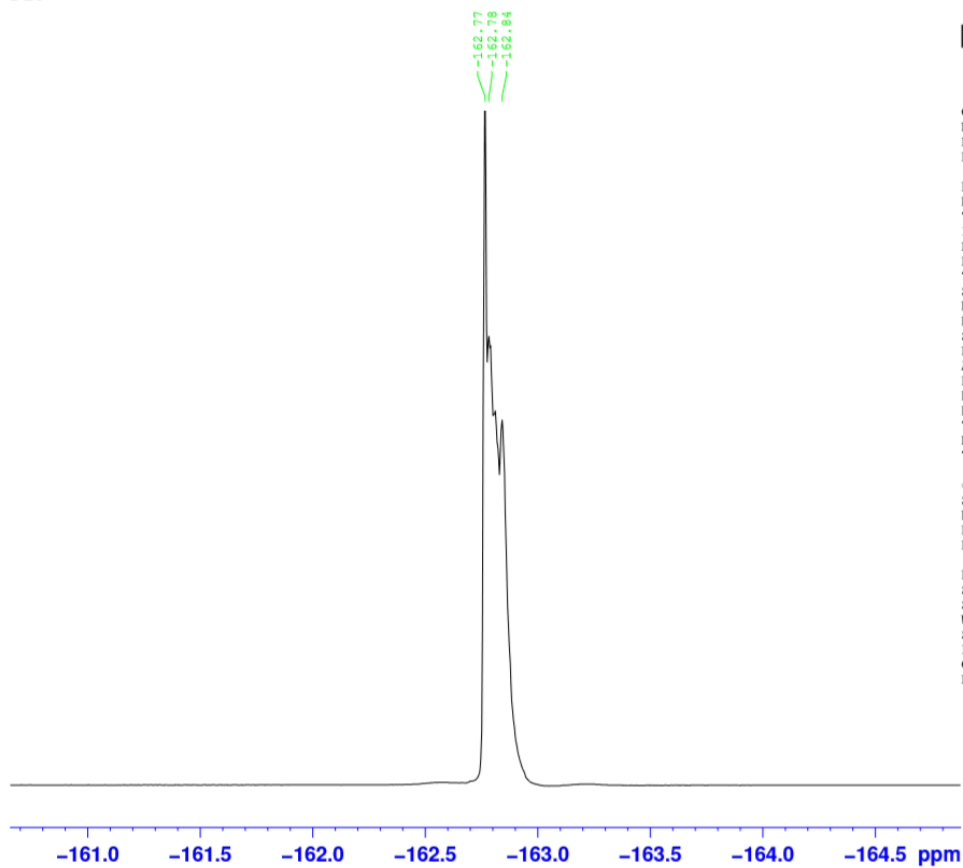
Current Data Parameters
NAME   FM36-DMSO-19F
EXPNO   1
PROCNO   1

F2 - Acquisition Parameters
Date_   20180417
Time   10.28
INSTRUM   spect
PROBHD   5 mm PABBO BB-
PULPROG   zgflqn
TD   131072
SOLVENT   DMSO
NS   16
DS   4
SWH   89285.711 Hz
FIDRES   0.681196 Hz
AQ   0.7340032 sec
RG   90.5
DW   5.600 usec
DE   6.50 usec
TE   296.0 K
D1   1.00000000 sec
TD0   1

======== CHANNEL f1 ========
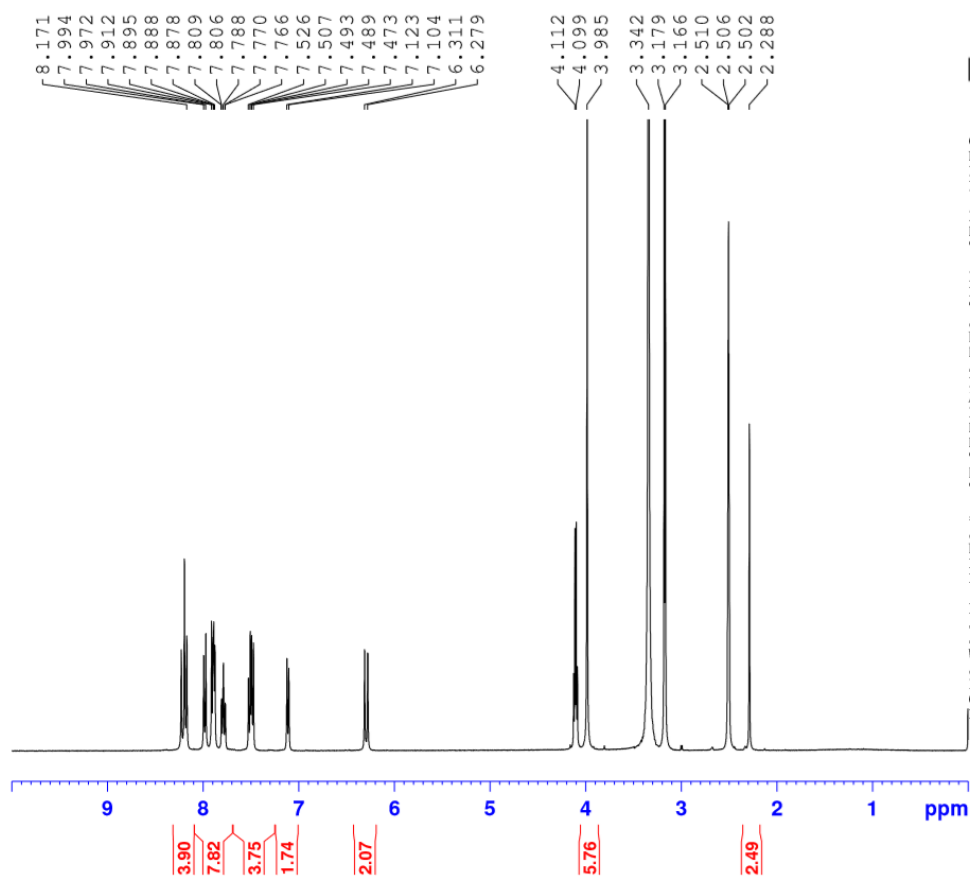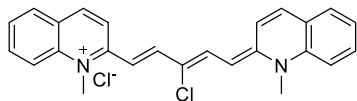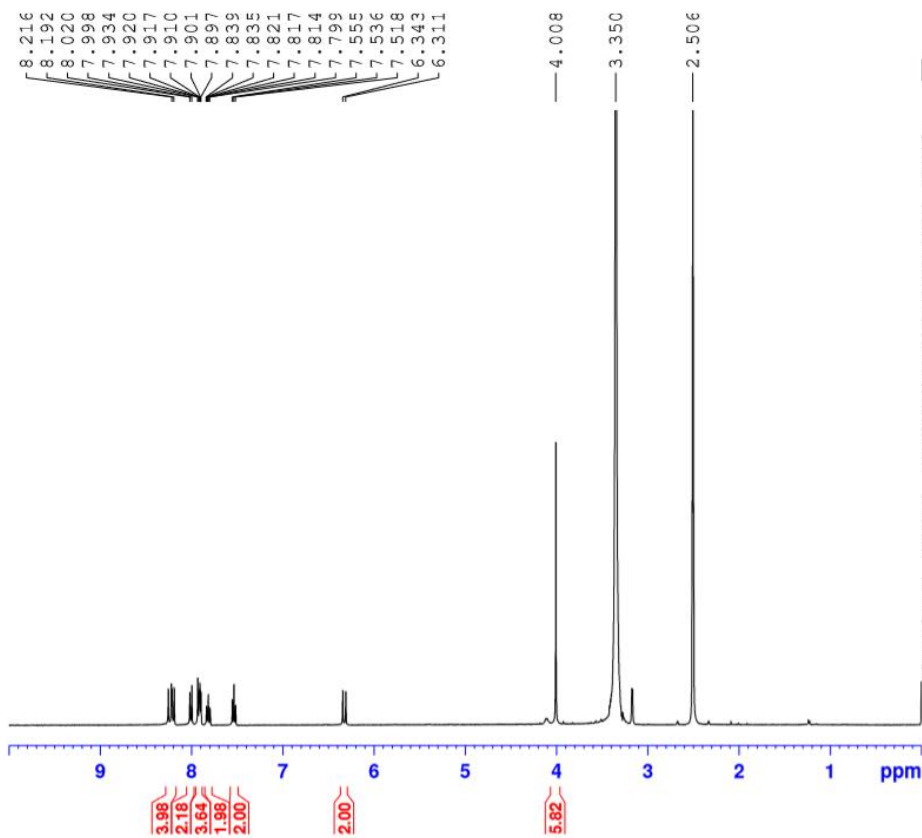SFO1   376.4701248 MHz
NUC1   19F
P1   14.00 usec
PLW1   20.00000000 W

F2 - Processing parameters
SI   65536
SF   376.5077760 MHz
WDW   EM
SSB   0
LB   0.30 Hz
GB   0
PC   1.00

−161.0   −161.5   −162.0   −162.5   −163.0   −163.5   −164.0   −164.5 ppm

Chemical Formula: $C_{25}H_{22}ClIN_2$
Molecular Weight: 512.8195

17a

Chemical Formula: $C_{32}H_{29}ClN_2O_3S$
Molecular Weight: 557.1050

17c

8.171
7.994
7.972
7.912
7.895
7.888
7.878
7.809
7.806
7.788
7.770
7.766
7.526
7.507
7.493
7.489
7.473
7.123
7.104
6.311
6.279

4.112
4.099
3.985

3.342
3.179
3.166
3.160

2.510
2.506
2.502
2.288

Current Data Parameters
NAME   fm43-ts-dmso-1H
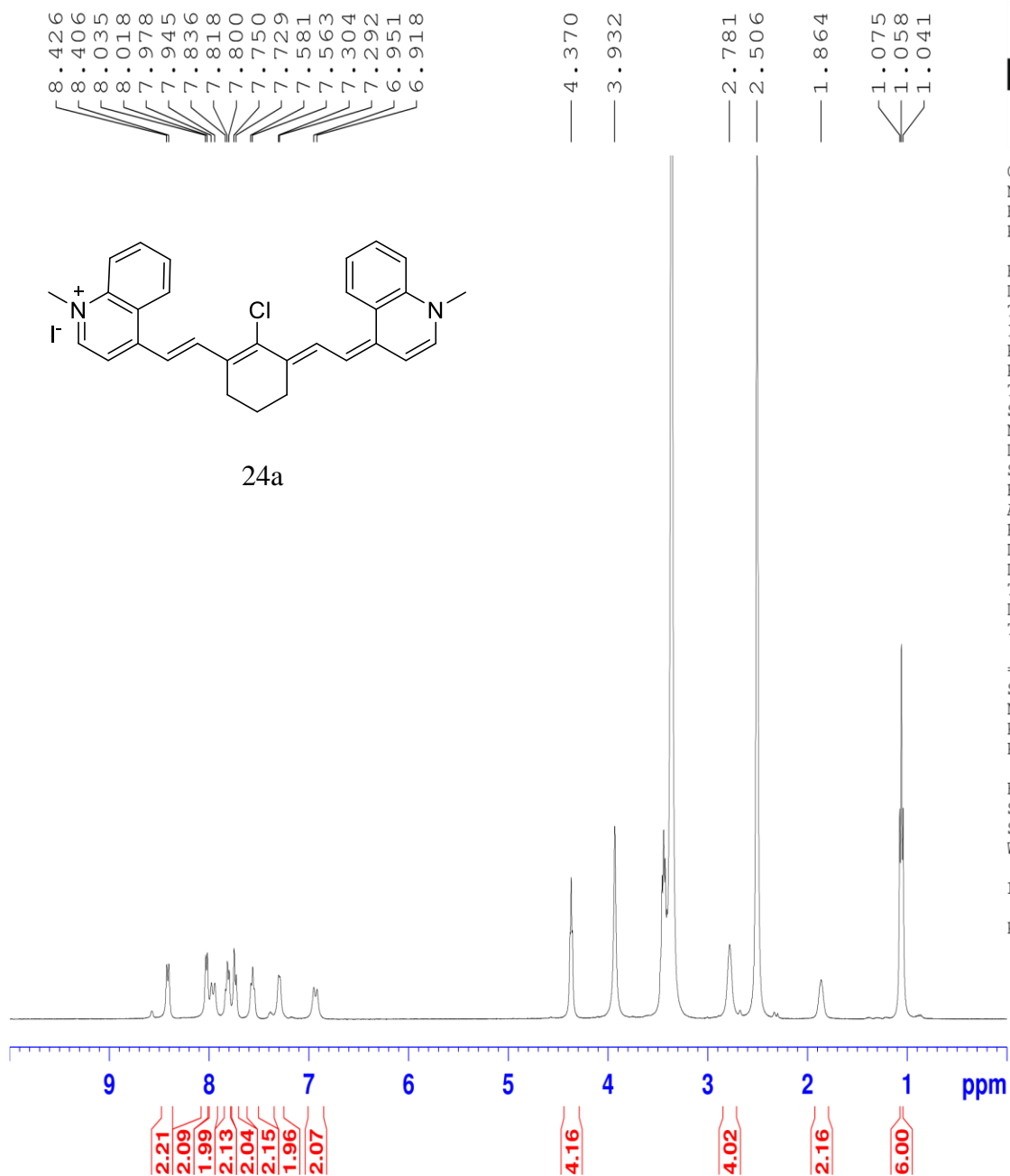EXPNO   1
PROCNO   1

F2 - Acquisition Parameters
Date_   20170308
Time   18.57
INSTRUM   spect
PROBHD   5 mm PABBO BB-
PULPROG   zg30
TD   65536
SOLVENT   DMSO
NS   64
DS   2
SWH   8012.820 Hz
FIDRES   0.122266 Hz
AQ   4.0894465 sec
RG   32
DW   62.400 usec
DE   6.50 usec
TE   298.0 K
D1   1.00000000 sec
TDO   1

======== CHANNEL f1 ========
SFO1   400.1424710 MHz
NUC1   1H
P1   13.55 usec
PLW1   16.00000000 W

F2 - Processing parameters
SI   65536
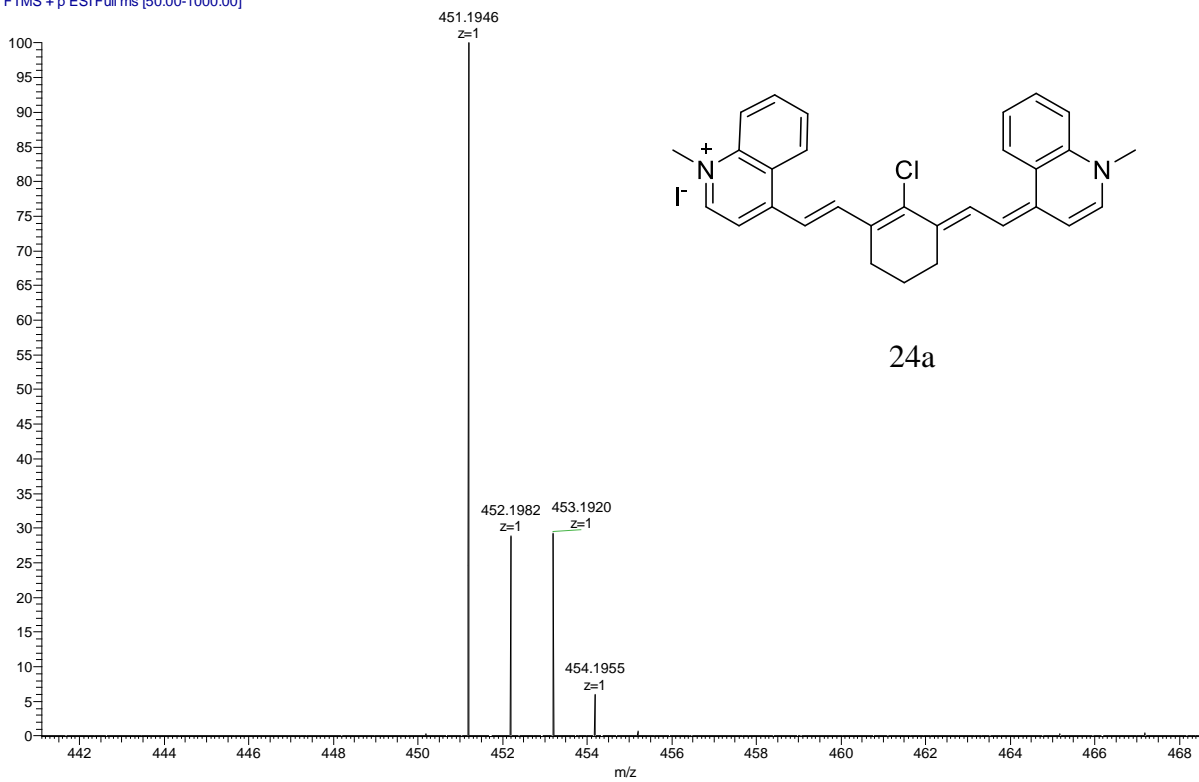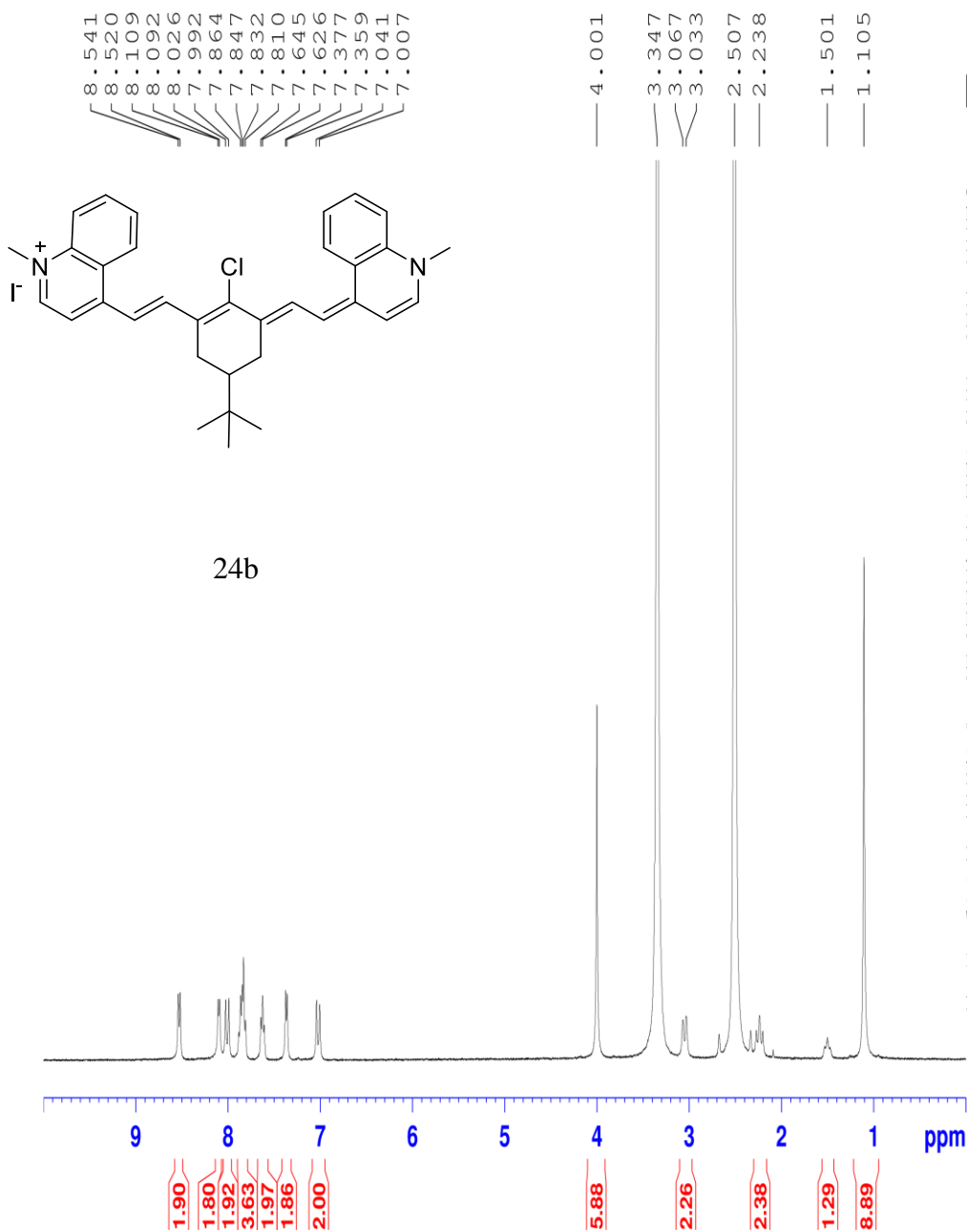SF   400.1400000 MHz
WDW   EM
SSB   0
LB   0.30 Hz
GB   0
PC   1.00

9   8   7   6   5   4   3   2   1   ppm

3.90 7.82 3.75 1.74   2.07   5.76   2.49

Chemical Formula: $C_{26}H_{25}ClN_2O_4S$
Molecular Weight: 497.0060

17b

Peak labels: 8.171, 7.994, 7.972, 7.912, 7.895, 7.888, 7.878, 7.809, 7.806, 7.788, 7.770, 7.766, 7.526, 7.507, 7.493, 7.489, 7.473, 7.123, 7.104, 6.311, 6.279, 4.112, 4.099, 3.985, 3.342, 3.179, 3.166, 3.160, 2.510, 2.506, 2.502, 2.288

Integration values: 3.90, 7.82, 3.75, 1.74, 2.07, 5.76, 2.49

Chemical Formula: C$_{25}$H$_{22}$Cl$_2$N$_2$
Molecular Weight: 421.3650

19d

8.426
8.406
8.035
8.018
7.978
7.945
7.836
7.818
7.800
7.750
7.729
7.581
7.563
7.304
7.292
6.951
6.918

4.370
3.932

2.781
2.506

1.864

1.075
1.058
1.041

BRUKER

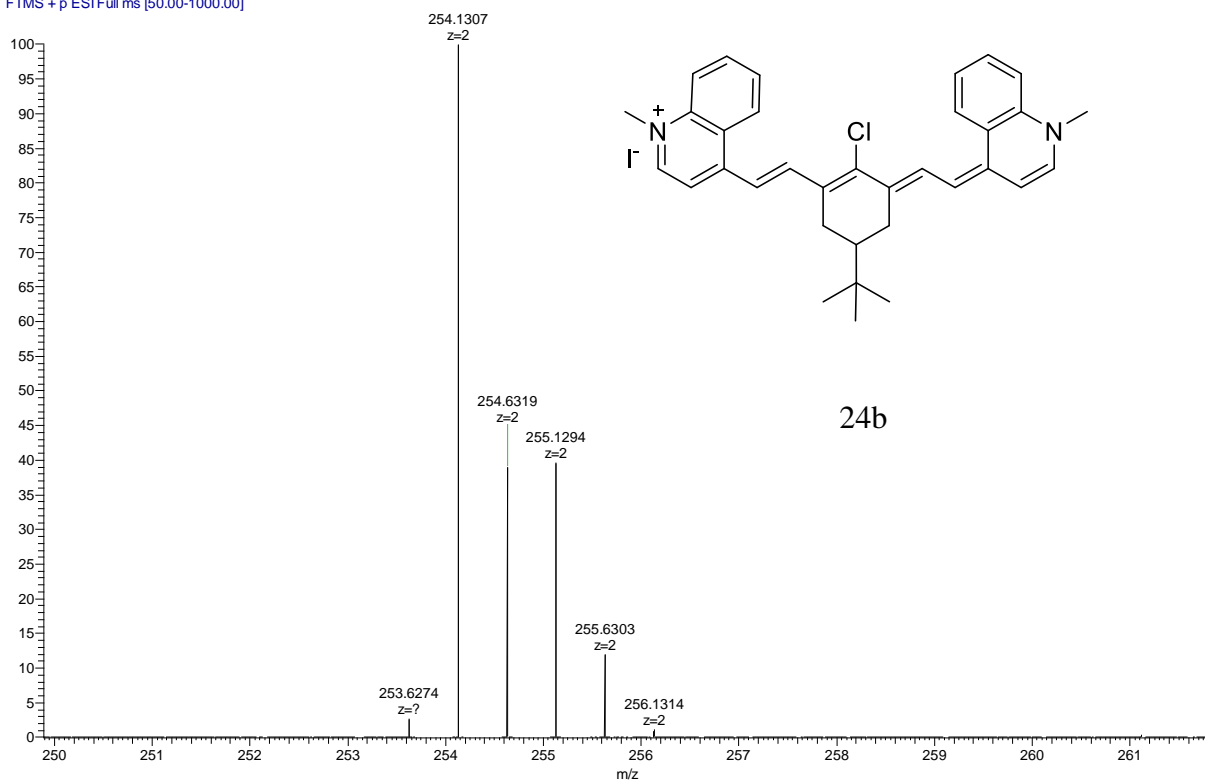Current Data Parameters
NAME   4meq-me-vils-1H-dmso
EXPNO   1
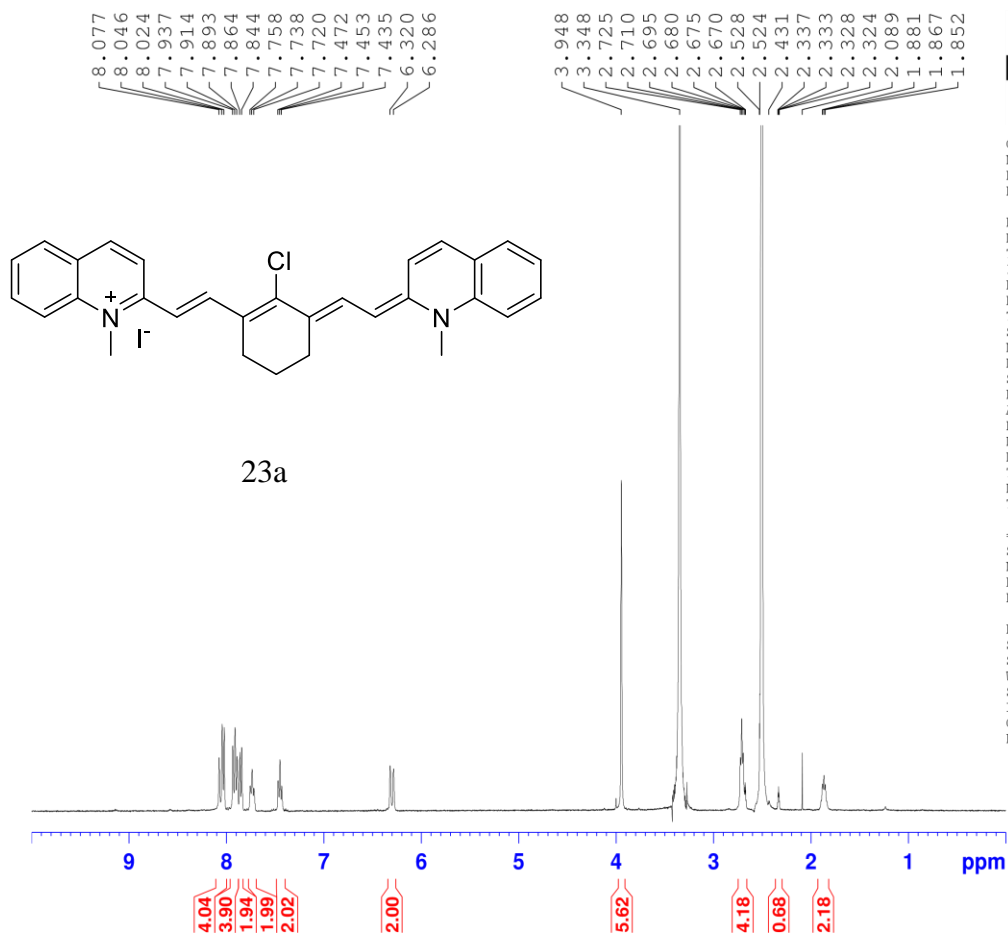PROCNO   1

F2 - Acquisition Parameters
Date_   20170828
Time   18.55
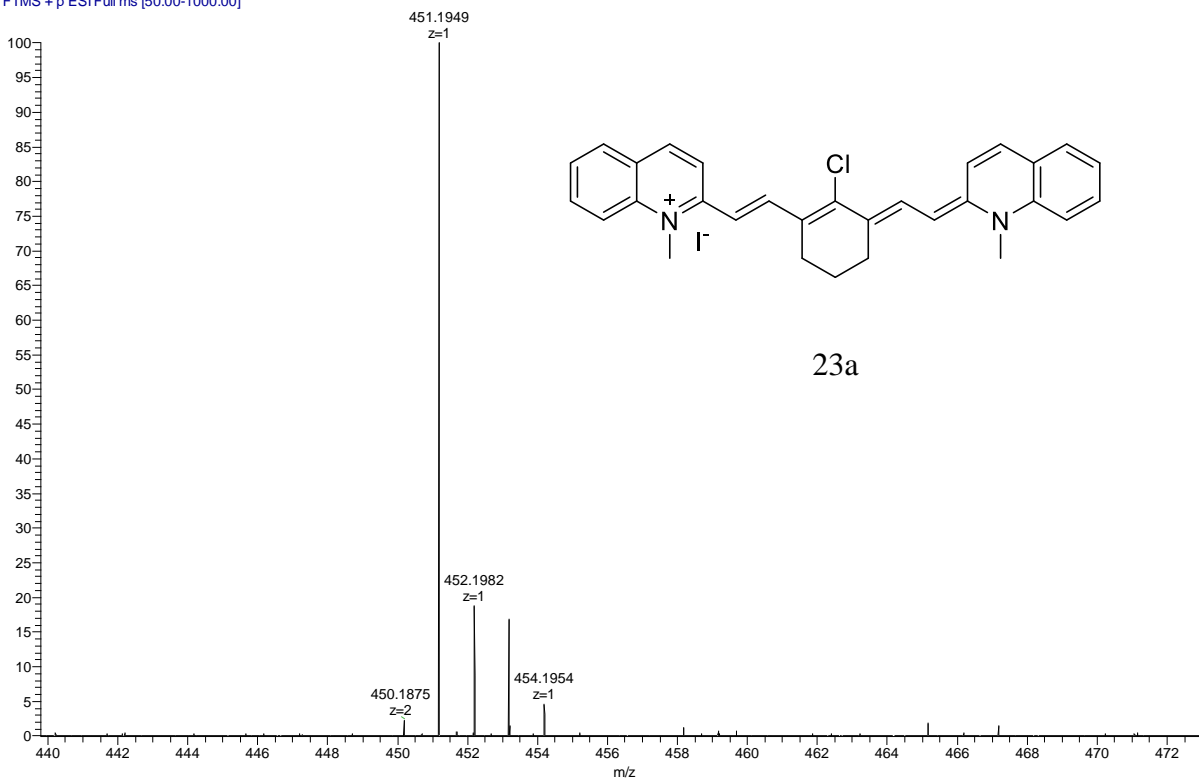INSTRUM   spect
PROBHD   5 mm PABBO BB-
PULPROG   zg30
TD   65536
SOLVENT   DMSO
NS   64
DS   2
SWH   8012.820 Hz
FIDRES   0.122266 Hz
AQ   4.0894465 sec
RG   32
DW   62.400 usec
DE   6.50 usec
TE   297.1 K
D1   1.00000000 sec
TDO   1

======== CHANNEL f1 ========
SFO1   400.1424710 MHz
NUC1   1H
P1   13.55 usec
PLW1   16.00000000 W

F2 - Processing parameters
SI   65536
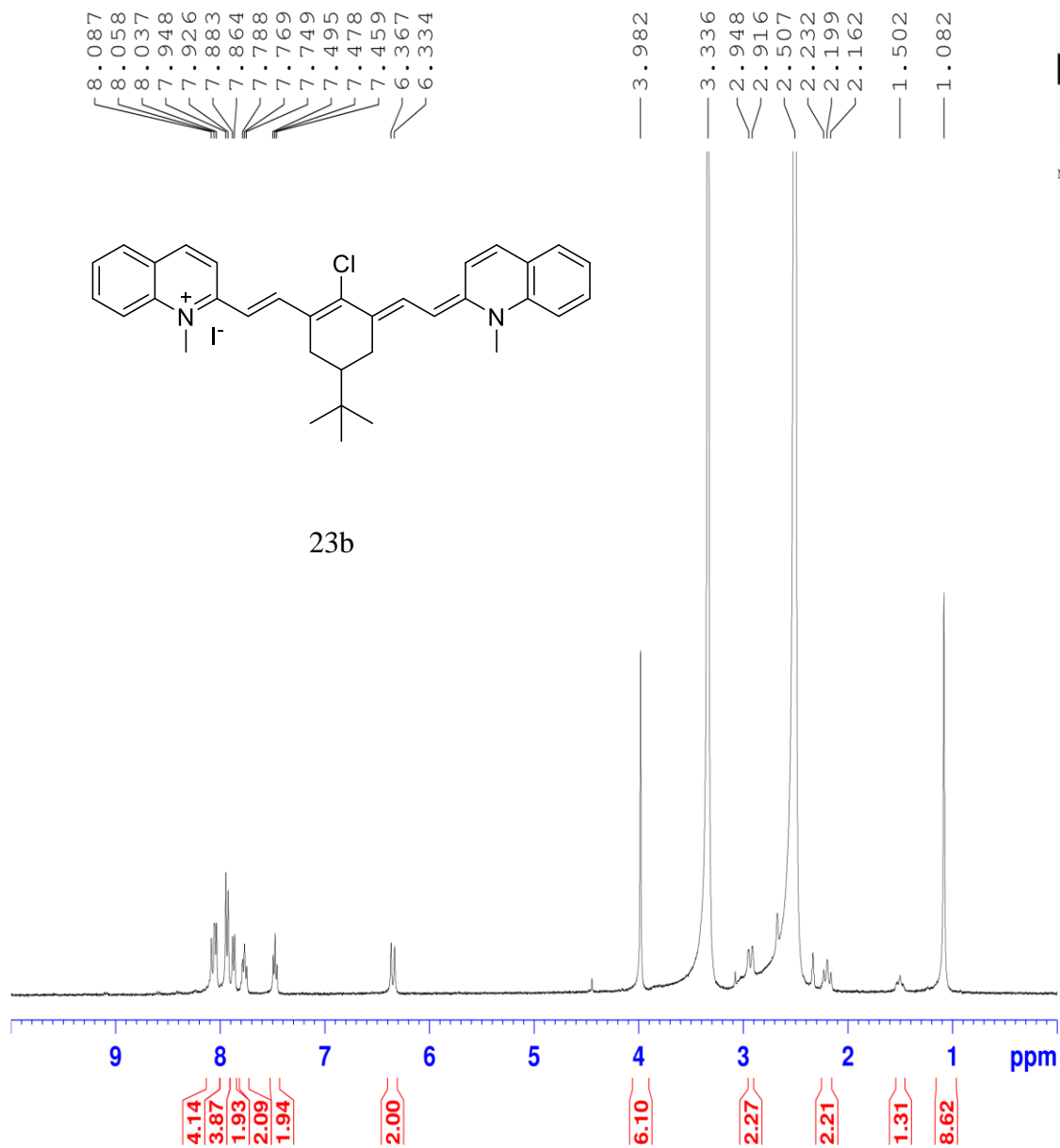SF   400.1400000 MHz
WDW   EM

LB   0.30 Hz

PC   1.00

24a

9   8   7   6   5   4   3   2   1   ppm

2.21
2.09
1.99
2.13
2.04
2.15
1.96
2.07

4.16

4.02

2.16

6.00

24a

8.541
8.520
8.109
8.092
8.026
7.992
7.864
7.847
7.832
7.810
7.645
7.626
7.377
7.359
7.041
7.007

4.001

3.347
3.067
3.033

2.507
2.238

1.501
1.105

24b

1.90 1.80 1.92 3.63 1.97 1.86 2.00   5.88   2.26   2.38   1.29 8.89

FM_61_ESIPOS_HENARY_041918 #163-171 RT: 2.29-2.40 AV: 9 NL: 7.47E7
T: FTMS + p ESI Full ms [50.00-1000.00]

8.077
8.046
8.024
7.937
7.914
7.893
7.864
7.844
7.758
7.738
7.720
7.472
7.453
7.435
6.320
6.286

3.948
3.348
2.725
2.710
2.695
2.680
2.675
2.670
2.528
2.524
2.431
2.337
2.333
2.328
2.324
2.089
1.881
1.867
1.852

BRUKER
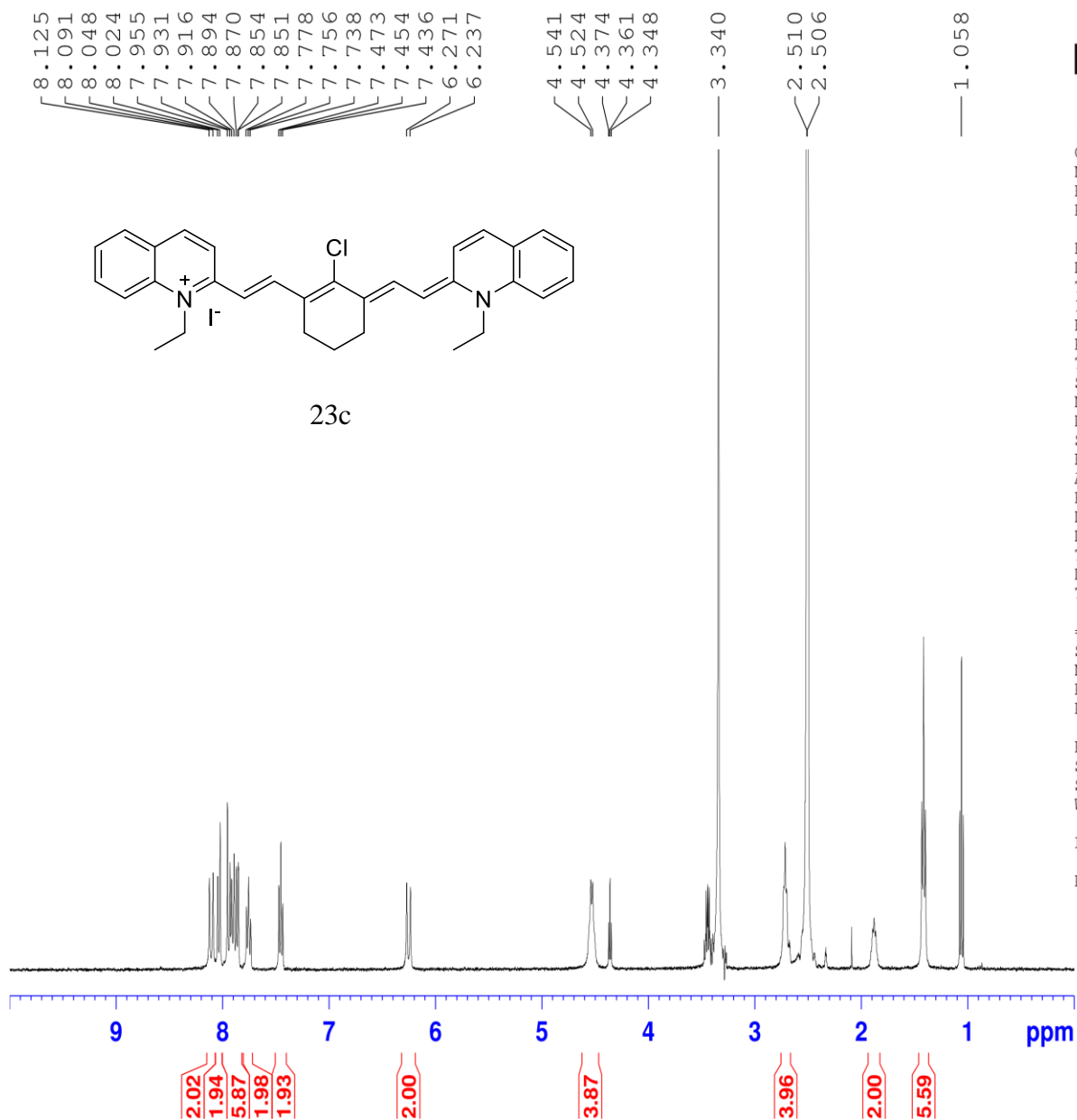
Current Data Parameters
NAME   2meq-me-vils-DMSO-1H
EXPNO   2
PROCNO   1

F2 - Acquisition Parameters
Date_   20170821
Time   20.50
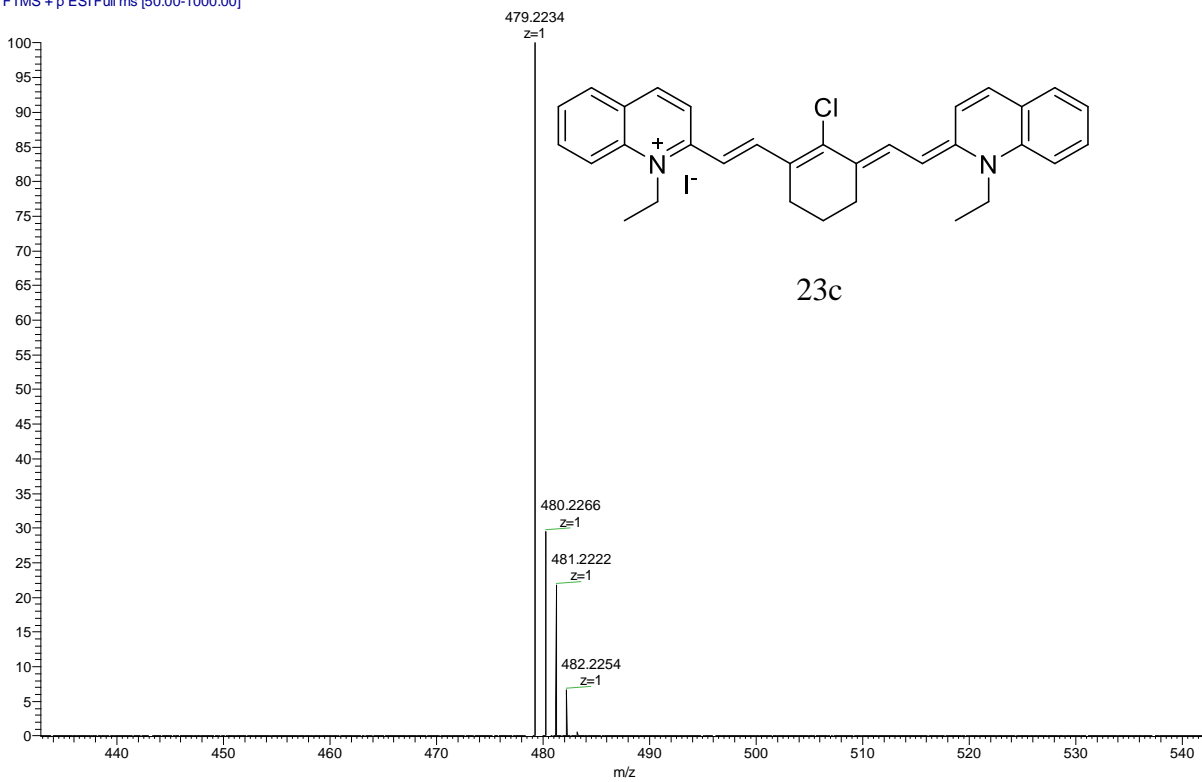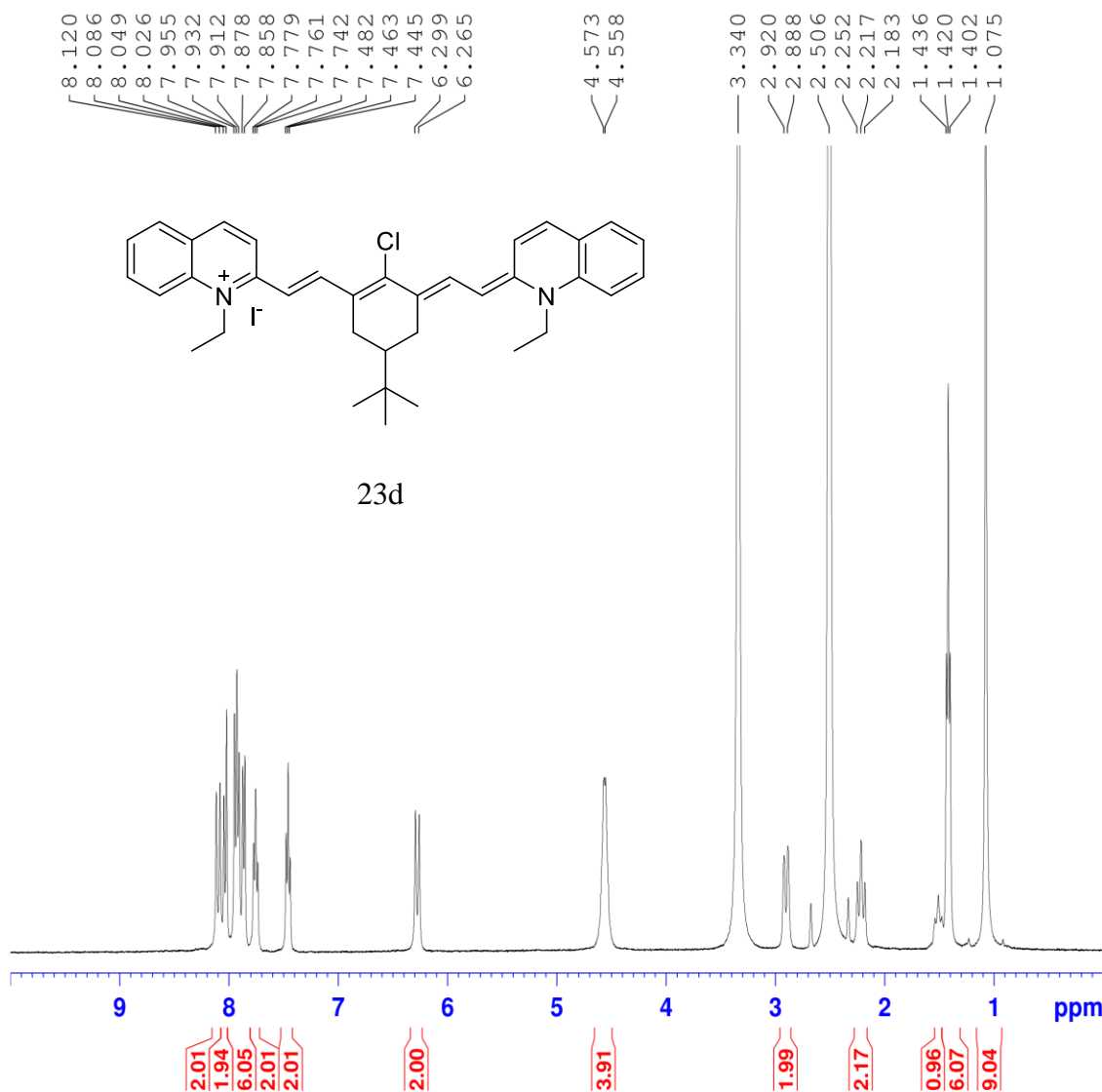INSTRUM   spect
PROBHD   5 mm PABBO BB-
PULPROG   zg30
TD   65536
SOLVENT   DMSO
NS   16
DS   2
SWH   8012.820 Hz
FIDRES   0.122266 Hz
AQ   4.0894465 sec
RG   32
DW   62.400 usec
DE   6.50 usec
TE   296.8 K
D1   1.00000000 sec
TD0   1

======== CHANNEL f1 ========
SFO1   400.1424710 MHz
NUC1   1H
P1   13.55 usec
PLW1   16.00000000 W

F2 - Processing parameters
SI   65536
SF   400.1400000 MHz
WDW   EM
SSB   0
LB   0.30 Hz
GB   0
PC   1.00

23a

9   8   7   6   5   4   3   2   1   ppm

4.04
3.90
1.94
1.99
2.02
2.00
5.62
4.18
0.68
2.18

23a

8.087
8.058
8.037
7.948
7.926
7.883
7.864
7.788
7.769
7.749
7.495
7.478
7.459
6.367
6.334

3.982

3.336

2.948
2.916
2.507
2.232
2.199
2.162

1.502

1.082

NAME   tbut-vils-2MeQ-dye2-DMSO-1H

23b

9   8   7   6   5   4   3   2   1   ppm

4.14
3.87
1.93
2.09
1.94

2.00

6.10

2.27

2.21

1.31

8.62

FM_60_ESIPOS_HENARY_041918 #145-149 RT: 2.04-2.10 AV: 5 NL: 7.32E7
T: FTMS + p ESI Full ms [50.00-1000.00]

23b

8.125
8.091
8.048
8.024
7.955
7.931
7.916
7.894
7.870
7.854
7.851
7.778
7.756
7.738
7.473
7.454
7.436
6.271
6.237

4.541
4.524
4.374
4.361
4.348

3.340

2.510
2.506

1.058

23c

9 8 7 6 5 4 3 2 1 ppm

2.02 1.94 5.87 1.98 1.93   2.00   3.87   3.96 2.00 5.59

23c

23d

8.120 8.086 8.049 8.026 7.955 7.932 7.912 7.878 7.858 7.779 7.761 7.742 7.482 7.463 7.445 6.299 6.265

4.573 4.558

3.340 2.920 2.888 2.506 2.252 2.217 2.183 1.436 1.420 1.402 1.075

2.01 1.94 6.05 2.01 2.01 2.00 3.91 1.99 2.17 0.96 6.07 9.04

23d

23f

23e

8.009
7.973
7.928
7.712
7.698
7.572

6.271
6.239

3.916
3.341
2.907
2.506
2.090
1.486
1.084

23f

8.17
2.09
2.09
2.06
6.00
2.06
1.07
8.91

9   8   7   6   5   4   3   2   1   ppm

F19

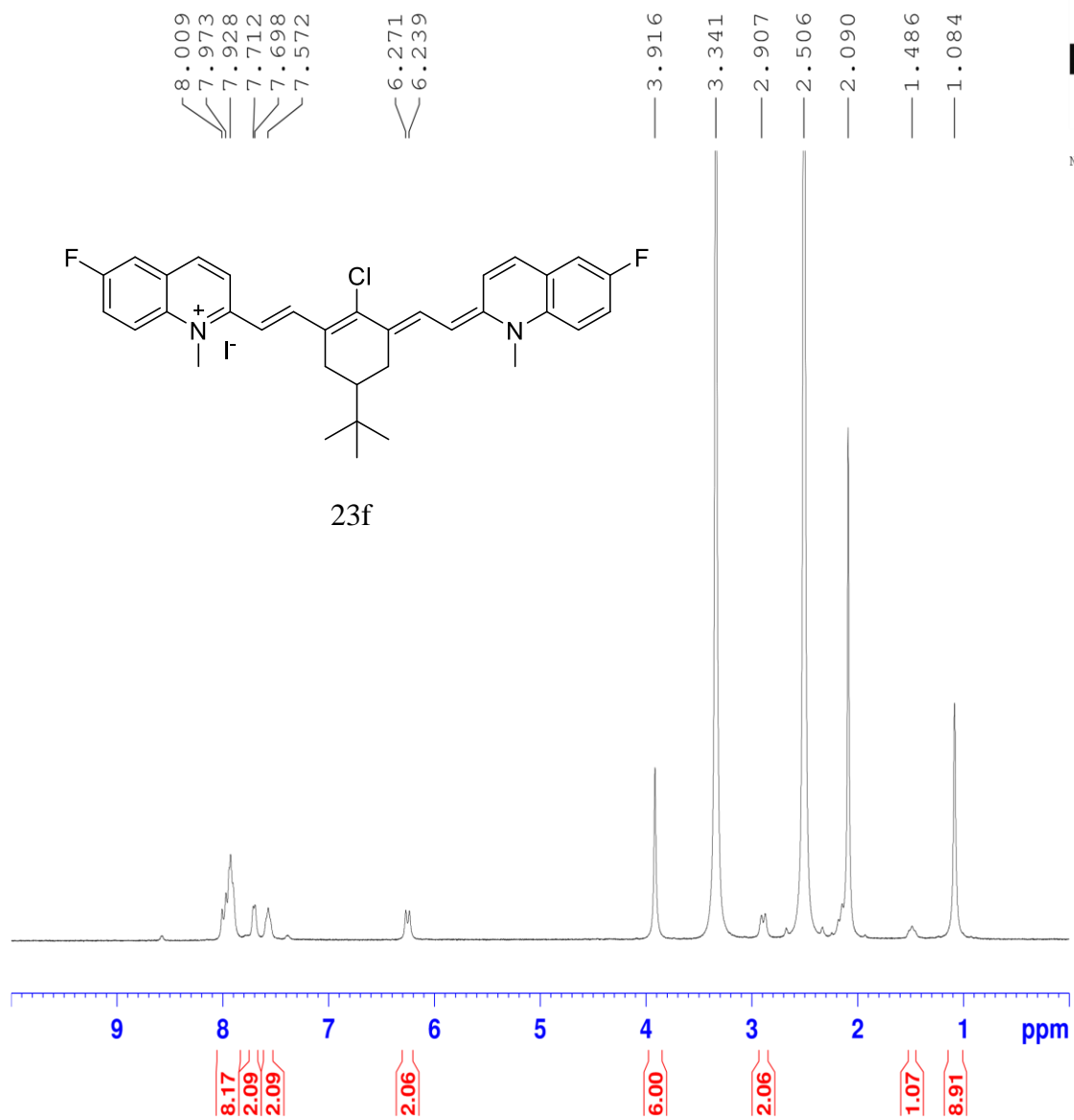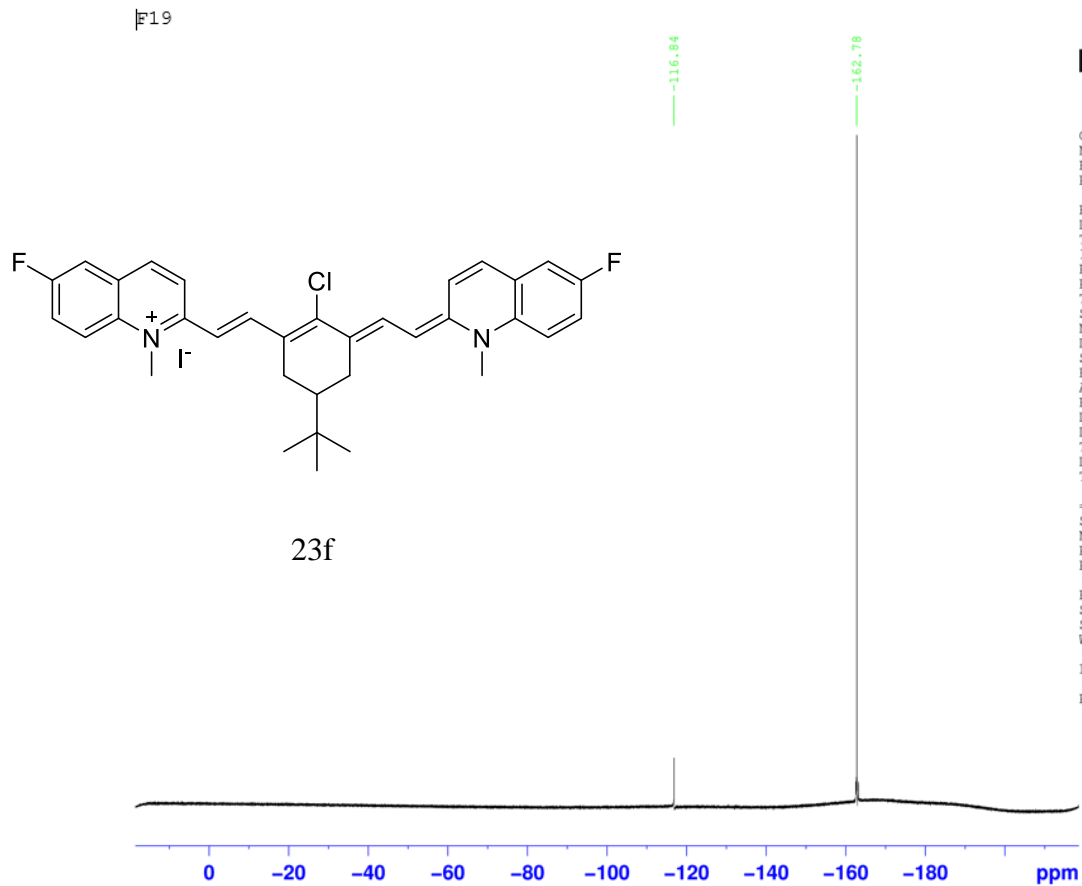23f

Current Data Parameters
NAME   fm67-DMSO-19F
EXPNO   1
PROCNO   1

F2 - Acquisition Parameters
Date_   20180417
Time   11.27
INSTRUM   spect
PROBHD   5 mm PABBO BB-
PULPROG   zgflqn
TD   131072
SOLVENT   DMSO
NS   16
DS   4
SWH   89285.711 Hz
FIDRES   0.681196 Hz
AQ   0.7340032 sec
RG   90.5
DW   5.600 usec
DE   6.50 usec
TE   295.4 K
D1   1.00000000 sec
TD0   1

======== CHANNEL f1 ========
SFO1   376.4701248 MHz
NUC1   19F
P1   14.00 usec
PLW1   20.00000000 W

F2 - Processing parameters
SI   65536
SF   376.5077760 MHz
WDW   EM

LB   0.30 Hz

PC   1.00